Abteilung für Hand-, Plastische und Ästhetische Chirurgie

Abteilung der Ludwig-Maximilians-Universität München

Vorstand: Prof. Dr. Riccardo Giunta

CAD-CAM workflow for the fabrication of Bioscaffolds and Porous Auricular Constructs with Polycaprolactone using Ultimaker 2+

Dissertation zum Erwerb des Doktorgrades der Medizin an der

Medizinischen Fakultät der Ludwig-Maximilians-Universität zu

München

Vorgelegt von Chenhao Ma

aus Handan, Hebei Provinz, China

2021

Mit Genehmigung der Medizinischen Fakultät der Universität München

Berichterstatter: Prof. Dr. Thilo Schenck

Mitberichterstatter: Prof. Dr. Matthias Pietschmann

Dekan: Prof. Dr. med. dent Reinhard Hickel

Tag der Mündlichen Prüfung: 19.05.2021

Abstract

In recent years, the application of three-dimensional fabrication to fabricate customized porous scaffolds for cell culture has received much attention from the field of tissue engineering and plastic surgery. In this study, we applied a more publicly accessible 3D printer, Ultimaker 2+ with biodegradable polymer-polycaprolactone (PCL) to fabricate both three-dimensional bioscaffolds and auricular constructs (both solid and porous) prepared to fill the gap as potential solutions for both cartilage defects and microtia respectively by managing of the CAD-CAM workflow. As an overview, the modified CAD-CAM workflow was regarded as the uniform preparation fabricating types of scaffolds to identify the general printability of PCL with Ultimaker 2+. For bioscaffolds, limit test was performed on original scaffold, the resolution for printing scaffolds by PCL was identified as 600 microns by applying method of uniform scaling and limit approaching. For customized auricular constructs, we extract the model from MRI/CT scan and use its mirror image for the general shape of model building in a relatively customized way to fabricate solid auricular constructs. Boolean operation was then applied for fabricating the inner porous microstructure to fabricate porous auricular constructs. As there were no significant differences among three groups of filaments regarding the respective dimensions for both bioscaffolds (n=9 for each group: PCL, PLA and ABS) and customized auricular constructs (n=5 for both solid auricular constructs and porous auricular constructs) indicated by the P value($P>0.05$) from ANOVA, the printing compatibility of PCL regarding each specific domain of scaffolds were identified. In Conclusion, our study had indicated a consistent CAD-CAM workflow for Ultimaker 2+ with PCL to fabricate three-dimensional bioscaffolds, solid auricular constructs and porous auricular constructs which could be potentially applied to fill the gap of cartilage engineering and microtia reconstruction through in-vitro cell culture, surgical simulation and in-situ cell culture respectively.

TABLE OF CONTENTS

1 Introduction

1.1 Clinical Problems

1.1.1 Cartilage Defects

A cartilage defect refers to a cartilage tissue abnormality caused by a congenital abnormality, trauma, or tumor resection. Although cartilage is a connective tissue with stiffness and flexibility, patients with cartilage damage are common in the clinic, and these injuries require attention for accurate evaluation of the cartilage and determination of the appropriate treatment options.(1) In particular, the lack of blood vessels, nerves, lymphatic tissue and other pathways for nourishing cartilage tissue consisting of one type and small numbers of cells, i.e., chondrocytes, with a relatively low proliferation rate are potentially responsible for the limited capacity of cartilage for spontaneous repair following injury. Thus, once cartilage is damaged, it is challenging for it to repair itself on its own and gain full recovery of its structure, function, and biomechanical properties.(2)

1.1.1.1 Anatomy

As a subtype of connective tissue, cartilage is composed of chondrocytes imbedded in a matrix accumulation of proteoglycans and collagen fibers. Compared with mineralized bone tissue, cartilage is less rigid but more flexible.(3)

The low rate of cartilage healing can be attributed to the fact that diffusion through the matrix is the only means of providing nutrition, as there are no blood or lymph vessels present for nourishing cartilage.(4) In addition, the lack of nerves passing through cartilage can explain the insensitivity of this connective tissue.

The perichondrium is the fibrous membrane that envelops cartilage and is consisted by two layers: an outer fibrous layer that contains fibroblasts to produce collagenous fibers and an inner chondrogenic layer that forms chondroblasts or chondrocytes. In adults, the perichondrium is present in the larynx, nose, trachea, ribs, external ear and epiglottis, while it is absent from the articular cartilage in the knee joints, attachment points of tendons and intervertebral disks in the spine.(5) Its function is to nourish cartilage as the diffusion of nutrients from capillaries in the perichondrium is vital for appositional avascular cartilage growth and repair. In addition, it also serves as a reservoir of stem cells to differentiate into chondrocytes for early bone development.

The calcification of cartilage is a marker of chondrocyte death, and calcified cartilage will be replaced by bone-like tissue.(6) Thus, calcium should be absent from the normal cartilage matrix, while its counterpart component chondroitin provides the inherent flexibility of cartilage tissue.

- Hyaline cartilage

As the most abundant type of cartilage tissue, hyaline cartilage is the type that forms the skeleton in the embryonic stage.(7) In adults, it persists as articular cartilage at the surface of joints, costal cartilage at the end of ribs, and other types of supporting cartilages in the nose,

trachea, and larynx. It has a glossy blue and white appearance and characteristics of high resilience.

- Fibrous cartilage

Fibrous cartilage is a tough tissue because it has a large proportion of dense, parallel-oriented collagen fibers. By occupying lacunae, its chondrocytes tend to arrange in rows between the coarse bundles of collagen fibers.(8) Fibrous cartilage is predominantly located at the insertions of ligaments and intervertebral disks; it shares similarities with other fibrous tissue with additional cartilage matrix and chondrocytes.

- Elastic cartilage

Elastic cartilage is more pliable due to its luxurious elastin fibers that form a mesh network of collagen, and it has a yellowish appearance owing to the abundance of elastic fibers cross-linked with insoluble elastin protein.(9) It serves as the component with the highest flexibility to form the external ear, epiglottis, and auditory tubes.

1.1.1.2 Treatment

Currently, the prevalent treatment choices for cartilage defects are microfracture, cartilage transfer, and autologous chondrocyte transplantation.(10)

- Microfracture

Microfracture is a treatment that stimulates the body to grow cartilage to fill the damaged area.(11) In this procedure, small holes are made in the subchondral bone at the defect site, exposing inner layers of bone tissue; this exposure will facilitate the formation of new cartilage by stimulating the resident bone marrow cells.

Advantages: It is the least invasive treatment option and is safe and reliable-it is most often performed, minimally invasive and can have a shorter recovery time than other conventional procedures; the prognosis is suitable for patients with indications.

Disadvantages: The new cartilage that fills in the gaps has different mechanical properties compared with healthy cartilage, further rehabilitation is required.(12) Mostly, the application of this technique is limited to joint cartilage, and it cannot be used for cartilage defects in the head or neck.

- Cartilage transfer

Cartilage transfer is a procedure of taking cartilage from one anatomical site and placing it at the area of interest to repair damage.(13)

Advantages: This procedure is recommended in cases of small areas of cartilage injury; immediate feedback occurs after this transfer for repair of the damaged cartilage with the healthy counterpart.

Disadvantages: Its application is limited to focal areas of cartilage damage in small size. The size of both the plug and the damaged area must be sufficiently small.

- Autologous chondrocyte implantation

It is an operation to harvest and collect chondrocytes as sample cells for expansion in cell culture.(14) The cells will be implanted into the area of cartilage damage after the number of cells has reached the expected level.

Advantages: Chondrocytes grown in vitro will be provided as a source of cartilage tissue to fill gaps.(14, 15) The potential applications of this technique tend to be more extensive, covering different types of cartilage tissue at different anatomical locations.

Disadvantages: This new approach is not mature and needs to be further optimized. Multiple surgeries and long periods of rehabilitation are required to achieve the best prognosis and results.

In summary, although these methods have a specific curative effect, there are inherent disadvantages, such as donor-site morbidity, inconsistent characteristics of the repaired area, and poor prognosis of cartilage integration.(16) With the development of regenerative medicine, significant progress has been made for cartilage engineering, which is capable to offer alternative approaches for repairing cartilage defects by solving the issues mentioned above.(17, 18)

1.1.2 Microtia

As a specific representative of cartilage defect, microtia is a congenital birth defect of the auricle of varying levels of severity, which ranges from an underdeveloped external ear to anotia, as the pinna is entirely missing. Microtia could either be an isolated congenital malformation or part of a syndrome. The overall prevalence of microtia is 2.06 per 10,000 births, which varies among different regions and races.(19)

1.1.2.1 Anatomy of the ear

The auricle is attached to both sides of the skull by ligaments and muscles and it is mainly composed of elastic cartilage covered by a thin connective tissue layer. It is supplied by anastomotic network derived from the superficial temporal and posterior auricular arteries, while it is innervated from the lesser occipital nerve and the great auricular nerve. On the other hand, the delicate cartilaginous framework acts as the skeletal of the auricle to form eminences, depressions and other important corresponding anatomical landmarks as below:

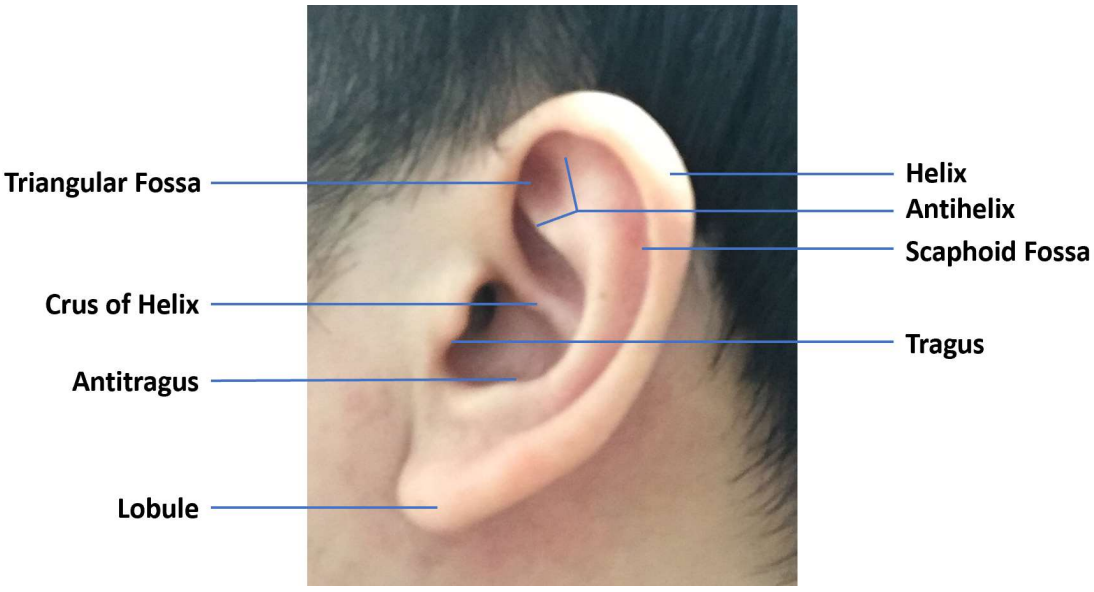

Figure 1. Structure of the ear

- Helix – the prominent rim of the auricle.
- Crus of helix – the interior end of the helix, a horizontal prominence.
- Antihelix – a curved prominence, parallel with and infront of the helix.
- Triangular fossa – a shallow depression between the two crura of the antihelix.
- Scaphoid fossa – a C-shaped groove depression between the helix and the antihelix.
- Tragus – a small pointed eminence projecting backward over the meatus
- Antitragus – an arch-shaped structure opposite to the tragus.
- Lobule – a lower part of the auricle where there is no cartilage.

1.1.2.2 Treatment

- Rib cartilage graft

Rib cartilage ear reconstruction was first introduced by Dr. Radford Tanzer in 1950s.(20) Followed by Brent-Nagata techniques or applying tissue expanders to modify stages of reconstruction, Brent-Nagata option encompasses threshold steps which includes the splitting and transposition of lobule, the construction of costal cartilage framework and its insertion into subcutaneous pocket, the covering with fascial flap.(21, 22) While the latter could be regarded as an alternative method by additionally inserting tissue expanders at postauricular mastoid region to stretch and grow extra skin to cover cartilage grafts.

Advantages: The risk of rejecting this cartilage framework is relatively low as it derives from one own body. In addition, the reconstructed ear can feel pain and heal as it is created from one's own rib cartilage as living tissue.

Disadvantages: It carries the risk of morbidity for donor site such as infection, scarring and chest wall deformity, Larger defects could even reach the limits of the potential pool of natural cartilage resources especially when patient is under 6 years old.

- Medpor implant graft

Medpor implant surgery utilizes a synthetic polyethylene framework to eliminate the need for harvesting rib cartilage, then it is covered with tissue from temporalis muscle fascia. As a biocompatible material, it provides an alternative option for aesthetic and reconstruction needs.

Advantages: First, this technique only requires one stage to insert pre-made implant into skin pocket. Further, it can be done at earlier age; finally, the concern regarding potential complications of donor site can be eliminated.

Disadvantages: As Medpor implant is not living tissue, Complications occurred on recipient site: such as infections, exposure and complete extrusion of implant induced by trauma can potentially result in the loss of the ear.

1.2 Cartilage Engineering

Cartilage engineering emerged as a new technique by multiplediscipline cooperation to fabricate biological substitutes composed of "tissue engineering triad"-scaffolds, cells and bioactive substances for restoring the functions of damaged cartilage.(18) By amplifying a small number of cells on a large scale and then inoculating them into a biodegradable scaffold, with gradual degradation of the scaffold, the cells will continue to proliferate, secrete matrix, and eventually regenerate functional living cartilage to repair the cartilage defect.(18, 23) In-vitro cartilage engineering and in-vivo cartilage engineering are defined as cultivating, propagating cells and growing cartilage outside and inside living organisms respectively.

Specifically, in the realm of plastic surgery, tissue-engineered cartilage is mainly applied for repairing cartilage lesions or reconstruction for the absence of cartilage tissue in the auricle, trachea, nose, and throat, among others.(24, 25) To achieve cosmetic goals (e.g., in reconstruction of the auricle or nose) or restore the original function (e.g., in tracheal defect repair), tissue-engineered cartilage often needs to be transplanted into subcutaneous or intramuscular environments where there is a lack of cartilage regeneration control signals and where the immune response tends to be more intensive. Therefore, tissue-engineered cartilage used for transplantation is required to have a stable cartilage phenotype, which means it is not susceptible to ossification or fibrosis in a non-cartilage microenvironment and has excellent biocompatibility to overcome rejection at the transplant site via an active immune response.(26) Additionally, tissue-engineered cartilage is often required to have substantial volumes, specific functions, such as unique personalized delicate forms, such as that of the auricle. The three vital components of cartilage engineering are cells, bioactive substances, and scaffolds.

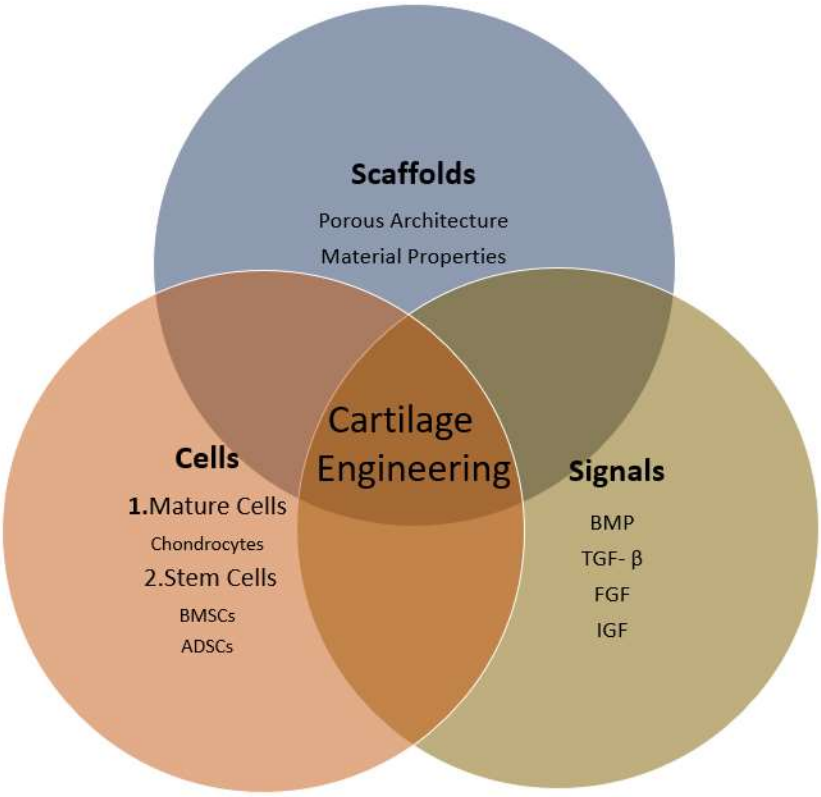

Figure 2. Components of cartilage engineering.

1.2.1 Cells

As the basis of cartilage engineering, the selection and source of cells have always been in the focus of attention in regenerative medicine research. Currently, cartilage cells and stem cells are two dominant types of cells being used regarding cartilage regeneration.

1.2.1.1 Chondrocytes

Cartilage cells, as the earliest and most primitive type of cells for cartilage engineering, have been studied for more than two decades. Cultured autologous chondrocytes are, in theory, the ideal cells for repairing human cartilage defects.(27) The autologous chondrocytes themselves have the cellular phenotypes needed for cells in cartilage tissue engineering and have no antigenicity, which thus prevents an immune response after transplantation. Autologous chondrocyte transplantation as a routine method in cartilage tissue engineering is also widely used in the clinic and has been proven to have an excellent therapeutic effect. A study has reported that cartilage at the defect site is repaired with hyaline cartilage after autologous chondrocyte transplantation.(28) However, the sources of autologous chondrocytes for transplantation are limited, the life of chondrocytes is finite,; additionally, they easily differentiate and lose their original chondrocyte phenotype after multiple cycles of propagation and proliferation during in vitro culture.(29) At the same time, a study has also confirmed that the activity of chondrocytes is age-related, with activity decreasing gradually with age. (30)On the other hand, although the limited sources of chondrocytes for autologous transplantation

could potentially be resolved through another alternative approach, i.e., allogeneic chondrocyte transplantation, this method has not been proven to provide a reliable source of cells because of the immunogenicity of the cells and the possibility of disease transmission.(31)

1.2.1.2 Stem cells

Stem cells are mainly classified into embryonic and adult stem cells. The former ones have a good capability for proliferation but because of the influence of laws and ethics on their use, research on embryonic stem cells has always had some limitations. Therefore, the latter ones have attracted extensive attention from most research institutes. Adult stem cells mainly refer to cells with further differentiation potential in adult tissues that exist in a variety of organs or tissues and can exhibit different degrees of regeneration and renewal in a pathological state or under the influence of external induction factors.(32) Bone marrow-derived mesenchymal stem cells and adipose-derived mesenchymal stem cells stand as the most popular representatives among various types of adult stem cells commonly being used.

- Bone marrow stem cells

Bone marrow stem cells are widely believed to be ideal candidate stem cells for cartilage engineering.(33) Harvesting this type of cell is relatively simple and minimally invasive; in addition, it is easy to isolate these cells from bone marrow, to proliferate and purify these cells in vitro and to stabilize the direction of differentiation into chondrocytes. There are four conventional approaches for separating bone marrow stem cells: density gradient centrifugation, the wall culture method, the flow cytometry sorting method and the immune magnetic bead sorting method; however, there are many problems in the clinical translation of bone marrow-derived mesenchymal stem cells, such as how to purify , identify and obtain bone marrow mesenchymal stem cells, in addition, effectively control the proliferation and process of differentiation of these cells into chondrocyte-like cells also remains as challenging issues to be further studied and solved.(34)

- Adipose-derived mesenchymal stem cells

Adipose-derived mesenchymal stem cells are rich in sources and have a strong ability to proliferate; current research suggests that these cells exhibit the most rapid growth of all stem cells. Previous results confirm that these cells also has the potential to differentiate into chondrocyte-like cells under extracorporeal induction.(35) The regenerative cartilage was successfully constructed by using these cells. However, the application of these cells as sources in cartilage engineering to repair cartilage lesions is only in the preliminary research stage, and a long-term experimental process is necessary before these cells can be used in clinical treatment.(36)

1.2.2 Signals

It is generally believed that cartilage injury repair is a complicated process involving various biological factors. Biological signals play essential roles and are critical in tissue engineering.(37) There are many kinds of biological regulatory factors, the most common of which are growth factors. Currently, primary growth factors commonly used are bone morphogenetic protein(BMP), transforming growth factor beta(TGF-β), fibroblast growth factor(FGF), and insulin-like growth factor.(IGF) (32) Different growth factors act on chondrocytes after being secreted, and their effects interact to form networks with specific spatial distributions.(38)

1.2.2.1 Bone morphogenetic protein

Since it was first discovered in 1963, the bone morphogenetic protein family has more than 20 members. Studies have confirmed that bone morphogenetic proteins can effectively promote the synthesis and metabolism of chondrocytes. Bone morphogenetic proteins is can increase synthesis and secretion of cartilage extracellular matrix, which has a positive impact on cartilage formation.(39, 40) At the same time, studies have also shown that bone morphogenetic proteins can promote the differentiation of these cells into chondrocyte-like cells and further maintain chondrocyte phenotype.

1.2.2.2 Transforming growth factor beta

As a class of multifunctional protein polypeptide, it plays an important role for repairing cartilage defects. Transforming growth factor beta has been classified into four subtypes: β1, β2, β3, and β4.(41) It regulates apoptosis, cell proliferation and differentiation through receptor signal transduction pathways on the cell. A previous study also showed that transforming growth factor beta could effectively promote the regeneration and differentiation of cartilage, and the effect of it subtype β3 induced differentiation was stronger than that of β1 and β2.(42) Subtype β3 can significantly increase the expression of Sox-9 and effectively promote the synthesis and secretion of protein oligosaccharides and type II collagen.

1.2.2.3 Fibroblast growth factor

Fibroblast growth factor is one type of polypeptide secreted by the pituitary gland and hypothalamus which can promote mitosis and growth of fibroblast cells and blood vessels formation. It mainly exists in acidic form as essential fibroblast growth factor 2, which have the same biological effect, but primary fibroblast growth factor occupies a prominent position in cartilage tissue engineering. The study confirmed that chondrocytes cultured in vitro can effectively maintain their cell phenotypes and maintain their differentiation status only under the action of this molecule.(43, 44)

1.2.2.4 Insulin-like growth factor

Insulin-like growth factor mainly refers to one specific class of amino acid sequences similar to insulin protein or polypeptide growth factor that can promote cell division.(45) It involves in chondrogenesis of mesenchymal stem cells and maintenance of mature cartilage. Furthermore, its binding protein represent a evolutionarily conservative protein family which regulate, store and transport insulin-like growth factor. Studies have confirmed that this molecule can effectively stimulate the proliferation of chondrocytes and promote the formation of cartilage substrates during cartilage development.(46). In summary, Insulin-like growth factors are important bioactive molecules regulating body development especially on endochondral ossification and chondrogenesis. Thus, it is expected to a vital element for promoting the cartilage engineering.

1.2.3 Scaffolds

Tissue scaffolds play an essential role as an alternative to the cartilage extracellular matrix (ECM) in cartilage engineering. Most researchers believed that the appropriate tissue engineering scaffolds must have excellent biocompatibility, absorbable degradation components, a good 3D structure as a microenvironment, and good plasticity.(47) In addition, the development of new materials and the appropriate selection of processing materials are essential to meet both the mechanical and biological requirements.(48) Finally, the customization of designing and manufacturing process is vital for meeting the geometric standards for controlling the preparation of scaffolds.(49)

1.2.3.1 Required criteria

Five criteria are needed to be taken into consideration for choosing materials and for designing and manufacturing bioscaffolds:

- Biocompatibility

The scaffold must be compatible: cells can adhere, function, proliferate, and usually differentiate through the scaffold. No or only a negligible reaction will be elicited so that inflammation can be prevented in order to prevent a rejection response.(50)

- Biodegradability

As the scaffolds only act as temporary constructs and will be replaced by the cells, biodegradability is required in order to achieve this result. The byproducts of degradation should be nontoxic and metabolizable.(48)

- Mechanical properties

Constructing scaffolds with appropriate mechanical strength is regarded as one of the significant challenges to engineering cartilage because the remodeling process of cartilage regeneration tends to be longer than other tissue counterparts. In addition, the healing rates vary with age, environment, and other individual health parameters.(51) Finally, a balance between mechanical strength and porous structure must be reached in order to achieve successful cell infiltration and vascularization.

- Architecture

Suitable architecture is critical for cellular penetration and nutritional diffusion within the scaffold. Metabolized waste can also exit within an appropriate porous interconnected structure.(52) Therefore, some critical parameters of geometric measurements, such as the density of pores, the mean pore size, and the depth of pores, must be considered when designing and fabricating scaffolds.

- Processability

Hardware compatibility and customized design and production suitable for individualized needs are highly valued.(53) Furthermore, in order to be accessible to clinical application and the medical market, reproducibility is also crucial for engineered constructs.

1.2.3.2 Materials

- Natural polymeric materials

Natural polymeric materials that is capable to be applied to form cartilage engineering scaffolds include fibrin, collagen, alginate, chitosan, chondroitin sulfate, hydroxyapatite, and hyaluronic acid.(49) Many natural polymeric materials can be extracted from biological tissues, with excellent biocompatibility. It is degradable by absorption or metabolization.(54) However, the degradation rate of most natural materials is difficult to control, and the mechanical strength is low.

- Synthetic polymeric materials

Specific subtype of candidate material can be either selected from the pool of synthetic polymers or modified to cover a range of potential advantages such as excellent biocompatibility and mechanical strength, a controllable degradation rate and a good shaping effect, Different needs can be met by adjusting the polymer proportions and relative molecular quantities. (55) Synthetic polymeric materials commonly applied in cartilage tissue engineering include polycaprolactone (PCL), polylactic acid (PLA), polymethyl acetate (PGA), and poly lactic-co-glycolic acid (PLGA).

- Polycaprolactone

As a type of synthetic polymer material, PCL is a semicrystalline, linear polymer characterized by, high porosity, biodegradablity, nontoxicity and good flexibility but poor hydrophilicity. The low degradation rate of PCL has been used in the repair of bone over a long regeneration time and allows PCL to function as a scaffold for a long time.(56) Thus, PCL is one of the ideal candidate materials for fabricating bioscaffolds and implants for cartilage engineering.

1.2.3.3 Manufacturing

With the continuous development of new materials, the core challenges faced in cartilage scaffold research began to shift toward the scaffold structure and preparation process. The aperture and 3D spatial structure of a scaffold are critical factors for cell proliferation, differentiation, and ECM formation during cartilage regeneration.(57) Among them, a porosity ranging from 250-500 μm can not only provide better proliferative conditions and facilitate ECM secretion but can also work as fabricated inner-structure formed by channels which are conducive to the transport of nutrients and gas exchange and impose a beneficial impact on cell proliferation, adhesion and migration, Finally, nutrients can be obtained through synovial fluid or perichondrium more efficiently as potential space is provided by the porous structure (58)

- Conventional manufacturing approach

Porous biodegradable scaffolds can be built up using traditional manufacturing approaches, such as gas foaming, particle leaching freeze-drying, and template approaches. The primary mechanism of the foaming approach is to induce the production of an inert gas (carbon dioxide or nitrogen) in the precursor solution. The resulting gas is mixed in a liquid and converted into a foam body, and then the temperature is lowered to stabilize the foam, resulting in the preparation of a porous scaffold.(59) With collagen as the scaffold substrate, porous scaffolds can be prepared by the foaming method, and glutaraldehyde can be applied as a crosslinking agent for stabilizing and adjusting the mechanical properties of the scaffold. The foaming method yields scaffolds with excellent biocompatibility and suitable porosity to meet the

adhesion and growth requirements of stem cells.(58) However, it is worth noting that although the foaming method shows some superiority in biocompatibility and scaffold porosity, the biomechanical strength of the resulting scaffolds is not satisfactory, which also limits further application of the foaming method in the preparation of porous scaffolds.(60) The particle filtration, freeze-drying and template methods are limited in the precise control of pore structure and connectivity of scaffolds, and the organic solvents used for preparation of bioscaffold may be harmful to cell growth; furthermore, the structure of human cartilage is complicated, so there are still issues regarding fabricating scaffolds via these conventional methods.(61)

- 3D fabricated scaffolds

As source of inputs for 3D printing are mainly from computer-aided design (CAD) 3D model or clinical computed tomography (CT)/magnetic resonance imaging (MRI) data;(64) This emerged technology can be used to accurately customize the shape and size of the implant to meet specific needs. In addition, for bioscaffold preparation, the ink used in 3D printing is the scaffold material, and in the process of slice-by-slice modeling, the pore structure of each layer can be adjusted by the thickness, spacing, and arrangement of the filaments to achieve the purpose of using different materials to print different structures for in vitro or in situ scaffolds.(65) The scaffold material prepared by 3D printing technology is not only controllable in its shape, internal pore structure, size, and distribution but is also easy to adjust, and the combinations of scaffold materials can be varied to simulate cartilage tissue formation in terms of both geometric arrangement and biological composition.(66) Therefore, its clinical significance is remarkable to use 3D printing techniques to study manufactured scaffolds with stable spatial structures, excellent mechanical properties, and biocompatibility for application in cartilage engineering.

1.3 Additive Manufacturing (AM)

Additive manufacturing alias 3D printing or direct digital manufacturing. Compared to traditional industrial manufacturing, products are not manufactured by hand or lathe; additive manufacturing uses laminated manufacturing technology to make products.(67) Its essential printing process is roughly divided into the following steps: first, CAD and other computer software programs are used to build a 3D model of the product, or 3D scanners are used to directly obtain 3D data to generate a 3D models of the item; then, the model is translated into a Standard Tessellation Language (STL) file, which is sent to a computer-aided manufacturing (CAM) system for processing. The prototype is then constructed according to the material used and the printing instructions of the model. The finished product also needs to be polished after being printed to make the surface smoother.(68) Its three major components: hardware, software and materials are introduced respectively as below.

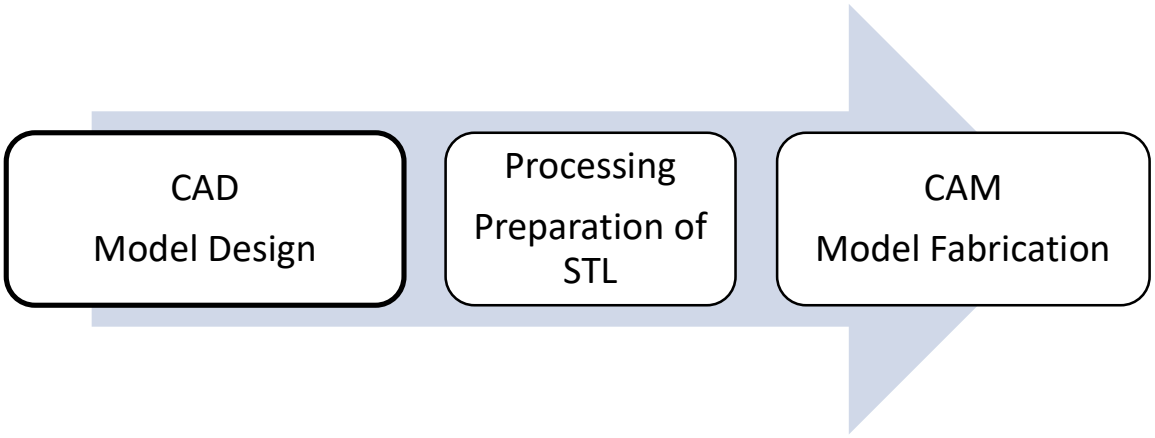

Figure 3. Workflow of additive manufacturing

1.3.1 Hardware

Currently, in terms of the operating mechanism and the range of compatible materials, as the hardware for additive manufacturing, 3D printers can be mainly classified into several categories: stereolithography (SLA), selective laser sintering (SLS), and fused deposition modeling (FDM).

1.3.1.1 Stereolithography (SLA)

This technology is used to apply photosensitive resin as raw material. Photosensitive resin is generally liquid and sensitive to a certain wavelength of ultraviolet light (normally from 250 nm to 400 nm). Immediately under exposure, a polymerization reaction and curing occur. Before printing in the resin tank filled with liquid photosensitive resin, a lifting table is set at the height of the next cross-section layer of the liquid surface; the focused laser beam under computer control scans along the liquid surface, and the scanned area resin is cured to obtain a sheet of resin of the cross-section. Liquid resin is exposed to light again and scanned and cured again, and these steps are repeated until the entire product is formed.(69) After one layer of curing is completed, a close distance is moved under the platform, and then liquid resin is applied superficially to the previous cured resin until a three-dimensional solid model is obtained. With a fast forming speed and a high degree of automation, this process is ideal for fabricating complex shapes with smooth surfaces. However, the quality of printouts also relay on the complexity of this hardware.

1.3.1.2 Selective laser sintering (SLS)

SLS is to prelay a layer of powder (metal powder or nonmetallic powder) on the platform. A laser under the control of a computer sinters the substantial part of the powder according to the interface contour information, and with continuous circulation, layers of molding accumulate.(70) This method has a simple manufacturing process, wide material selection range, low cost, and fast molding speed and is mainly used in the field of industry to make rapid molds directly.(71)

1.3.1.3 Fused deposition modeling (FDM)

FDM is to heat and melt a filamentous material, while the three-dimensional nozzle, under the control of a computer, selectively coats the material on the workbench according to the section contour information before being quickly cooled to form a section.(72) Following the completion of the first layer fabrication, the machine workbench drops to a height (that is, the layered thickness) and then build up the next layer, the entire model will be formed by repeating this flow. For this process, the molding material type is many, the molding part strength is high, and the precision is high; however, this process mainly applies to the molding of small plastic parts.(73)

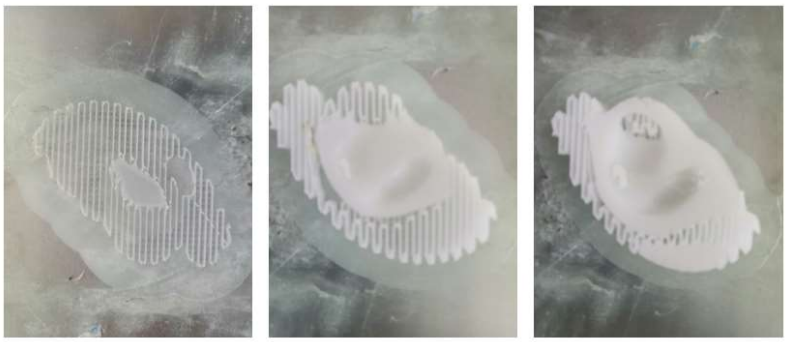

Figure 4. Layer-by-layer style additive manufacturing process of FDM 3D printer-Ultimaker

- Ultimaker 2+

As one of its representatives, we currently work with Ultimaker 2, a white, plastic FDM 3D printer. Its build size is 223 × 223 × 205mm. While its printing resolution could be adjusted between 600 microns and 20 microns. A flat glass severs as a print bed under appropriate heating temperature for adhesion of printouts. By assembling with shaft, both print bed and extruder could move along Z axis on vertical plane and along X,Y axis on horizontal plane respectively (74)

1.3.2 Software

Software for 3D printing are mainly used for the preparation of input information as model and processed command to deliver to the hardware. Several domains are classified to meet different purposes: CAD software is for model design, Medical imaging extraction is for obtaining and processing the anatomy area of interest, Slicer software is to slice selected model and generating G-code which is a universal language that can be identified by 3d printers.

1.3.2.1 CAD software

- Tinkercad

Tinkercad is a free, user-friendly, online platform for 3D design, with a collection of tools covering most essential functions. It is ideal for drafting and creating a model from scratch as an introduction to AutoCAD and other advanced CAD software.(75)

- AutoCAD

AutoCAD, a commercial CAD software developed by Autodesk that integrates advanced toolsets and updated extensions, could be used to address more complicated tasks, such as smoothing, meshing and other advanced operations with a specific purpose.(76) Thus, it is an ideal platform for making fine adjustments for designed models.

- Microsoft 3D Viewer

Microsoft 3D Viewer is a 3D object viewer included in the Windows 10 ecosystem, with high compatibility with both upstream software for input and downstream software for output. It is a suitable candidate terminal for evaluating and presenting designed models.(77)

1.3.2.2 Medical imaging data extraction

- Materialise Mimics

Materialise Mimics is an image processing software for 3D modeling, and it is mainly used for creating 3D designs in STL format from 2D medical images, such as CT, micro-CT, and MRI scans, in Digital Imaging and Communications in Medicine (DICOM) format by segmentation methods.

- Materialise 3-matic

Materialise 3-matic is a postprocessing software for smoothing and modifying the extracted design output by topology optimization methods. All important complex structures are kept during the entire process since work directly affects the triangulated surface.

1.3.2.3 Slicing and printer control software

- Cura

Cura is software for slicing the upstream CAD model to prepare for downstream 3D fabrication: slicing divides the model into multiple layers and then sends these 'instructions' to the printer, which then creates the object layer by layer.(78) Printer control is realized by modifying parameters in the interactive interface in Cura, which are sent in code to the printer as part of the STL file.(79) Basic settings of the AM process can be controlled, and the settings can be modified to meet a variety of needs.

1.3.3 Materials used in 3D printing/Filaments

PLA is a polyester consisting of lactic acid units that is odorless, low-warp, ecofriendly biodegradable and easy to print.(80)

Acrylonitrile-butadiene-styrene (ABS) is a copolymer with high toughness and impact resistance. It is a thermoplastic composed of butadiene, styrene, and acrylonitrile at different proportions. As a standard material compatible with the Ultimaker 2+, it is durable and stable over a broad range of temperatures.(81)

PCL, a biodegradable polymer that tends to start to melt at low temperatures, has the potential to be used in bioabsorbable implants and scaffolds because degradation occurs through the hydrolysis of its ester bonds in the human physiological microenvironment.(82)

It is also similar to the synthetic implant material Medpor-porous polyethylene, which has been widely applied for plastic surgery in clinics.

Filament material	Properties	Application	Printing temp	Strength	Flexibility	Ease of printing
PLA	Easy to print	Prototypes	180-210°C	Medium	Medium	High
ABS	Strong and durable	End-use parts and casings	230-250°C	High	Low	Medium
PCL	Safe, nontoxic and biodegradable	Medical implantation	80-160°C	Low	High	Low

Table 1. Comparison of properties of three types of filament materials.

2 Experimental Approaches

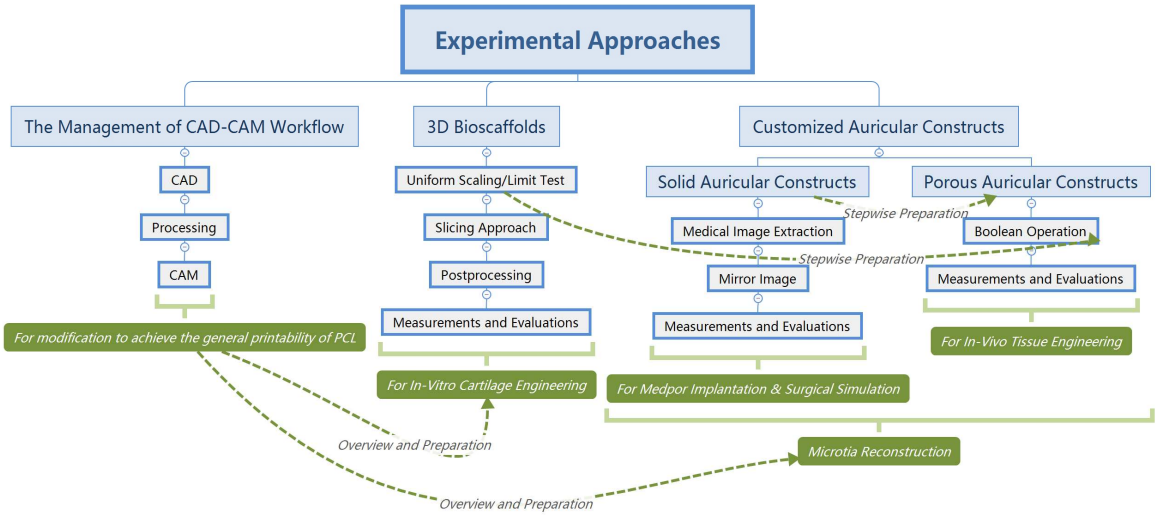

Figure 5. Roadmap for experimental approaches

2.1 Gaps and Implications

2.1.1 The printability of PCL: Management of CAD-CAM workflow

As a low-cost 3d printer, Ultimaker 2+ is not compatible with PCL in default settings, This gap can potentially be filled by modifying settings in through management of CAD-CAM workflow to achieve its general printability with PCL.

2.1.2 Cartilage engineering: Customized 3d PCL bioscaffolds

Regarding material properties, the material, as a building block for the production of a scaffold, must be biocompatible to execute function and avoid adverse reaction for biorecognition and must allow cell adhesion.

Regarding scaffold characteristics, the geometry of the architecture influences nutrient transfer, cell adhesion, and cellular interactions through the pore distribution, surface area, and porosity.

Thus, a customized 3d geometric structure of PCL bioscaffolds is called for cartilage engineering.

2.1.3 For microtia reconstruction：Customized auricular constructs

2.1.3.1 For improving conventional approaches: Solid auricular constructs

While traditional Medpor implants can only fit individual patient's need by modification through subtractive process such as contouring with scalpel and other manual tools. The gap as less flexibility of customization could be potentially filled by applying additive manufacturing to fabricate customized solid auricular constructs substitute.

Simulating the complex 3D framework of the auricle by carving costal cartilage requires significant cumulative surgical experience to meet the patient's customized needs. While its traditional reference for this procedure is a 2D drawing based on the normal side of auricle, it cannot reflect its detailed three-dimensional spatial structure. Thus, a mirrored solid auricle construct from customized CAD-CAM workflow is called for surgical simulation.

2.1.3.2 For developing tissue engineering approach: Porous auricular constructs

Despite the requirements for in-vitro cartilage engineering, regarding in-vivo engineering for the regeneration of auricle, the candidate scaffold should also take the form of complex anatomical shapes to mimic the general contour in macroscopic view while maintain the porous structure in micro view. This gap could be potentially solved by additively fabricating PCL porous auricular constructs through CAD-CAM workflow.

2.2 Roadmap for experiments and hypothesis

2.2.1 The management of CAD-CAM workflow

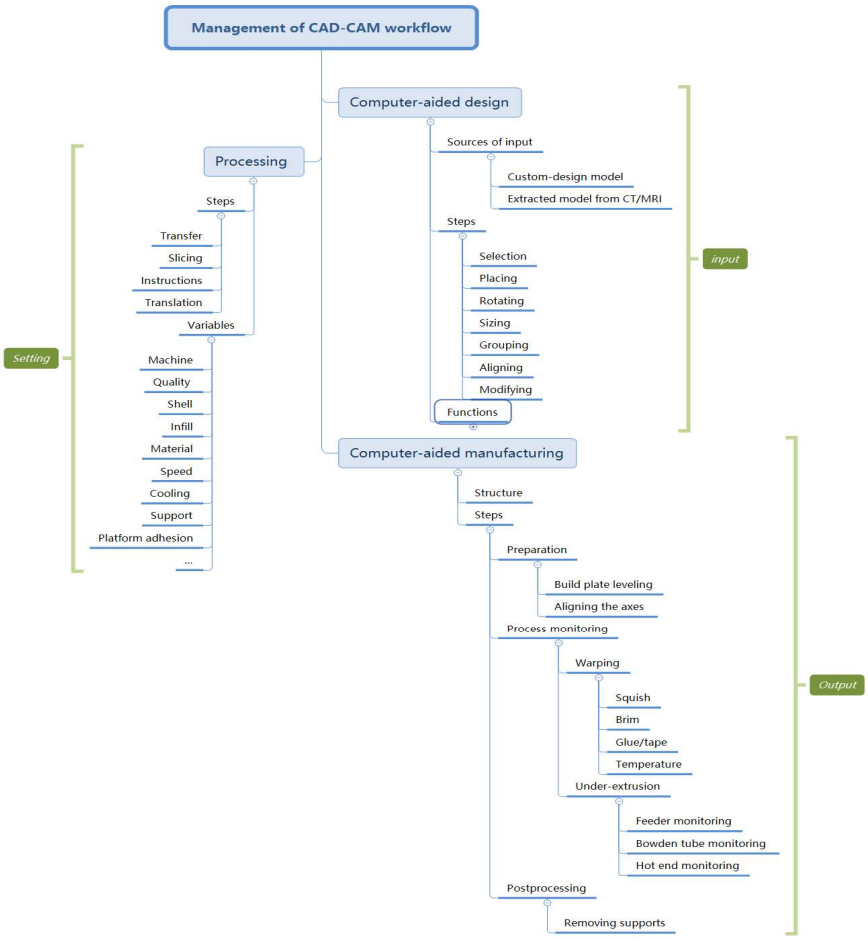

Figure 6. Roadmap for the management of CAD-CAM workflow

To get started for this workflow, a 3D model constructed by computer-aided design was required as an input resource; this model could be either a custom-designed construct or an extracted model based on scanned data such as CT. Through a series of steps, such as selection, grouping and aligning etc. A customized model could be fabricated in the design software to fit individual need. The function of computer-aided design include customization, evaluation, reflection of medical scans, and cost-effectiveness as a preparation for additive manufacturing

Then, the target model was transferred into Cura, open-source slicing software, for processing. After steps regarding modification on the control panel and profile of printing settings, instructions were given through information from parameters of some important variables: such as quality, shell, infill, cooling and other domains were adjusted to fit the need for achieving general printability with PCL, the design was then translated into G-code-the programming language to tell printer how to move and extrude as an instruction throughout the entire print process. The design was transferred to the hardware for manufacturing.

Based on the description of its mechanical structure, several threshold steps such as preparation, process monitoring and postprocessing were illustrated for trouble shooting regarding manufacturing with PCL and other reference material. The hardware then manufactures the object with thin layers slice by slice, the feeder supplies plastic filaments which were then extruded on to the build plate after being melted in the hot end of the print head. Through this layer-by-layer manufacturing process, the final models were printed.

Logically, this whole section was also regarded as general preparation and overview for following sections that would be expected to follow this workflow as repeated cycle.

2.2.1.1 Hypothesis 1

The management of CAD-CAM workflow was served as the effective preparation and uniform overview regarding the fabrication of printouts for both bioscaffolds and customized auricular constructs, its purpose is to modify and identify the general printability of PCL with Ultimaker 2+.

2.2.2 3D Bioscaffolds

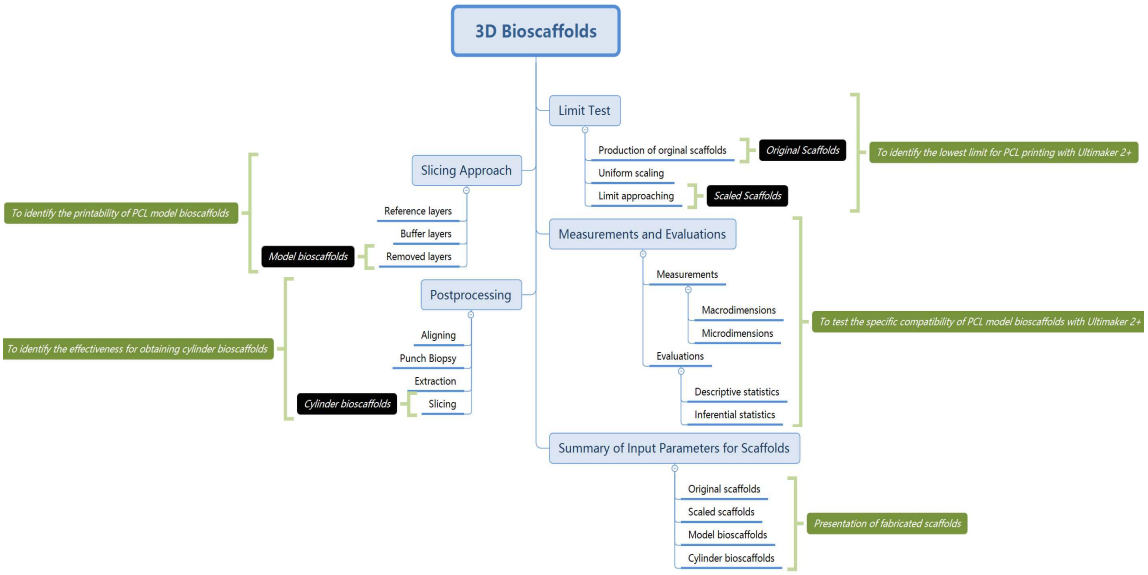

Figure 7. Roadmap for fabrication of 3D bioscaffolds

This process starts from the production of original scaffolds by customized design, then followed by uniform scaling and limit approaching to test the lowest limit for the Ultimaker 2+ with PCL and obtain the scaled scaffolds to work on. Logically, this limit test imbed in this section also serves as stepwise preparation for determining the pore size for porous auricular constructs in the following chapter. Slicing approach is performed by calculating reference, buffer and removed layers in order to achieve the model bioscaffolds for measurements and evaluations (n=9 for PCL, PLA and ABS). Finally, postprocessing was performed through steps such as aligning, punch biopsy, extraction and slicing to obtain the cylinder bioscaffolds. To conclude this, a summary for parameters for each kind of scaffolds were described.

2.2.2.1 Hypothesis 2-1

Limit test was performed to approach and identify the lowest limit for PCL printing with Ultimaker 2+.

2.2.2.2 Hypothesis 2-2

To test the printing accuracy and specific compatibility of PCL model bioscaffolds with Ultimaker 2+. Which could further indicate its potential application as in-vitro cartilage engineering for cartilage defects.

2.2.2.3 Hypothesis 2-3

Postprocessing was performed to determine the effectiveness of the systematic approach to manually obtain cylinder bioscaffolds.

2.2.3 Customized Auricular Constructs

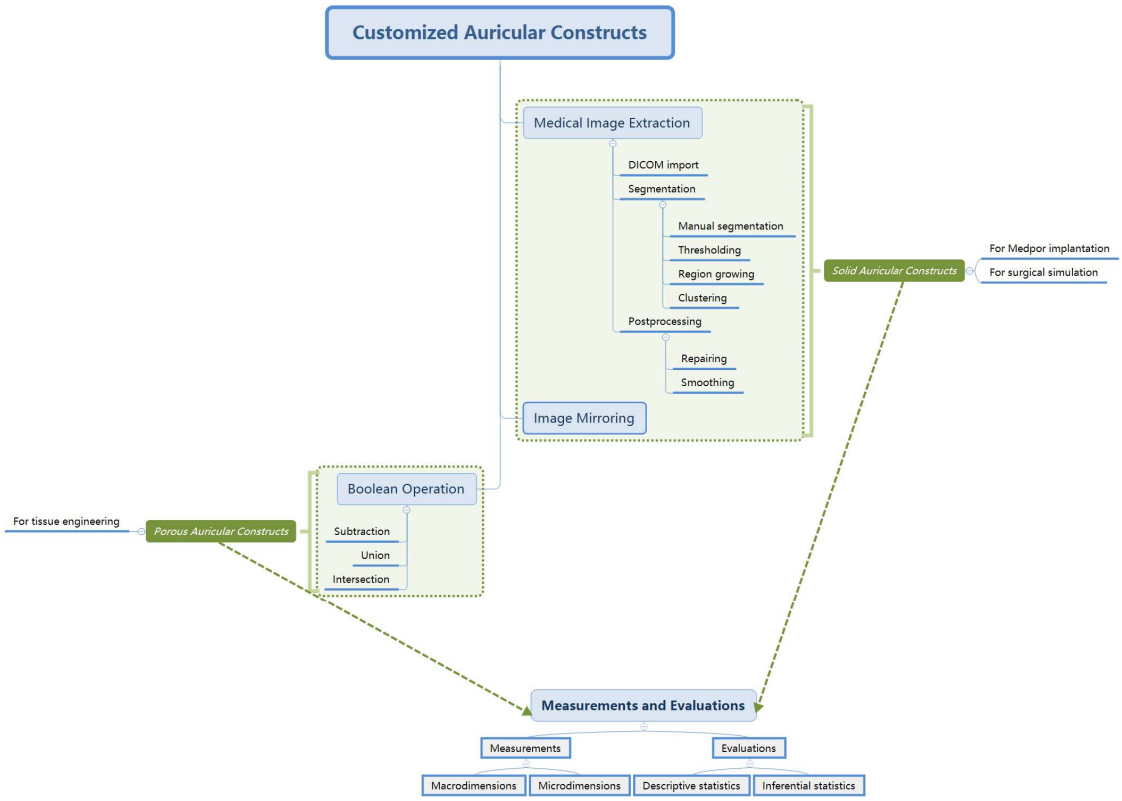

Figure 8. Roadmap for fabrication of customized auricular constructs

For the fabrication customized auricular constructs, the raw data were first extracted from CT images: By importing DICOM file, a series of segmentation methods were applied for extraction of model such as manual segmentation, thresholding, region growing and clustering, then followed by postprocessing through repairing and smoothing to remove potential noise. Image mirroring was applied to the gain symmetric model to simulate the repair of a unilateral defect. Solid auricular constructs have been fabricated by following the steps described above. Logically, it also serves as the stepwise preparation for porous auricular constructs below: As

several instructions from boolean operations (subtraction, union and intersection) were applied to the solid auricular construct to create a mesh with a uniform pore distribution, Porous auricular constructs were fabricated. Measurements and evaluations for types of constructs were performed to test the printing accuracy and compatibility of PCL with Ultimaker 2+ for printing both solid auricular constructs(n=5 for PCL, PLA and ABS) and porous auricular constructs(n=5 for PCL, PLA and ABS).

2.2.3.1 Hypothesis 3−1

To test the printing accuracy and specific compatibility of PCL solid auricular constructs. Which might further indicate its potential application as Medpor implantation and surgical simulation for microtia reconstruction.

2.2.3.2 Hypothesis 3-2

To test the printing accuracy and specific compatibility of PCL solid auricular constructs. Which might further indicate it potential application as in-situ tissue engineering for microtia reconstruction.

3 Materials and Methods

3.1 Materials

3.1.1 3D Fabrication

The materials for the model design and fabrication (CAD-CAM workflow) include three major elements: hardware, software and filaments.

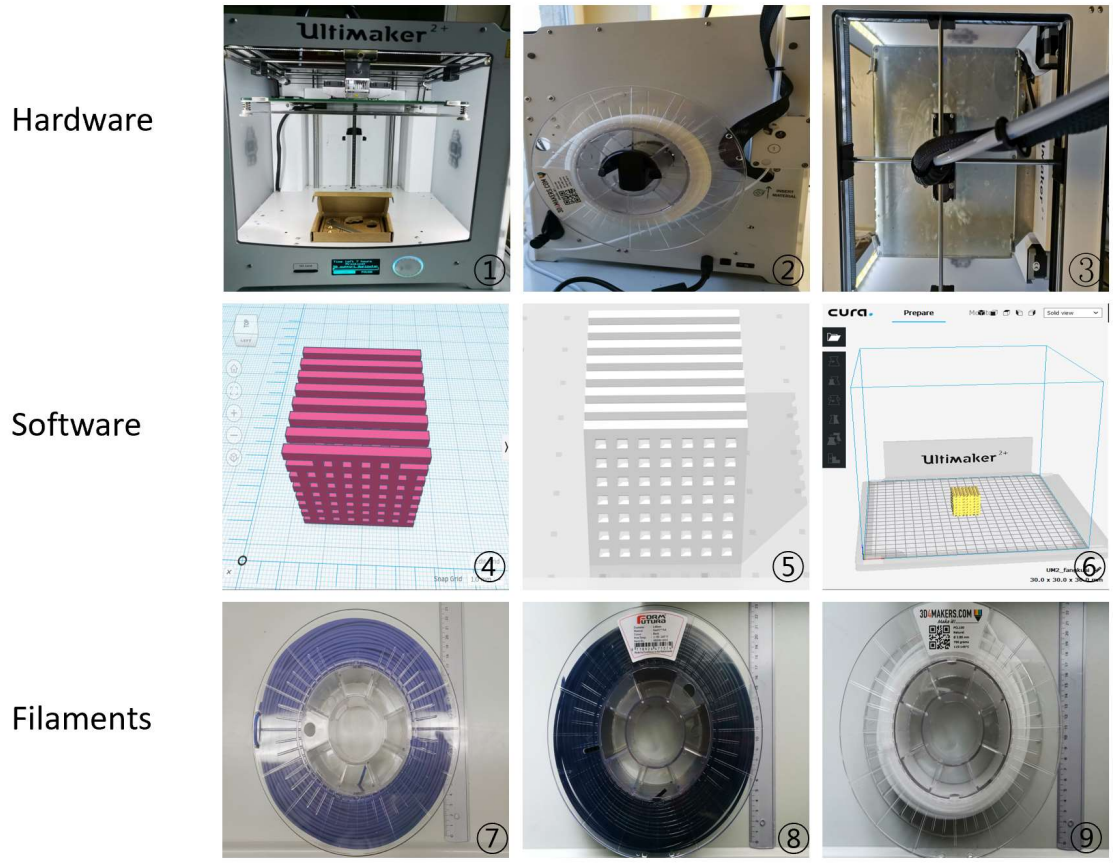

Figure 9. Presentation of materials for 3D fabrication.

1-3: Hardware: front, back and top views of the Ultimaker 2 with the Upgrade Extrusion Kit. 4-6: Software: CAD (Tinkercad), evaluation (Microsoft 3D Viewer) and CAM (Cura). 7-9: Filaments: 2.85-mm ABS, PLA, and PCL filaments, respectively.

3.1.1.1 Hardware

The Ultimaker 2 (Ultimaker BV, Utrecht, Netherlands), a relatively economically accessible and user-friendly FDM printer, was used as the hardware unit for 3D fabrication after

upgrading to the Ultimaker 2+ with the installation of an extrusion kit (Ultimaker BV, Utrecht, Netherlands) 1. Interchangeable nozzles of different sizes (0.25, 0.4, 0.6, and 0.8 mm) provide another controllable variable to modify the balance between printing speed and accuracy. 2. The geared feeder was equipped to increase reliability and customize the correct pressure to potentially extend the range of materials compatible with the open-filament system. 3. Optimized airflow was achieved for smoother printing by setting up new fan caps to secure a uniform airflow distribution below the nozzle. More details of the main features of this FDM printer are shown below.

Feature	Parameter	Note
Build volume	8.8 x 8.8 x 12 inches	Physical space to hold printouts during processing
Compatibility of materials	Open-filament system: PLA, ABS, CPE, CPE+, PC, etc.	PCL is potentially compatible by customizing settings
Layer resolution	600 to 20 microns	Balance between faster speed and greater detail can be achieved in this range
Build speed	Up to 24 mm^3/s	How fast the filament can be extruded
Travel speed	Up to 300 mm/s	How fast the print head can move

Table 2. Parameters for the main features of the Ultimaker 2.

Note: Range of resolution was indicated for reference material.

3.1.1.2 Software

The primary tool used for model design is Tinkercad v2.0 (Autodesk, San Rafael, CA, USA), a free online collection of software tools with easy-to-use features. This platform is suitable and was used for building the macrostructure of the scaffold from scratch. AutoCAD 2018 (Autodesk, San Rafael, CA, USA) is the ideal software for creating precise 2D and 3D drawings with excellent geometrical characteristics by modifying complex solid structures, surfaces and mesh objects and is ideal for designing the inner microstructure, such as the size, shape, and arrangement of pores. Microsoft 3D Builder (Windows 10, Version 1703; Microsoft, Redmond, WA, USA) was used to evaluate the general structure and the distribution of the inner connections. The target measurements of the designed standard scaffold were obtained through the built-in measurement system of Microsoft 3D Viewer (Windows 10, Version 1703; Microsoft, Redmond, WA, USA). The STL file was then transferred to the graphical user interface platform Cura 3.6.0 (Ultimaker BV, Utrecht, Netherlands) to adjust the slicing and printing settings. Materialise Mimics 20.0 and its affiliated software Materialise 3-matic 9.0 were used to extract MRI/CT data and postprocess the extracted model, respectively.

Domain	Function	Software
Model design	General structure	Tinkercad
	Delicate substructures	AutoCAD
Model evaluation	Preview and measurements	Microsoft Viewer & Microsoft Builder
Printing control	Slicing and settings	Cura
Model extraction	CT/MRI data extraction	Materialise Mimics
	Postprocessing and smoothing	Remesh 3-matic

Table 3. Summary of the functions of software categories for the workflow

Note: AutoCAD is a more advanced alternative for Thinkercad to design complicated structure.

3.1.1.3 Filaments

	Company	Color	Diameter (Tolerance)	Roundness	Density
ABS	Formfutura, Netherlands	Blue	2.85mm (+/-0.05 mm)	99%	1.05 g/cm3
PLA	Formfutura, Netherlands	Black	2.85mm (+/- 0.05 mm)	99%	1.24 g/cm3
PCL	3D4MAKERS, Netherlands	White	2.85mm (+/- 0.05 mm)	99%	1.1 g/cm3

Table 4. Technical information for filaments

Note: technical information is important because different company might supply same type of filaments with different parameters.

3.1.2 Medical Images

CT images were obtained with approval from the medical ethics committee of Plastic Surgery Hospital, Chinese Academy of Medical Science, Peking Union Medical College (Beijing, China). All measurement data collection was carried out according to the code of ethics with written informed consent from the patient.

3.1.3 Measurements

An electronic vernier caliper (150 mm, Wiha, Schonach, Germany) was used to measure dimensions of both the 3D cell culture scaffold and the auricular construct. An Axio Observer (ZEISS, Oberkochen, Germany) light microscope was used to measure the pore size and other microstructures. With the affiliated software ZEN (ZEISS, Oberkochen, Germany), we could acquire, process and analyse images in multiple dimensions. The predefined measurements in the software design were regarded as the standard measurements for reference.

3.1.4 Statistical Analysis

Descriptive statistics for summary and inferential statistics for comparison were obtained by ANOVA and one-sample t-test using GraphPad Prism 8.01 (GraphPad, San Diego, CA, USA). $P<0.05$ was regarded as statistically significant.

3.2 Methods

3.2.1 CAD-CAM workflow

To start printing, a designed 3D model of purpose is required as an input resource; this model could be either a custom-designed construct or an extracted model based on scanned data (CT/MRI).

Then, the target model is imported into Cura, open-source slicing software, for processing. After modification of the printing settings or other parameters, the design is converted into G-code -the programming language to tell printer how to move and extrude throughout the entire print process.. The design is transferred to the hardware by either inserting a micro-SD card with the G-code file or directly connecting the hardware to the desktop using a USB cable.

The hardware then manufactures the object with thin layers slice by slice. The feeder supplies plastic filaments which are then extruded on to the build plate after being melted in the hot end of the print head. Through this layer-by-layer manufacturing process, the final model is printed.

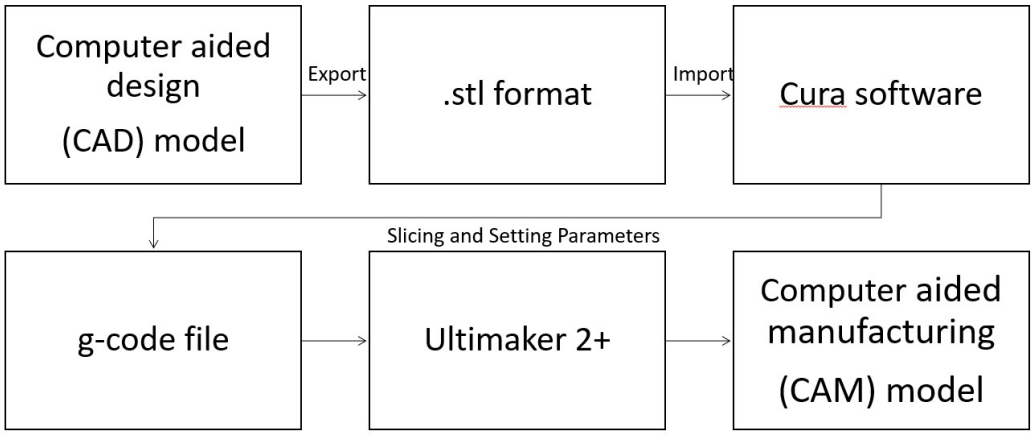

Figure 10. CAD-CAM workflow of Ultimaker 2+

3.2.1.1 CAD

The CAD procedure can be customized for a variety of purposes as the initial input of this workflow. (See presentation of the designs in the respective parts of the results.)

The spectrum of AM has expanded to include many possibilities under the guidance of CAD, and this essential step has several inherent advantages, as follows: 1. Custom models can be tailored to individual needs for size and shape in three dimensions. 2. This type of interactive model can provide real-time feedback for further evaluation. 3. Complex geometries can be easily designed or extracted from real-world scans. 4. Rather than manually removing material, as in traditional subtractive manufacturing, AM with CAD directly and significantly reduces the material costs and required time.

The general procedures for CAD include the following steps:

1. Selection of original shapes for starting the model.

2. Moving and placing the model in the 3D coordinate system.

3. Rotating or spinning the model by specific degrees to achieve specific angles.

4. Sizing the model in particular directions to match the expected measurements.

5. Grouping multiple units into a single model with different parts.

6. Aligning multiple units to achieve a systematic arrangement.

7. Modifying the original model with repeated cycles of adjustment.

3.2.1.2 Processing

Processing plays a critical role in checking and preparing the STL file as G-code ready for printing. As the software for slicing and preparation, Cura not only controls the printing settings but can also be customized by applying additional functions, such as infill patterns and supporting structures for specific purposes.

In Cura, all setting options are presented on the right control panels and are categorized into several domains. To gain access to all sub-settings in more detail, enabling any counterpart of interest in the preference tab is required. Below are explanations of the main domains/variables of the settings, which include the machine, quality, shell, infill, material, speed, cooling, support, and platform adhesion etc.

- Machine

Settings for matching the specific type and version of 3D printer. The nozzle diameter can be selected. For our process, the smallest nozzle, at 0.25 mm, was regarded as the reference size throughout the manufacturing process. This setting has priority compared with settings in the hardware domain, which means that this setting will override the chosen nozzle size on a display panel of the Ultimaker 2+.

- Quality

Settings related to quality of the 3D-printed product. As one of the most modified variables, the layer height refers to the thickness (mm) of the unit layer being printed. Thinner layer height can increase the mechanical accuracy in the Z dimension, to fabricate final construct with a smoother surface. This parameter is indirectly related to the print speed. As accuracy is our primary concern and has a higher priority than time; 10μm, the lowest layer thickness, was selected as the reference setting for our workflow.

- Shell

Settings associated with the external structure. Regarding variables in this domain, the wall thickness indicates the outside wall thickness of the model in the X-Y plane; dividing by another included variable, the wall line width, yields the number of walls. For instance, the wall line width was set as 0.4 mm in this workflow; with a wall thickness of 1.2 mm, and 1.2 mm=n * 0.4, n=3 walls will be printed. In theory, a wall thickness of 3 times the line width is an optimal balance for both accuracy and efficiency. More predefined walls would reduce the quality as too much fill would leak out of the final printed product, forming strings.

- Infill

Settings associated with the internal structure. The infill density refers to the number of filaments used on the inside of the printed product and is presented as a percentage. Another alternative way to adjust the infill density is to set the distance between the patterned units.

For our project, 80% was set as the reference value to offer enough support for our constructs.

- Material

Settings related to the mechanics of filament extrusion. These settings are related to the process in which the filament is pulled back by the feeder to prevent leakage from the printer head during the process of traveling from one target site to another. By enabling retraction in our customized setting, stringing threads that might decrease the potential accuracy of the printed product were prevented, which was required for constructing a clean final model.

- Speed

Settings for the mechanical speed of print carriage along 2D X-Y plane. The extrusion of filaments would also be calculated accordingly. Thus, generally, a higher print speed will decrease the print quality because of the need to increase the temperature for melting the plastic to maintain the extrusion rate. To avoid this unstable balance, 45 mm/s was set as the reference speed for our workflow.

- Cooling

Settings for cooling melted plastic during the printing process. By enabling this option in our setting panel, the fans affiliated with the print head kept working throughout the process, ensuring that the printed material was appropriately cooled before the next layer was printed on top of it. Especially for layers with a short print time and layers with bridges/overhangs, cooling will increase the print quality.

- Support

Settings for adding support structures. As some of our models have a large proportion of empty space or overhanging structures (such as the porous auricular construct), to support these floating parts and prevent collapse of the model, this option is required. On the other hand, postprocessing by manual removal of the supporting structures might be tedious; a way to avoid this is setting the proper orientation of the model to ensure the largest adhesive base area for the construct.

- Platform adhesion

Options for how the model is fixed to the build plate. Brim was chosen for our workflow as it had the best results in preventing warping of the printed product by extending the buffering area of the adhesive base in the corner space.

3.2.1.3 CAM

After the STL file was processed to G-code and exported to the 3D printer through the transfer of data from the micro-SD card, the model could be fabricated under the guidance of the CAD and Cura settings. The model was fabricated slice-by-slice by AM; this approach not only increased the replicability and accuracy of the process but also decreased the cost by preventing

the unnecessary waste of materials, which could be an issue with traditional subtractive manufacturing approaches.

- Structure of the Ultimaker 2+

  - Print head: The unit mainly responsible for filament extrusion.
  - Bowden tube: The tube that holds filaments while they move through.
  - Print head cable: The cable that connects the electronic circuit to the drive print head.
  - Build plate: The glass plate that serves as the surface onto which the product is printed. Clamps are used to secure the X-Y position, while a screw can be adjusted to modify the Z position of this plate.
  - Control button: By physical rotating or pushing this button, actions to guide the behavior of the 3D printer can be selected and confirmed.
  - Display screen: An interactive display through which operators can communicate information to and receive feedback from the Ultimaker 2+.

Figure 11. Front view of the Ultimaker 2+

.

- Teflon (TFN) coupler: The area in which the loaded filaments meet the hot end to be prepared for the process of extrusion.
- Nozzle: Nozzles 0.25, 0.4, 0.6 and 0.8 mm in size can be interchanged for different purposes; as our main concern was to achieve the highest accuracy, the 0.25-mm nozzle was chosen as our standard nozzle.
- Fan shroud: The shroud is used to keep the fan from cooling the nozzle, which slows the heating process and results in a temperature error being shown on the display screen. In addition, the bending of the shroud could slow the cooling process.

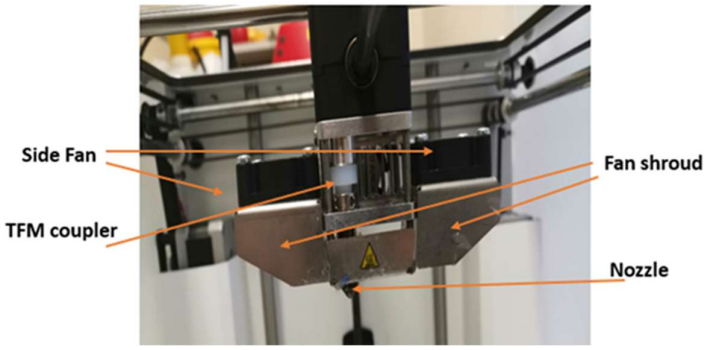

Figure 12. Structure of the printer head

- Spool holder: The hanging structure for holding the spool of filaments; the purpose of this reel design is to help the filaments move in a circular style during loading.
- USB cable socket: By connecting the Ultimaker 2+ with a computer, the Cura file could be updated directly in a real-time manner to monitor and control the behavior of the 3D printer without STL input from a micro-SD card.
- Power cable socket and power switch: Never turn on the power switch before plugging in the power cable.
- Geared feeder: Included in the Extrusion Upgrade Kit, the geared feeder improves the pressure control system and prevents grinding of the material. In addition, the feeder can be adjusted based on the individual requirements of different types of filaments.

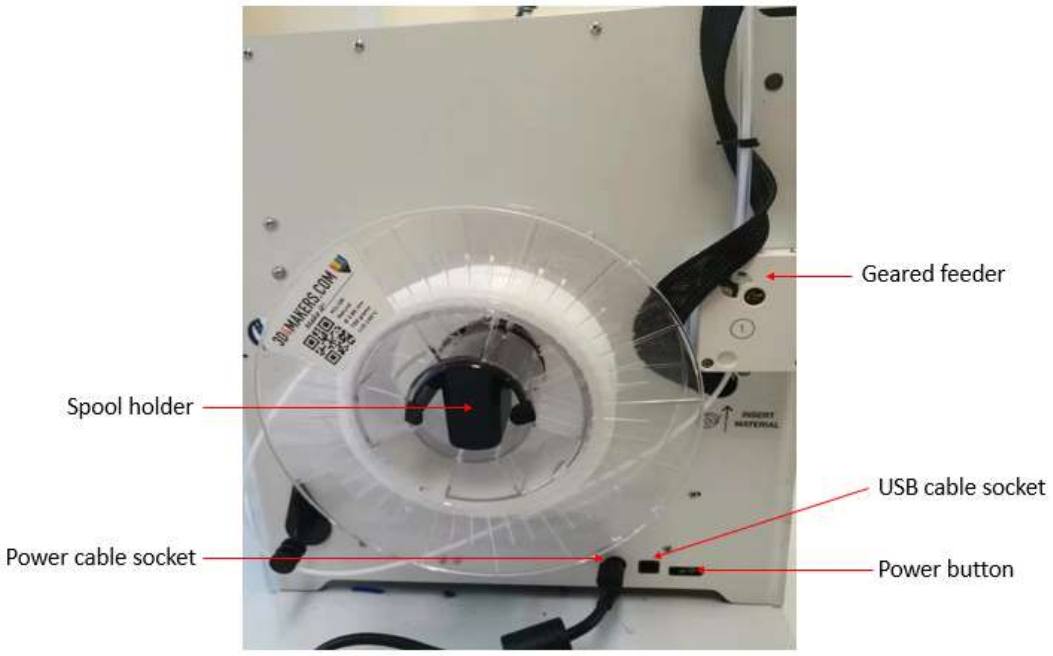

Figure 13. Back view of the Ultimaker 2+

- Threshold steps for AM using the Ultimaker 2+

The main steps for additive manufacturing can be classified into different domains in primary stages of preparation, process monitoring and postprocessing respectively.

- Build plate leveling

Logic: Bed leveling is essential for the uniform placement of plastic filaments and the solid fixation of the bottom of the structure for adhesion to support the whole printed product.

Procedures: On the display screen of the Ultimaker 2+, go to Maintenance > Build Plate. Following the homing step, the print head will locate itself at the back center of the X-Y horizontal plane.

To set the height, continue rotating the button near the display screen until a 1-mm gap between the bed and nozzle is reached. Leveling of the front, left and right of the build plate is achieved by adjusting the screw to modify the Z position of the bed to ensure a 1-mm gap, as mentioned above. A sheet of A4 paper should be applied to measure this distance as the final fine-tuning step; moving it in and out in this gap with little friction serves as proof that the distance between the bed and nozzle is sufficiently small without contact.

- Aligning the axes

Logic: For proper positioning of the printer head during the printing process, it is essential to align the axes to maintain accuracy and precision in the X-Y plane.

Procedures: Apply a 2-mm hex-head screwdriver to loosen the related pulleys to adjust the alignment of the rod; after correctly positioning the rods, retightening the pulleys to complete the general procedures.

For mechanics, the position of the rod is mainly controlled by long horizontal belts. Loosening the pulleys attached to the belts is recommended to free the sliding blocks: the back pulley corresponds to the long right belt, and the front pulley corresponds to the long left belt. After making adjustments by moving the side blocks and measuring the distance to the pulleys on the respective axes, tighten the pulleys to restrict free movement of the side blocks and complete all procedures.

- Warping

Logic: Warping refers to the bending up of an edge corner caused by shrinkage of the expanded plastic during the 3D manufacturing process. The main logic to avoid warping is to prepare a bed for printing with four threshold variables: squish, brim, glue/tape and temperature.

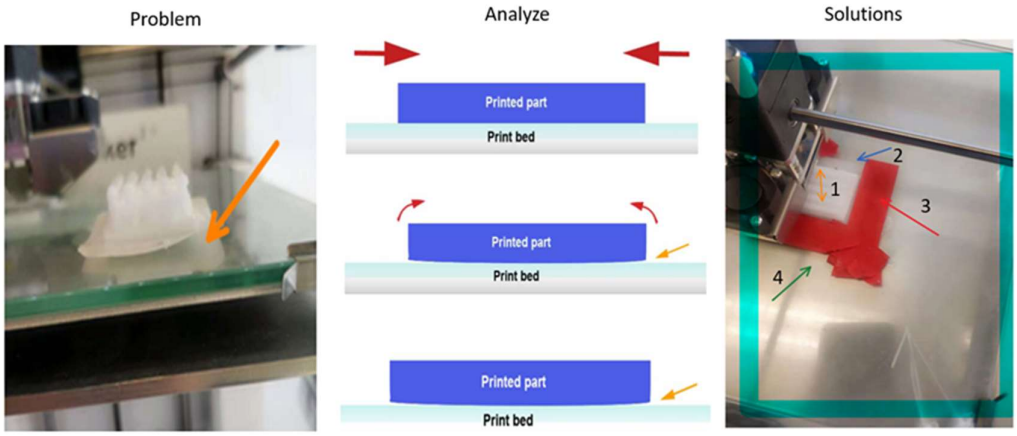

Figure 14. Warping issues and solutions

1. Squish. 2. Brim. 3. Glue/tape. 4. Temperature.

Squish: This variable refers to firmness with which the printed layer is pressed onto the build plate to secure the bonding of the first layer as a solid foundation for the upper layers of the printed product. This is mainly controlled by the distance between the nozzle and the glass bed. If warping occurs during processing, manual releveling is required, and the bottom of the printed product should be monitored and adjusted accordingly.

Brim: This variable refers to the flat area of a single bottom layer surrounding the printed product; this feature could be added in the built-in setting options in Cura. A brim resists the pulling forces exerted during the cooling process and can easily be removed after the completion of manufacturing.

Glue/tape: These can be applied to promote surface adhesion. Glue should be applied evenly on the target area of the plate, while tape should be used on the corner area of objects to create more adhesive surfaces.

Temperature: Heating is required to keep the material under the glass transition temperature to ensure that the extruded filaments remain flat and bind evenly to the glass bed. This can be adjusted on the display of the Ultimaker 2+ by choosing the proper build plate temperature. In addition, cooling should be monitored and controlled for the manufacturing of each layer because excessive cooling will cause concentric contraction of the material. This variable can be modified on the control panel in Cura.

- Under-extrusion

Logic: Under-extrusion refers to a situation in which an appropriate amount of material cannot be supplied for manufacturing. Under-extrusion can be confirmed by the observation of a thin, uneven or missed layer during processing monitoring.

Procedures: The balance between temperature and flow rate must be controlled properly.

Temperature is important; when it is too low, the plastic cannot melt and tends to be more viscous, and when it is too high, clogs can easily form as the properties of the material in the nozzle have changed. An appropriate temperature should be set based on the recommendations on the spool of filament. The temperature can be modified either on the display screen of the Ultimaker 2+ during processing monitoring or on the setting panel in Cura.

The flow rate is defined by the nozzle size, print speed and layer height. A high preset temperature allows a faster flow rate; in contrast, a lower preset temperature leads to a faster flow rate, which could lead to under-extrusion by exceeding the printing capacity and not providing sufficient melted material to meet the volume required for extrusion. The flow rate can be adjusted by modifying the related variables in Cura.

For feeder monitoring: As the source of material, the feeder is potentially responsible for under-extrusion, and this diagnosis can be confirmed by the observation of filaments moving poorly or grinding during the manufacturing process. The tension in the tube should be kept at an appropriate level. If the tension is too low, the feeder will not have sufficient grip, which could be diagnosed when the surface of the material is completely smooth, without any visible marks as proof of an appropriate tension level. If the tension is too high, however, squeezing will occur and produce noise. The tension can be adjusted on the feeder of the Ultimaker 2+ accordingly.

For Bowden tube monitoring: As the next stop for the material, the Bowden tube is another possible source of under-extrusion: Particles resulting from grinding could become stuck in this component, causing friction. In addition, coiled filaments could also produce more friction than their straight counterparts; thus, movement of the spool of filaments should be monitored and adjusted accordingly.

For hot end monitoring: After ruling out previous potential issues, the hot end should be checked, as nozzle blockage is another common cause of improper extrusion. Once confirmed, unclogging is necessary: to do this, the nozzle should be heated up and a needle should be inserted into the nozzle from the bottom. Another alternative is to remove the clog by performing a cold pull from the top after uninstallation of the tube. If these steps failed, then the nozzle must be replaced by unscrewing the old nozzle and attaching a new nozzle to the hot end.

- Removing supports

Logic: Support removal is necessary when the support option is applied in Cura, which would be preconfirmed based on both the geometric design and the orientation of the model on the plate.

Procedures: Start by removing the majority of the supports manually since this is a fresh print and they can simply be pulled off; do this around the printed product, and remove the easily accessible parts. Avoid fragile areas of the product to prevent damage or collapse during this procedure. After general removal, flush cuts should be applied to snip off the rest of these structures; the goal is to separate the supports from the model so that the model can be pulled off as one large unit. Large supports will be out of the way, allowing supports in trickier areas to be removed later. Do not cut too close as this may cause pitting, which might be difficult to remove during sanding. When all main supports have been removed, start sanding away small nubs to smooth the surface. Sand in a circular motion without leaving deep marks; the goal is to blend the nubs into the surface of the product.

3.2.2 3D biocaffolds

In this section of the study, we applied both CAD and CAM to fabricate customized 3D scaffolds for cell culture via a relatively standardized workflow with a low-cost commercial 3D printer, the Ultimaker 2+, and biodegradable PCL filaments (inherently compatible PLA and ABS counterparts were regarded as reference materials). The process was monitored using a limit test, and the measurements of the mold scaffold were evaluated by comparison This work will serve as the foundation for future testing of the candidate scaffolds in cell culture and proliferation.

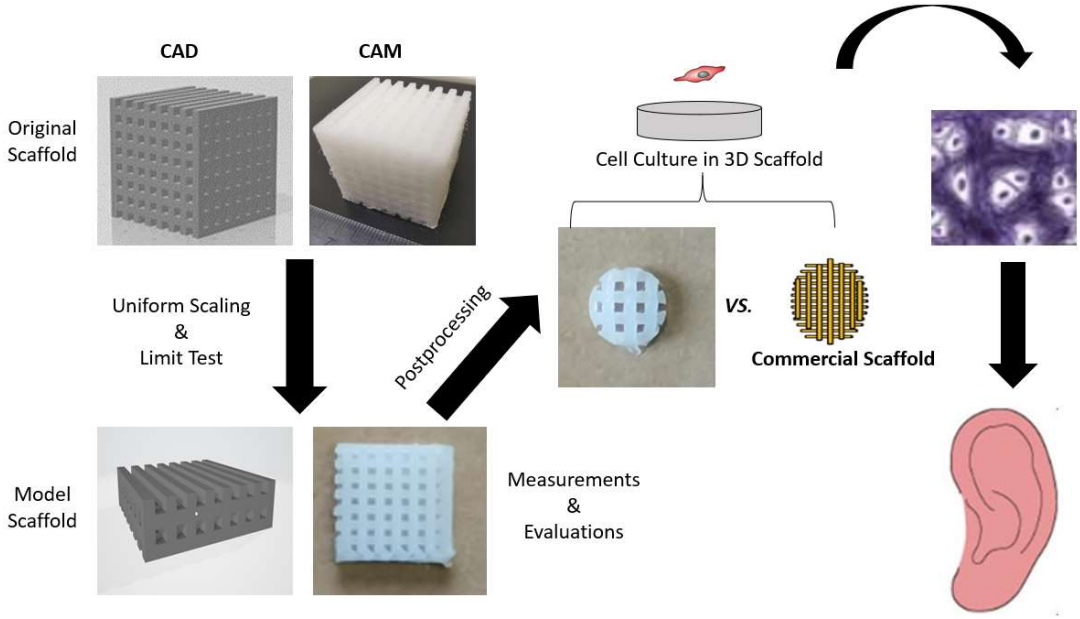

Figure 15. Roadmap for the fabrication of 3D bioscaffolds

Note: Pictures on the left shows the workflow for fabricating and postprocessing bioscaffolds, while the right counterparts indicated further investigation for its potential application for further study.

Uniform scaling was performed to approach and identify lowest limit of PCL scaffold fabricated by Ultimaker 2+.

Measurements and evaluations were conducted to compare the measurements of dimension of PCL with reference material to test its potential compatibility.

Postprocessing was completed by applying punch biopsy to extract cylinder shape scaffold from model scaffold.

3.2.2.1 Limit test

- Production of original scaffolds

1. The procedures for designing the original scaffolds involved the steps below:
2. Select a basic cube shape as the original unit to start with.
3. Place the unit at an appropriate location on the working plane.
4. Modify the cube by changing its dimensions of length, width and height to 30, 2 and 2 mm respectively.
5. Replicate the modified rectangular unit to n=8 units as the basic building materials.
6. Aligning the 8 units in parallel with a 2-mm gap to form a structure serving as the base layer.
7. Replicate this layer to create 15 copies as layer units.
8. Rotate one of these layers by 90 degrees horizontally on the X-Y plane.
9. Place the rotated layer onto the base layer to form a crossed-layer structure.
10. Use this structure consisting of two crossed layers with 16 rectangular units as a unit of the whole structure to form the final original scaffold by repeating the steps 7 times and placing the units onto the base layer one by one accordingly.

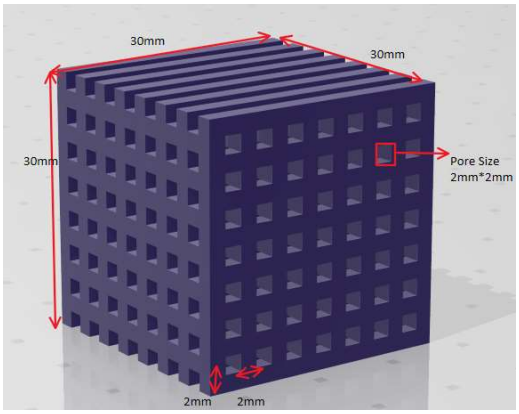

Figure 16. Parameters for design of the original scaffold

Note: As a cubic original scaffold with uniform measurements in each dimension at the same level, it serves specific purpose, as limited dimensions are required to be measured for comparison across dimensions because respective measurements are equal in both macro and micro levels.

- Uniform scaling

A limit test was implemented by uniform scaling, which refers to modification of the size the original scaffold changing the ratios of the dimensions.(Fig. 16) Changing the size of the model without sacrificing either the relative macro (side length of cube) or micro (pore size) structures is an ideal systematic method to approach and determine the lowest limit for the printing process.

The method of uniform scaling was applied for modifying parameters of the target model in each direction while maintaining its original shape. This method could be performed in either

the CAD software by scaling down each unit of measurement (1 mm). A constant ratio could be applied to calculate the expected values of the other dimensions. For instance, if the edge length of the scaffold was changed to 15 mm, then the pore size would shrink down to 2/(30/15)=1 mm because there is no change in the ratio of the dimensions. Thus, the pore size of the 10-mm model would be 2/(30/10)=2/3 mm.

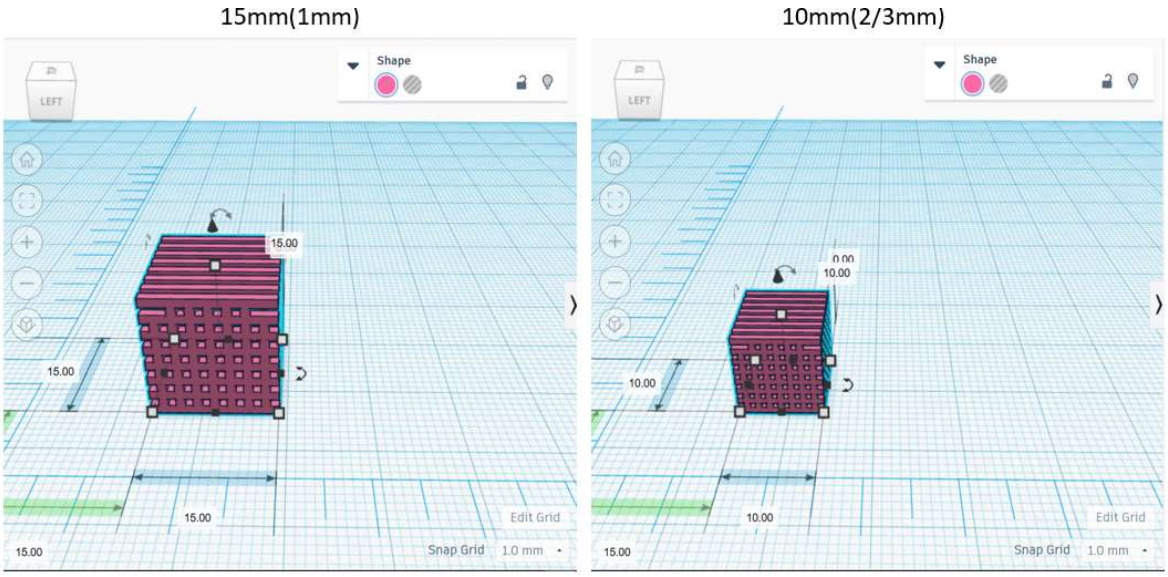

Figure 17. Process and methods for uniform scaling

Note: This is inputs from customized design to simulate the process of uniform scaling. Only two representative scaffolds with specific value were provided as samples for theoretical deduction.

- Limit approaching

To test the print limit of the Ultimaker 2+ with different types of filaments, 15-mm cubic scaffolds were scaled down by 1 mm at each step of the uniform scaling process, and the limit was identified if it meets one of the following criterias:

1. Hardware could not fabricate scaffolds appropriately during printing process.
2. The general structure of scaffolds collapsed after printing process.
3. Scaffolds could be sliced by Cura software during printing preparation.

3.2.2.2 Slicing approach

The model scaffolds were designed using the slicing approach which refers to the removal of cross-sectional layers one by one from the simulated final test scaffold, with fifteen layers, to approach the model scaffold, with four layers. Since the 3D cell culture scaffold for comparison had three layers in total, the bottom layer of the model scaffold served as a buffer area to be removed later during postprocessing but was required because the base layer for facilitating adhesion was too slim and difficult to remove after printing. Logically, to remove this default layer physically, an additional layer needed to be added to serve as a buffer area that could be removed later during postprocessing. Nine model scaffolds were designed and fabricated accordingly with each type of filament.

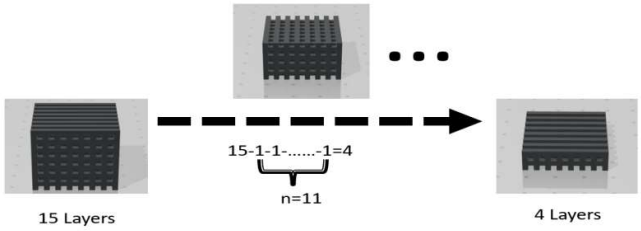

Figure 18. Process and methods for the slicing approach

Note: This describe the logic for calculating the layers needed to removed from scaled scaffolds to fit the needs for both buffering and geometric values from reference conventional scaffolds.

3.2.2.3 Measurement of model scaffolds

- Measurement of the reference model

Standard measurements as a reference for comparison could be acquired using the CAD software. Four dimensions, the edge length, height, width of rectangular unit and pore size, were set as dimensions of interest, as shown in the figure below.

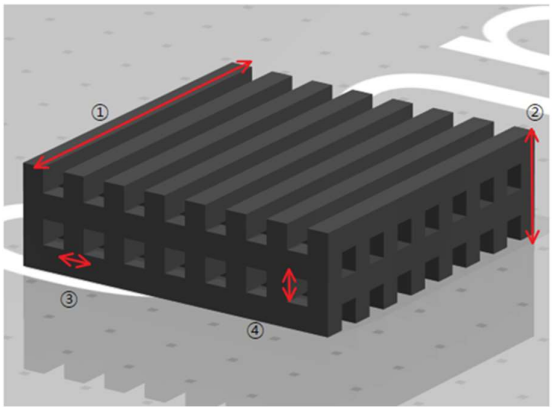

Figure 19. Dimensions of measurement for the model scaffold

① Edge length. ② Height. ③ Width of rectangular unit. ④ Pore size.

- Measurement of the fabricated scaffolds

Scaffolds fabricated using different types of filaments were measured with different methods for the macrostructures and microstructures, as follows:

Macrodimensions: The edge length and height were measured using electronic calipers three times for each dimension for each model scaffold, and then the mean was calculated as the final value for each scaffold.

Microdimensions: The width of the rectangular unit and the pore size were acquired using a built-in measuring tool in the software affiliated with the light microscope. By setting both the

start and end points, a red line of interest was defined according to the dimension of interest to objectively acquire the linear distance as a real measurement.

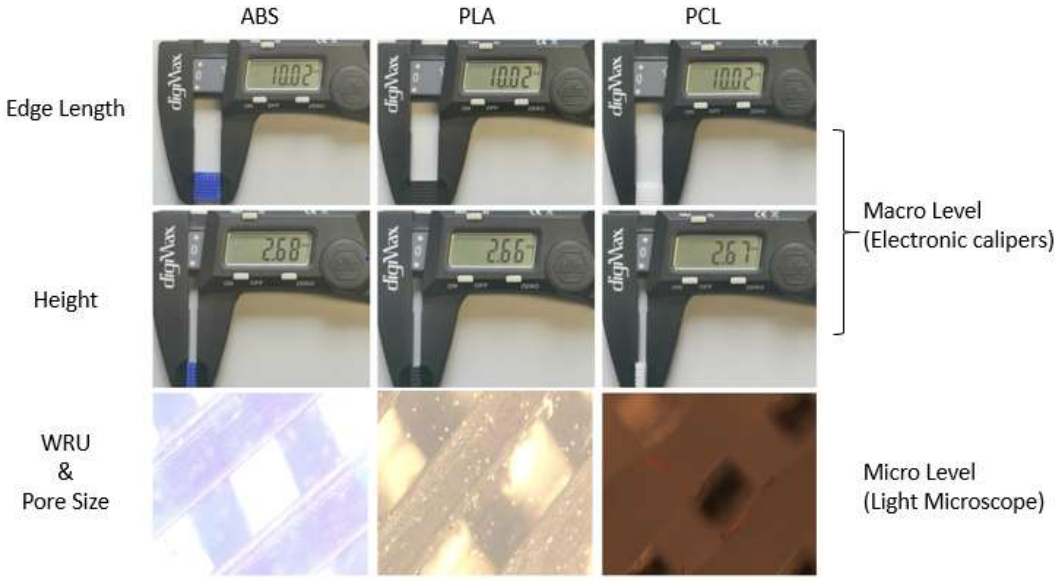

Figure 20. Tools and methods for measuring the model scaffolds

- Evaluation of the model scaffolds

Data were analyzed using GraphPad Prism 8. For descriptive statistics, data are presented as the mean, standard deviation (SD) and sample size. For statistical analysis of the consistency and accuracy of the PCL model scaffold, unpaired one-sample t-tests were performed with standard measurements in software, and one-way ANOVA was performed to compare the three types of materials ABS, PLA, PCL regarding four dimensions. $P<0.05$ was set as the threshold value for statistical significance.

3.2.2.4 Postprocessing

Postprocessing was performed to obtain a cylindrical 3D cell culture scaffold with three crossed layers from a square model scaffold with four layers using a biopsy punch to acquire the target parts and shape.

The general procedure was as follows:

- Mark the center of the square scaffold; this mark should coincide with the center of the circle produced using the biopsy punch.
- Apply the biopsy punch at the correct location of the square model scaffold to acquire the desired cylinder.
- Use a needle to extract the cylinder from the tube of the biopsy punch.
- Apply slicing tools to remove the slim bottom and buffer layers to achieve the final three-layered 3D model for cell culture.

Instead of relying solely on direct 3D fabrication, this indirect 3D printing process merges the CAD-CAM workflow method and the customized postprocessing method described above and

reaches improved accuracy in producing this small cylindrical scaffold with great detail and a delicate shape by avoiding the inconsistent final results of direct 3D printing.Since it is hard to PCL melted filament to follow the round edge of cylinder shape on the track of direct 3D printing method.

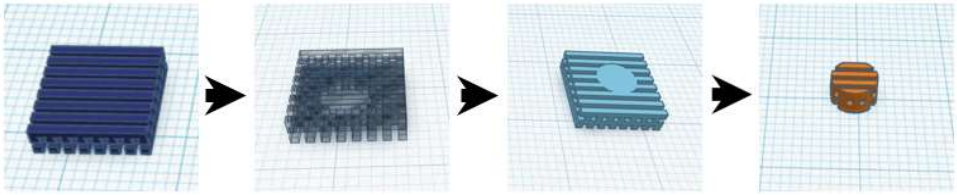

Figure 21. Simulation of postprocessing steps

Note: the is a replication of this method in design software for simulation of punch biopsy on the scaled scaffolds.

It was my workflow/logical outline presented by CAD software as a simulation for our postprocessing method. 1.Started from model scaffold on the left, 2.The center of model scaffold with the center of the round hole of biopsy punch were aligned. 2.By using tube-shaped tool-biopsy punch to obtain the cylinder scaffold. 3.The model scaffold was left with round holes 4.The cylinder scaffold was extracted.

3.2.2.5 Summary

Starting from the design of the original scaffold, which was a cube with an edge length of 30 mm, eight rectangular units in each layer were used to form square pores by rotating adjacent layers with the same design by 90 degrees. Thus, a uniform model was constructed with an equal distribution of pores to serve as the foundation for a series of modification procedures mentioned above.

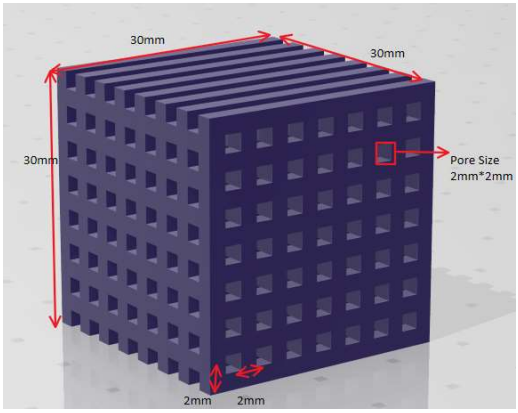

Figure 22. Parameters for design of the original scaffold (Suspended)

Regarding the models obtained after each step of the proceeding methods, the 1st is the original scaffold, the 2nd represents the scaffold with a 10-mm edge length and a 2/3 pore size to reach the lowest limit of fabrication with PCL after the limit test, the 3rd represents the model scaffold with four layers yielded by the slicing approach, and the 4th scaffold represents the final cylindrical scaffold intended for cell culture yielded by postprocessing.

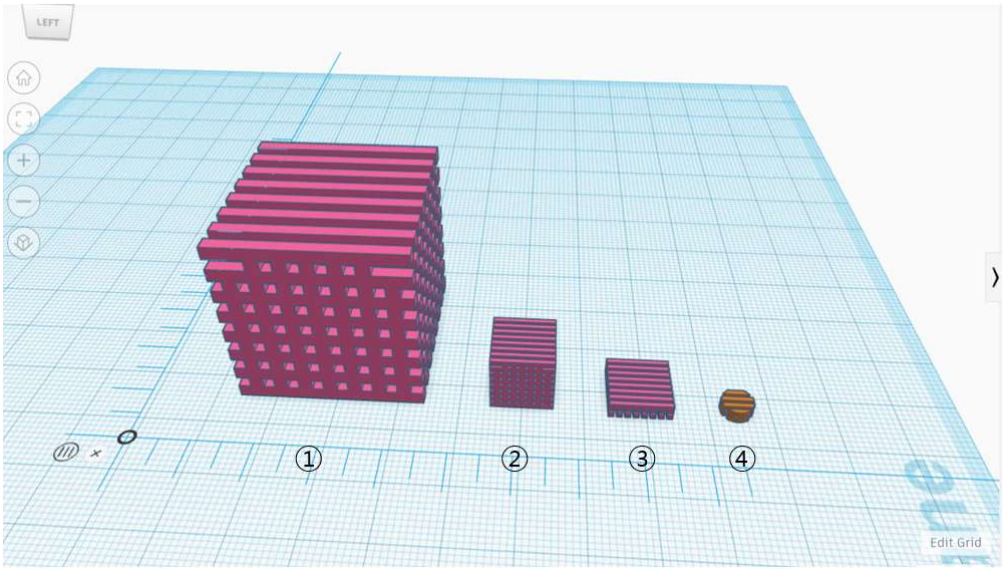

Figure 23. Presentation of the design of all types of scaffolds

Note: This is a presentation in methods sections as input with set parameters in software for simulation and summary.

In terms of all of the parameters, the scaffolds derived from the 1st scaffold should be at a certain scale ratio. The height difference between the 2nd and 3rd scaffolds resulted from the slicing approach applied to remove the top layers and keeping only four layers, while the height difference between the 3rd and 4th scaffolds resulted from the physical slicing performed during the postprocessing procedure. There was also a difference in the edge length/diameter since the diameter of the hole produced by the biopsy punch was 5 mm. However, the pore size of the 2nd, 3rd and 4th scaffolds was the same because all scaffolds were derived from the original scaffold by downscaling the dimensions which were never subsequently modified in the following series of applied methods.

Standard design/ Dimensions (mm)	Original scaffold ①	Scaled scaffold ②	Model bioscaffold ③	Cylinder bioscaffolds ④
Edge length/diameter	30	10	10	5
Height	30	10	3/8	2
Pore size	2	2/3	2/3	2/3

Table 5. Summary of design parameters for all types of scaffolds

Note: These values were pre-set as the parameters for both designing and planning, these values could also be verified by either theoretical calculations or extraction of standard measurements from designing software.

3.2.3 Customized Auricular Constructs

For the fabrication of a customized auricular model and porous auricular model, the raw data were first extracted from CT images by segmentation and then postprocessed by smoothing and wrapping. The final model was mirrored to simulate the repair of a unilateral defect. Boolean operations were applied to the customized solid construct to create a mesh with a uniform pore distribution and fabricate a porous auricular scaffold.

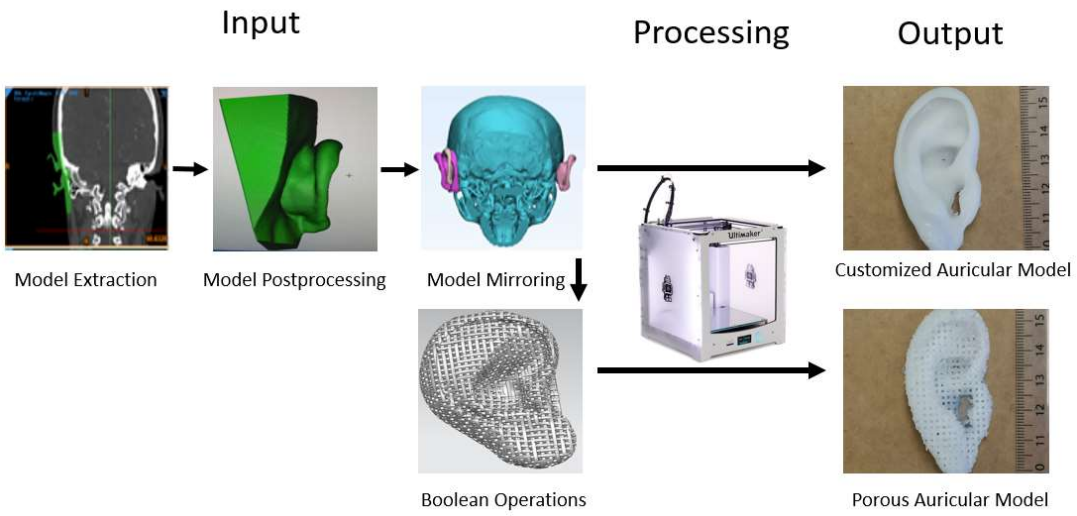

Figure 24. Roadmap of customized porous auricle fabrication.

3.2.3.1 Medical imaging extraction

- DICOM Import

Medical imaging data were acquired from the CT images of a female patient, with anonymization according to the patient's wish, from Plastic Surgery Hospital, Chinese Academy of Medical Science, Peking Union Medical College, Beijing, China. 2)Data were stored in DICOM format, which is for transferring and processing scan data. The file was imported into Materialise Mimics and prepared for subsequent steps for extrapolation. The DICOM data were loaded into the working platform (DICOM > Import > Select data > Load).

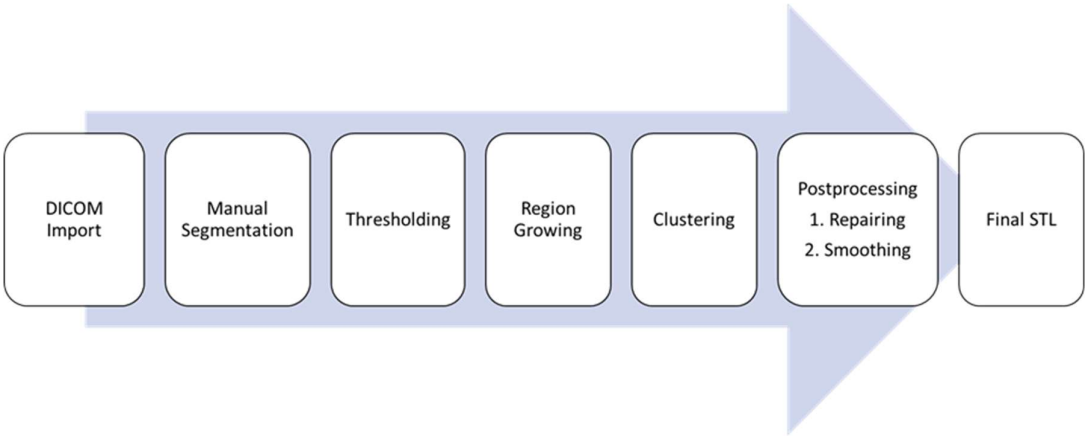

Figure 25. Workflow of medical image extraction and postprocessing.

- Segmentation

As a main step of image processing, segmentation refers to the extraction of the region of interest from the pool of imaging data. By locating objects in each slice, the purpose of this step is to identify the target area formed by gradually accumulated volumetric data slice by slice.

- Manual Segmentation

Manual segmentation refers to the process in which a plastic surgeon specializing in microtia reconstruction segments CT images by hand in a "slice-by slice" manner. The accuracy is related to the image quality.In this study, the boundaries of the ear were identified in general, and a paintbrush tool was applied to draw along the contour, highlighting the region of interest. The purpose is to locate the region of interest from general perspectives.

- Thresholding

The imaging data were divided into separate regions with different ranges of grayscale values. These ranges consisted of peaks and valleys; one peak represents one region, while a valley located between two peaks represents a threshold value used as a cut-off point. Different tissues were defined in different ranges of values surrounded by the boundaries of the threshold. Thus, this method is ideal for extracting the contour shape of a homogeneous aggregation of the same type of tissue.

In this study, a predefined range of grayscale values for soft tissue, the main composition of the auricle, was set as a reference to be applied for this procedure. This effectively converted a grayscale reading to a binary reading under target intensity to represent the tissue for presenting a space of interest by excluding other areas out of this grayscale range. Then, cropping was applied for volume restriction.

The threshold was set as a range from Minimum -700 Hounsfield Unit to Maximum 225 Hounsfield Unit.

- Region growing

The principle of this method is to start from seed points and merge neighboring pixels with similar properties. The surrounding pixels are approached from the initial seed in a progressive way based on the classification criteria. In contrast, the region is separated into subsections if the homogeneity standard is not met. The two mutually interactive variables in this approach are the number of seed points and the homogeneity criterion.

In this study, seed points were positioned at the center of the extracted volume and expanded to fill the space of the region of interest. As the boundaries of the auricle were clearly identified with the removal of potential noise in previous steps, this procedure was ideal for merging neighboring pixels to form an object with a high level of homogeneity.

- Clustering

By classifying target regions into groups with certain features, objects with shared attributes tended to aggregate as a defined cluster. The criteria for supervised clusters can be decided and

customized according to individual needs, while unsupervised clusters can be formed semiautomatically by the system.

In this study, by applying the clustering method, potential noise from areas with different attributes could be excluded to further filter the extracted region of interest and obtain an auricle with more clearly identified edges.

- Postprocessing

For converting a crude 3D construct into a smooth model ready to be printed, a series of procedures for postprocessing and final refinement were conducted.

  - Repairing

Potential errors and discontinuities along the boundaries derived from the previous segmentation method were fixed by filling in gaps and unnecessary anatomical parts, such as the base area for the auricle to attach to the skull and the remaining substructure of the middle ear.

  - Smoothing

Model was refined by applying an automatic global smoothing filter and a local smoothing brush tool to remove step artefacts and unphysiological holes.

3.2.3.2 Image mirroring

The final exported STL file was imported into AutoCAD Design Software, and the constructed model was mirrored to the simulated affected side relative to the facial midsagittal plane defined by several anatomical landmarks, such as the foramen magnum center, external occipital crest, and nasal bone suture. In addition to image mirroring, delineation and restoration were performed on the skull model as a pilot trial to define the relative spatial relationship after removing the simulated affected side. This model was also positioned on the simulated side with an appropriate orientation regarding matching and symmetry. The rear view was set as the reference angle for visual evaluation as a potential prospect for future surgical planning in reality

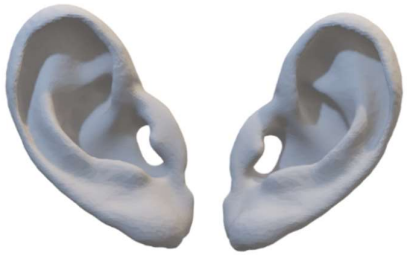

Figure 26. Mirror image simulation

3.2.3.3 Boolean operations

Boolean operations are advanced 3D modeling methods used to create uniform features, such as holes, which could mimic the distribution of pores in our complex auricular model in a more consistent and systematic manner.

In fact, in AutoCAD software, this is one of the few ways to produce an empty space in a solid model. Interactions with each unit during our design procedure are also necessary. The three Boolean operations are union, subtraction, and intersection algorithms.

Union: It combines two units into one object.

Subtraction: It removes the volume of one object from another to create hollow structure.

Intersection: It obtains the interference area by removing the areas outside of the intersection.

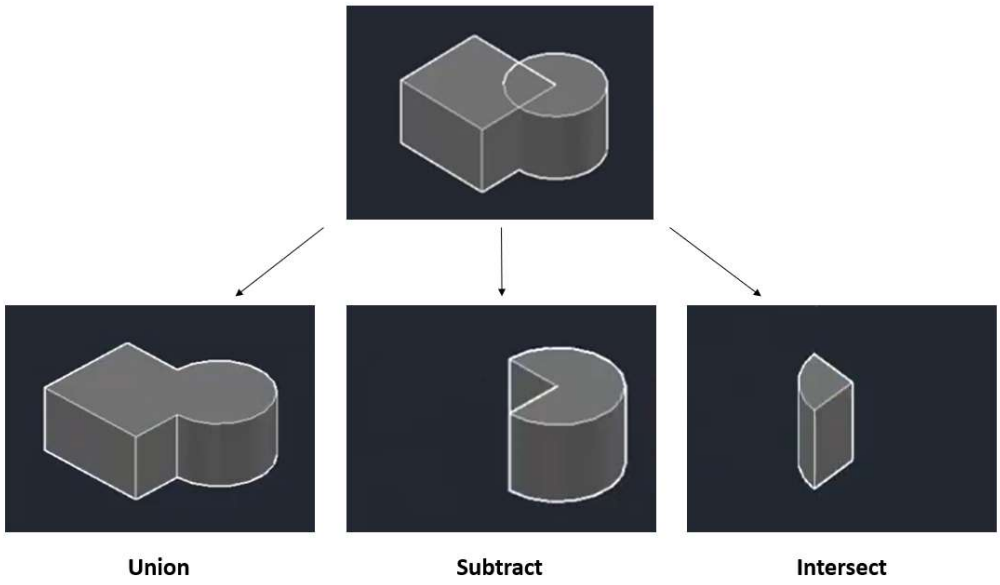

Figure 27. Simulation of Boolean operations

Steps in AutoCAD:

Start with two separate entities attached to each other physically as cube and cylinder with shared area shown above.

- Union

The process of fusing regions and objects into one entity.

Steps: Clicked “Solid” tab => Clicked “Union” panel => Clicked on the first object and press ctrl to select second object => Pressed “Enter” after selection is complete => two separate entities were fused and are reflected as one entity.

Steps: Press “Enter” after selecting both objects (when the cube and cylinder become dashed). Both objects become fused and are reflected as one entity by continuing to move the objects

until they move as one. The whole process is cleaner if different colors are used to represent each object.

- Subtraction

The process of subtracting one object from another to create shape of interest.

Steps: Clicked “Solid” tab => Clicked “Subtract” panel => Select cylinder and press “Enter” to retain this geometry => Select cube and press “Enter” to subtract this geometry => The cross area was removed from the cylinder.

- Intersection

The process of creating a new shape from the overlapping regions of two or more objects..

Steps: Select the two objects, and press “Enter”. The intersection operation is performed, and the overlapping region is extracted

Intersection: The process of creating a new shape from common portion shared by two or more objects.

Steps: Clicked “Solid” tab => Clicked “Intersect” panel => Clicked on the first object and press ctrl to select second object => Pressed “Enter” after selection is complete => Common section of the geometry is retained while all of other geometries are removed

To apply the concepts and methods mentioned above to our model, we first shaped a base with many scaffold units with 2/3 mm pores and then systematically executed Boolean operations to merge the base with our solid auricular model. Finally, through a step-by-step extraction modeling process, the final porous ear model was constructed.

- Combined instructions

Detailed commands and exact sequence for this flow was shown as below

Convergent Modeling => Line => Stretching => Moving Object => Offset Face => Modeling => Moving Object => Array Geometry features => Array Geometry features => Enclosure Modeling => Moving Object => Moving Face => Extraction Modeling (1) => Subtraction (1) => Extraction Modeling (2) => Subtraction (2) …Automatic Cycle of Boolean Operations Completed.

3.2.3.4 Measurements and Evaluations

- Dimensions

Four macro-dimensions of the both solid and porous auricular constructs were measured using electronic vernier calipers, including the physiognomic ear length, morphological ear length, physiognomic ear breadth and morphological ear breadth. All dimensions were defined as shown below.

Morphological ear length: From the Darwinian tubercle (which is the slight projection occasionally present on the edge of the external human ear) to the tragion, where the deepest point is located (a point in the depth of the notch just above the tragus of the ear).

Morphological ear width(breadth): From the otobasion superius to the otobasion inferius (the upper and lower points at which the pinna is attached to the scalp, respectively).

Physiognomic ear length: From the superaurale (the highest point of the upper edge of the helix of the ear) to the subaurale (the lowest point of the inferior border of the ear lobule).

Physiognomic ear width(breadth): From the preaurale (the most anterior point of the ear, just before the point of helix attachment to the head) to the postaurale (the most posterior point of the ear, located on the free edge of the helix).

- Measurements

Measurements were performed three times for each dimension, corresponding means were calculated for the final statistical analysis.

Reference values for the models were achieved by performing measurements in the software by marking the start and end points on the model. A line was set to measure the distance between these marked points to obtain the measurements as reference values.

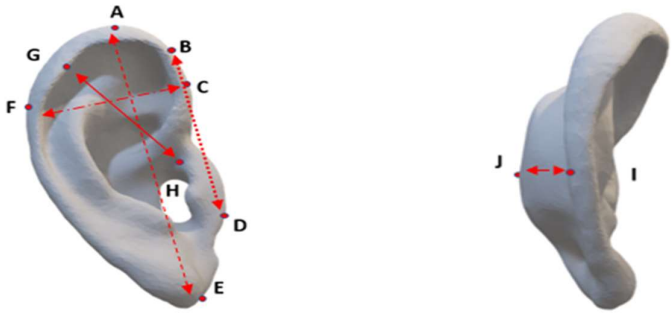

Figure 28. Dimensions of measurement for the virtual auricular model

Physiognomic Ear Length （A-E）, Morphology Breadth （B-D）, Physiognomic Ear Breadth （F-C）, Morphology Length （G-H）, Height （I-J）

For the printed constructs, the anatomical points were marked in red, and electronic calipers were applied to measure the distance between the marked points and obtain the measurements.

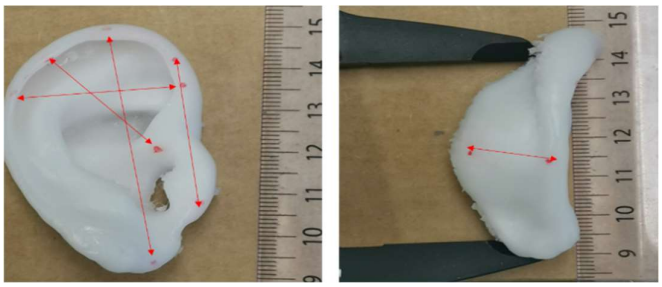

Figure 29. Dimensions of measurement for the printed auricular constructs

For the porous auricular constructs, two micro-dimensions include both the pore size and width of the rectangular unit (WRU) were measured under a light microscope. A line was drawn

along the target dimension, and the length of the line was read automatically by the interactive application affiliated with the light microscope.

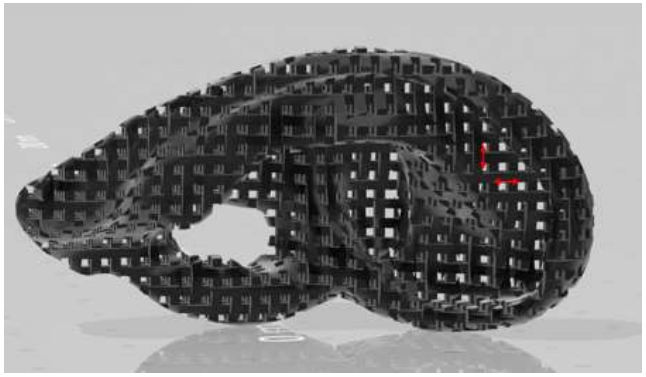

Figure 30. Dimensions of measurement for the porous auricular constructs

Note: only representative value in specific area for microdimensions was marked and measured across porous auricular constructs as Boolean operation have been performed to obtain relatively standardized porous structure within this model.

- Evaluation

In addition to descriptive statistics, for evaluation, ANOVA was conducted to compare the three types of materials, while one-sample t-tests were performed to compare the samples printed with specific materials and the standard reference sample measured by CAD software regarding macro-dimensions for solid auricular constructs and both macro-dimensions and micro-dimensions for porous auricular constructs.

4 Results

4.1 CAD-CAM Workflow

4.1.1 CAD

Different kinds of models were designed for different purposes in this project, as presented below. An original model was designed from scratch (e.g., original scaffold and custom-designed auricular model), a pre-existing model was imported for modification in terms of scale or shape (e.g., model scaffold and simulated cylindrical scaffold for cell culture), a simple construct was modeled for the addition of features from the printing settings (e.g., cubes with inner structure infill patterns), a model was extracted from CT/MRI data (e.g., the solid auricular model), an anatomical was extracted after spatial positioning (e.g., image mirroring of the auricle), and an extracted anatomical model with additional complicated design features was produced (e.g., the porous auricular constructs after the Boolean operations). More details are described in later sections.

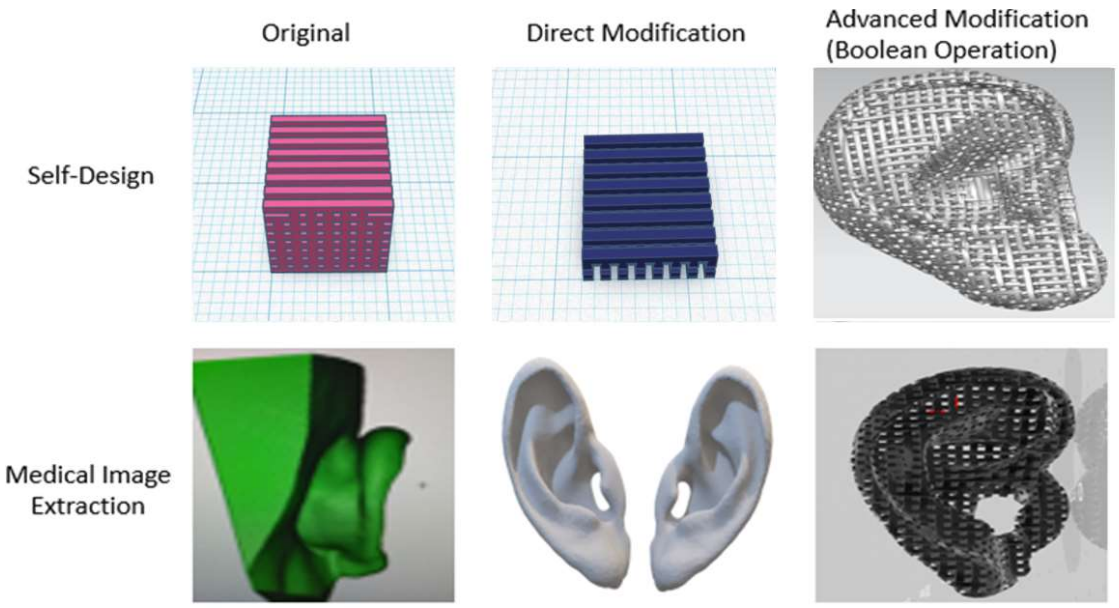

Figure 31. Presentation of CAD samples

4.1.2 Processing

The results of parameters for the slicing and printer settings are presented below.

- Quality

The layer height, initial layer height, line width, wall line width, outer wall line width, inner wall line width, top/bottom line width and infill line width were set as 0.06 mm, 0.2 mm, 0.4 mm, 0.4 mm, 0.4 mm, 0.4 mm, 0.4 mm, and 100%, respectively.

- Shell

The wall thickness, wall line count, number of top surface skin layers, top/bottom thickness, top thickness, number of top layers, bottom thickness and number of bottom layers were set as 1.2 mm, 3, 0, 0.8 mm, 0.8 mm, 8, 0.8, and 8, respectively.

- Infill

The infill density was set as 50%, while the infill pattern was defined as a grid.

- Material

The flow rate, retraction enabling, retraction at layer change, retraction distance and retraction speed settings were set as 95%, yes, no, 5 mm and 40 mm/s, respectively.

- Speed

The printing speed, initial speed, wall speed, outer wall speed, inner wall speed, top/bottom speed, travel speed, initial layer speed, skirt brim speed, print acceleration and print jerk were set as 45, 45, 22.5, 22.5, 45, 22.5, 22.5, 300, and 5 mm/s, respectively.

- Cooling

The print cooling enabling, fan speed, regular fan speed, maximum fan speed, regular/maximum speed threshold, initial fan speed, and regular fan speed at height settings were set as yes, 100%, 100%, 100%, 10%, 0% and 0.2 mm, respectively.

4.1.3 CAM

CAM was completed based on the CAD input and controlled by the processing steps maintained by Cura. Through the slicing-style fabrication process, the main printed samples output were as follows:

- Original designed scaffold.
- Model scaffold after modification.
- Custom-designed auricular model with porous structure.
- Solid auricular model from CT data.
- Mirrored auricular model extracted from CT data.
- Porous auricular model extracted from CT data.

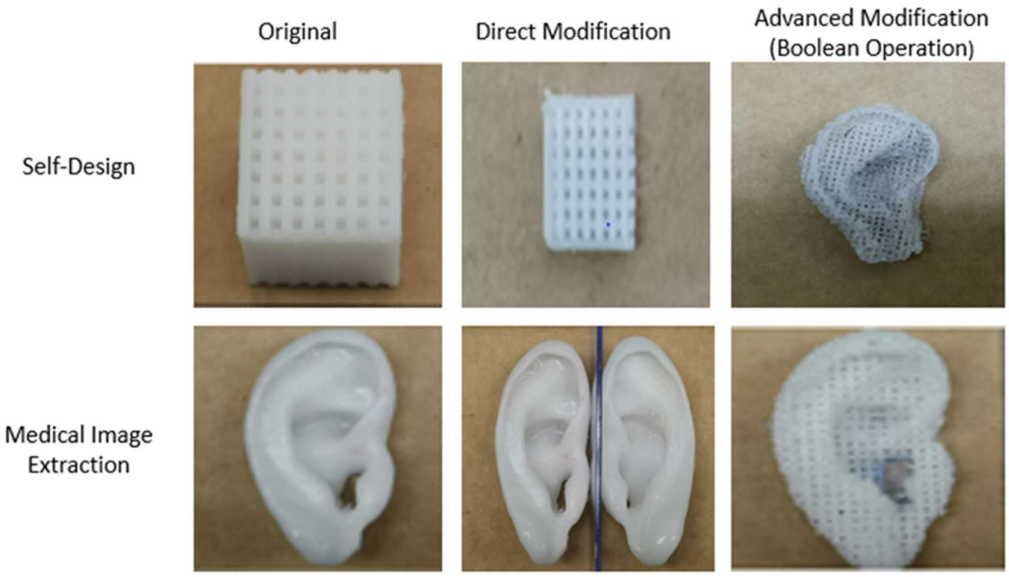

Figure 32. Presentation of CAM samples

4.2 3D Bioscaffolds

4.2.1 Limit Test

The method of uniform scaling was applied to approach the potential limit of the pore size by millimeter decrements in the edge length of the cubic scaffold outputs by the Ultimaker 2+ for the fabrication of scaffolds using three types of filaments.

The limit was achieved when the modified scaffold could not be fabricated appropriately. The final test scaffold was then obtained, and its parameters were identified as the standard for model scaffolds.

For the summary of measurements, the macrodimension (edge length) could easily be measured, and the microdimension (pore size) could be calculated based on the uniform ratio between these two units. The scale was calculated as limit = dimension scale*2/30.

Thus, the final test scaffold was a cubic scaffold with an edge length of 10 mm and a pore size of 2/3 mm for PCL filaments and 5 mm and 1/3 mm for PLA and ABS filaments.

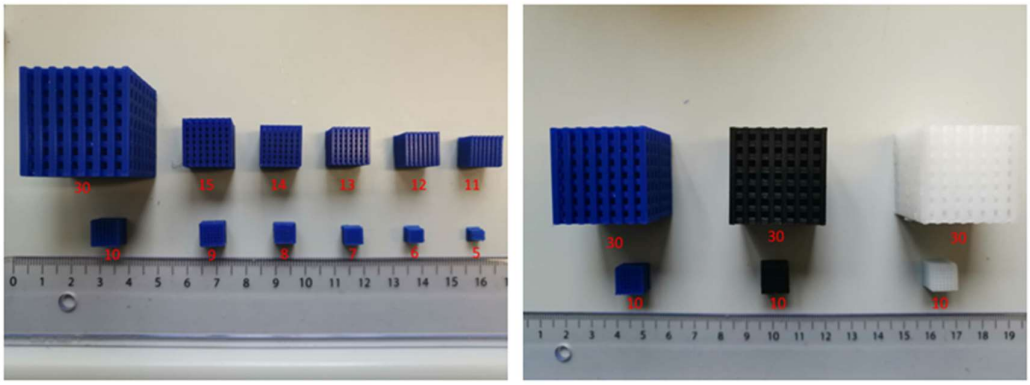

Figure 33. Limit test

Uniform scaling was performed as pictures shown on the left, the limit was approaching until it push to its lowest limit, picture on the right showed the identified scaled scaffold for PCL and other two reference group.

Dimension Scale (Limit*)(mm)	15 (1.000)	14 (0.933)	13 (0.867)	12 (0.800)	11 (0.733)	10 (0.667)	9 (0.6)	8 (0.533)	7 (0.467)	6 (0.400)	5 (0.333)	4 (0.267)
ABS	√	√	√	√	√	√	√	√	√	√	√	x
PLA	√	√	√	√	√	√	√	√	√	√	√	x
PCL	√	√	√	√	√	√*	x	x	x	x	x	x

Table 6. Summary of the limit test

√. Fabrication available. ×. Fabrication unavailable. *. Identified limit

Limit of PLA and ABS is 0.33mm while PCL is 0.66mm as figure indicated.

4.2.2 Slicing Approach

After slicing approach, the 3d model bioscaffolds was fabricated with fours layers left, as the top three layers set reference from most commercial scaffolds, while the bottom layer would be regarded as the buffer layer ready (temporary support structure) removed to be removed by postprocessing. Repeating this workflow described above, 9 printout outs for each type of filaments are fabricated. The final results are presented as below:

ABS PLA PCL

Figure 34. Results of 3D fabricated model bioscaffolds

4.2.3 Measurements and Evaluations

The descriptive statistics and results of the statistical analysis are presented below. For the descriptive statistics, the data are presented as the mean, SD and sample size. For the statistical analysis of the consistency and accuracy of the PCL model scaffold, unpaired one-sample t-tests were performed with the reference measurements, and one-way ANOVA was performed among the three types of materials regarding four dimensions. $P<0.05$ was set as the threshold value for statistical significance.

Dimension(mm)/Material	ABS			PLA			PCL		
	Mean	SD	N	Mean	SD	N	Mean	SD	N
Edge Length	10.03	0.054	9	10.00	0.065	9	10.01	0.054	9
Height	2.670	0.022	9	2.673	0.021	9	2.667	0.031	9
WRU	0.661	0.013	9	0.662	0.008	9	0.666	0.009	9
Pore Size	0.669	0.011	9	0.664	0.010	9	0.673	0.007	9

Table 7. Descriptive statistics for dimensions of the model scaffolds

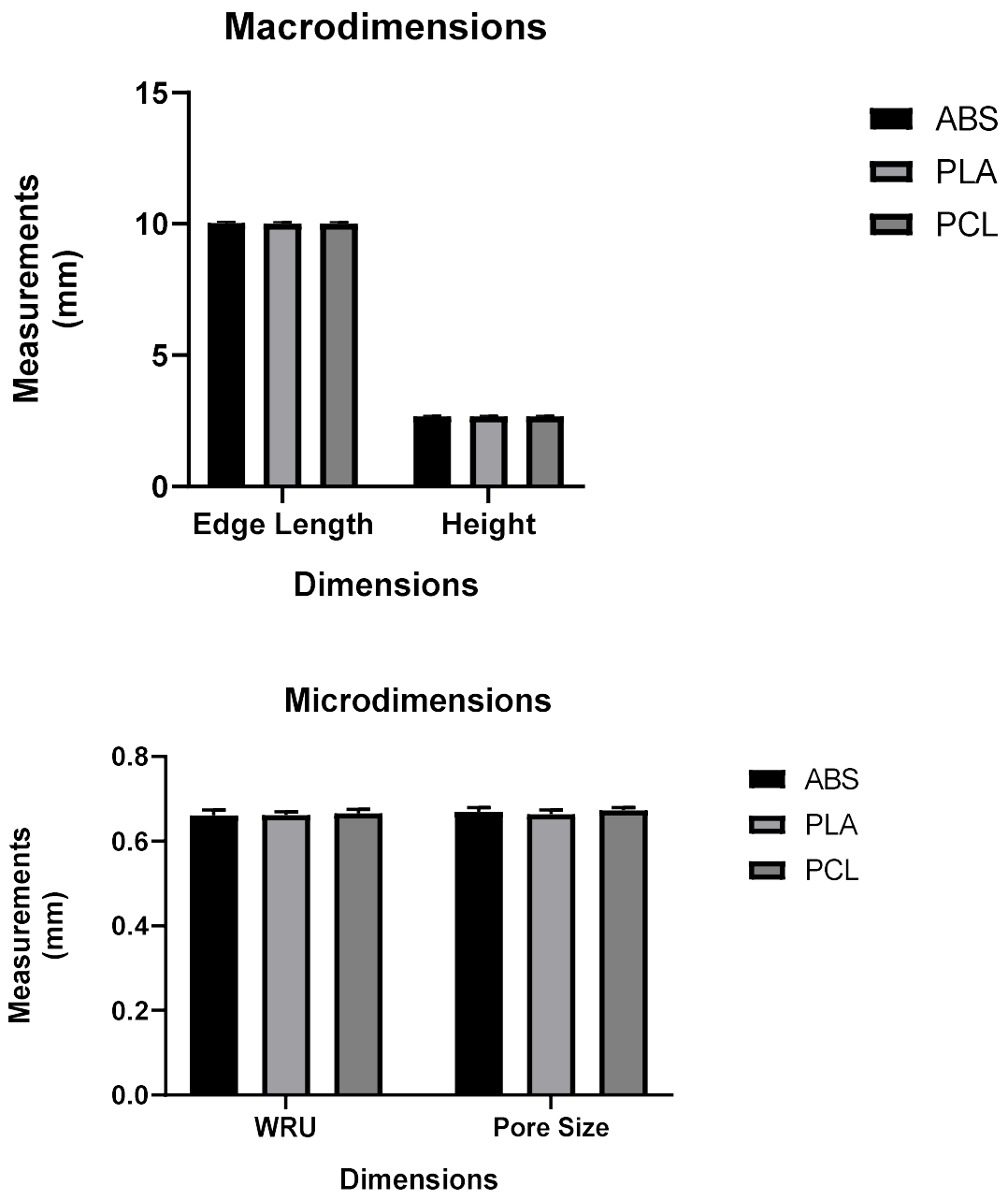

Figure 35. Summary of dimensions of scaffolds of different types of materials

For testing the consistency and accuracy of the printed PCL products, both ANOVA (for comparison with both the PLA and ABS products as references) and one-sample t-tests (for comparison with the reference measurements determined in CAD) were performed for all dimensions.

The P values for each were greater than 0.05. Thus, there was no significant difference in these parameters, demonstrating the relative consistency and accuracy of the PCL model scaffold achieved by this CAD-CAM indirect 3D printing workflow.

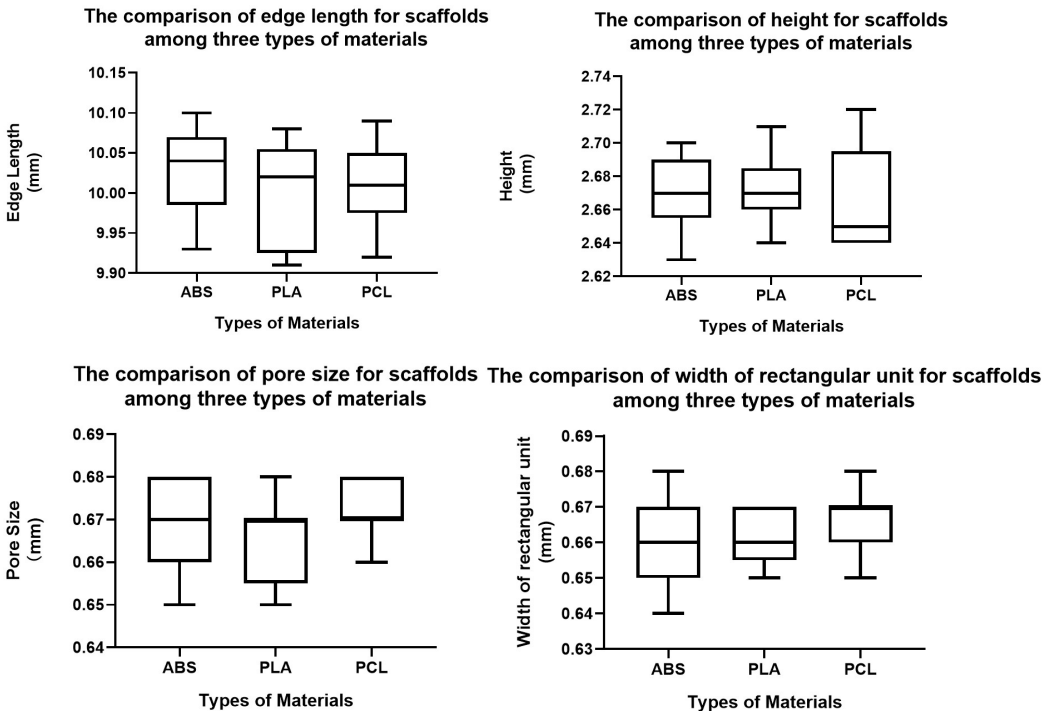

Figure 36. Comparison of dimensions of model scaffolds of three types of materials.

Statistical test	ANOVA	One-sample t-test		
Dimensions		ABS	PLA	PCL
Edge Length	0.6360	0.1757	0.9735	0.5665
Height	0.8530	0.8507	0.6406	0.7539
Width of rectangular unit	0.1545	0.7599	0.1388	0.1950
Pore Size	0.6316	0.1687	0.1523	0.9164

Table 8. Statistical analysis of dimensions of model scaffolds of three types of materials.

Note: The significant threshold P value was set as $P<0.05$, P value for all statistical test were not significant.

4.2.4 Postprocessing

Manual postprocessing was applied to the square model scaffold to obtain a cylindrical 3D cell culture scaffold. The main purpose was to remove the bottom layer while punching a round hole on the model to acquire the punched cylinder. The steps and results for this postprocessing procedure are shown below:

- Apply slicing tools (B) to remove the bottom layer (B) of the model scaffold (A).
- Apply a biopsy punch (D) to the remaining scaffold to manually extract cylinder shaped scaffold by cutting out(E).
- Use a needle (F) to obtain the final 3D cell culture scaffold (G) from the biopsy punch.

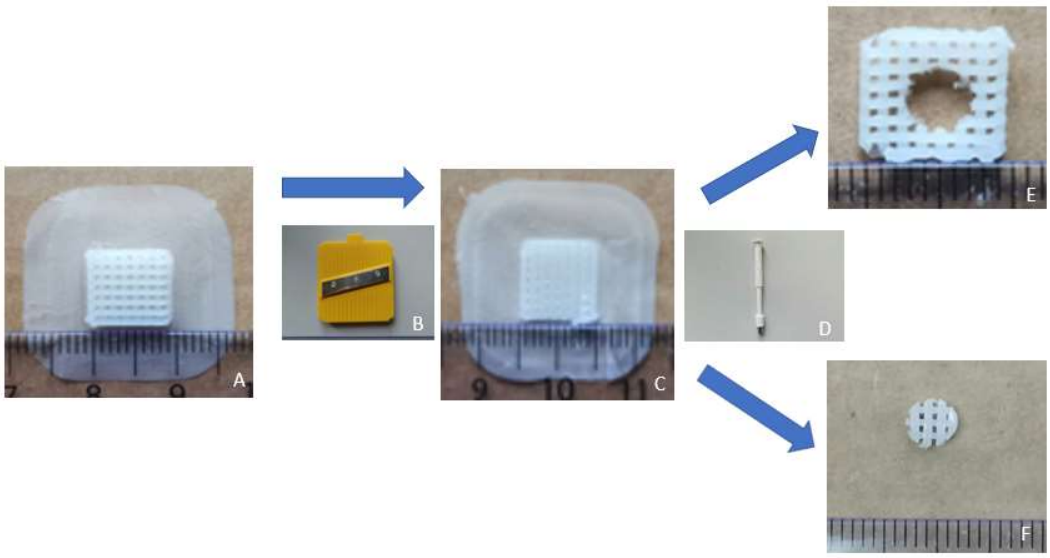

Figure 37. Procedure for postprocessing.

4.2.5 Summary

Starting from the original scaffold to create a scaled scaffold, the limit was identified when the scaled scaffold could not be fabricated properly. Then, the model scaffold was extracted and evaluated, followed by postprocessing to remove the nonporous bottom layer and obtain a cylindrical cell culture scaffold.

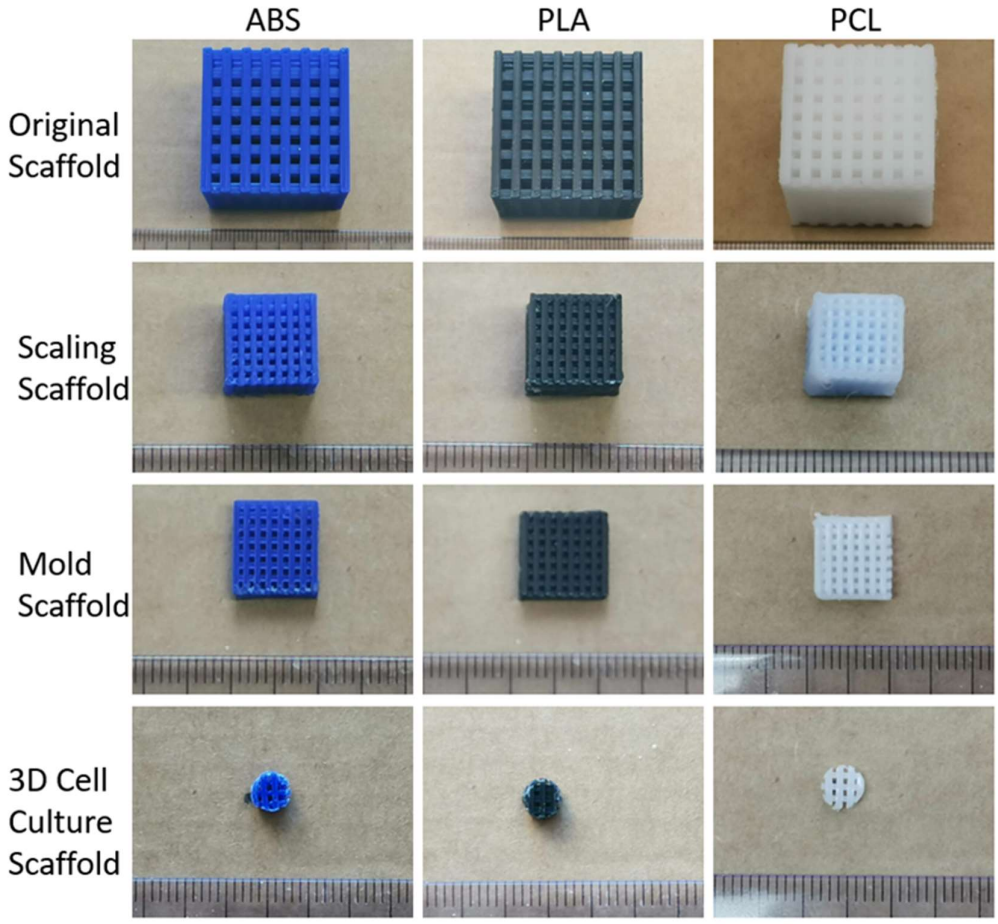

Figure 38. Presentation of all types of fabricated scaffolds

4.3 Customized Auricular Constructs

4.3.1 Medical Imaging Extraction

The 3D CT data of the skull of the patient were collected, and sliced images of the reference auricle were processed and exported as an STL file using Materialise Mimics. Contours and key landmarks were refined with additional focus by applying additional intensity-based segmentation methods. Then, the exported model was postprocessed in 3D matics. The procedures and results for each step are presented below. Finally, the solid auricular model was fabricated using the FDM 3D printer Ultimaker 2+ and was ready for further evaluation.

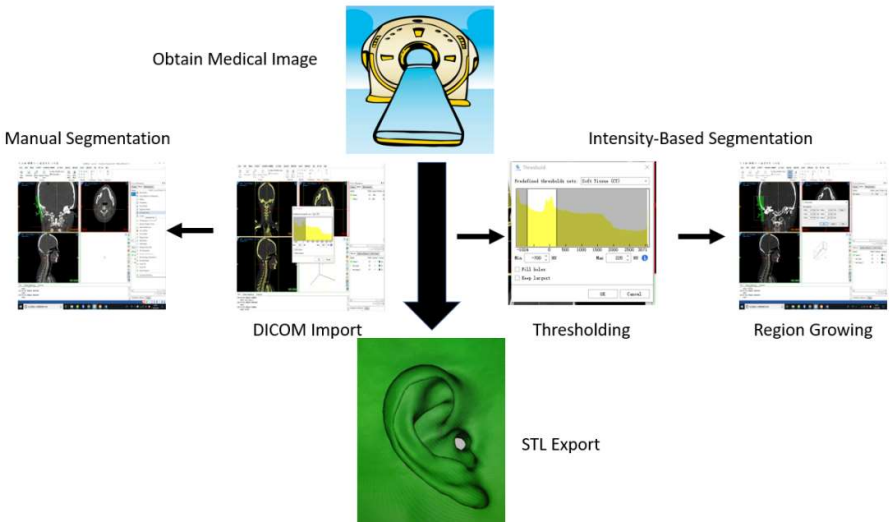

Figure 39. Model extraction from DICOM data

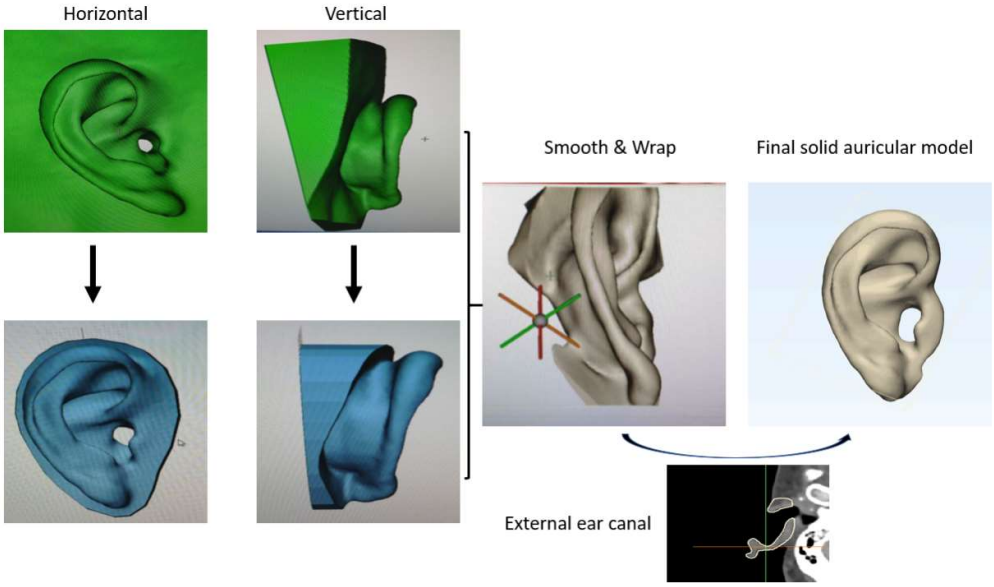

Figure 40. Postprocessing of the extracted model

4.3.2 Image Mirroring

The original auricular construct and the mirrored counterpart are presented below for comparison. The 3D mirrored construct is far superior the previous model created based on traditional 2D images and manual drawing of the outline from a real patient on the contralateral side. Thus, this approach could potentially help plastic surgeons carve costal cartilage to mimic the complex shape of the auricle on the affected side using a model for the purpose of simulation.

After this procedure, solid auricular constructs were fabricated and serve as stepwise preparation for porous auricular constructs.

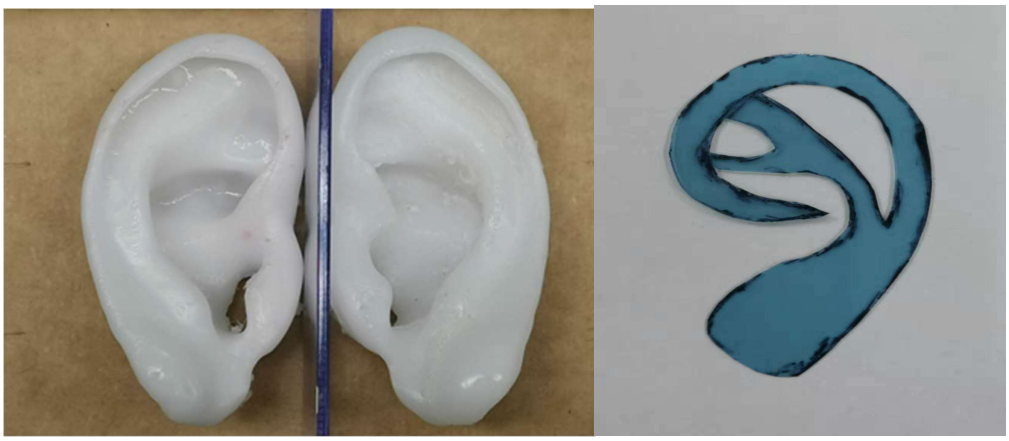

Figure 41. Comparison of 2D and 3D models for surgical simulation

4.3.3 Boolean Operations

Boolean operations were first applied in our trial study for the predesigned ear model, and the general procedures are presented in the figure below. Following preparation of the aggregated scaffold units with a uniform pore size of 2/3 mm, under mapping from the ear contour by merging and subtracting with Boolean operations, the final porous ear construct was produced. The same workflow was conducted for the extracted customized solid model for further evaluation.

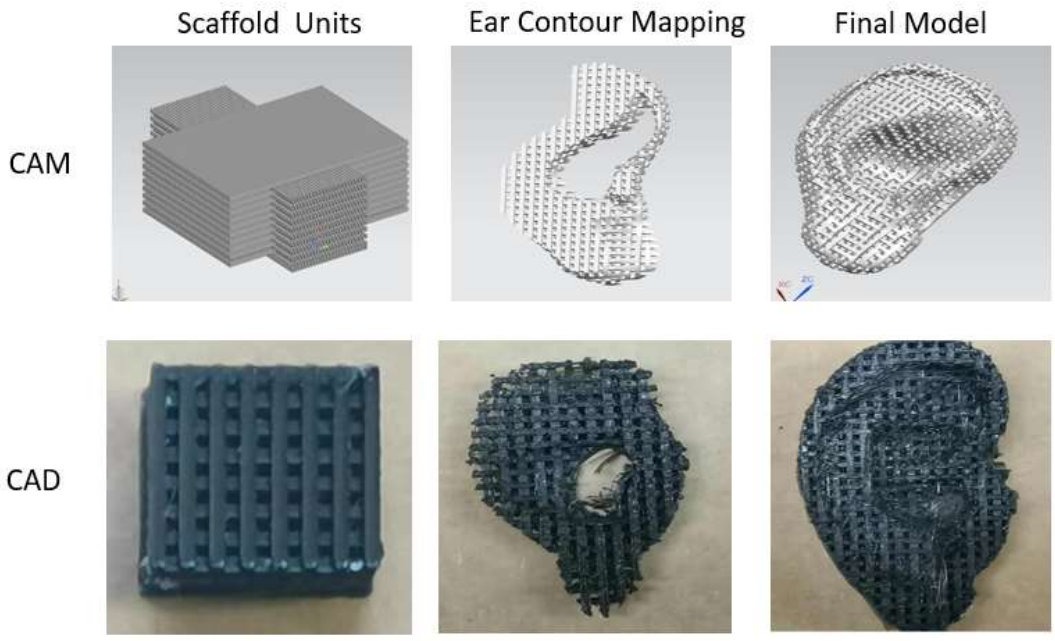

Figure 42. Presentation of the results of the Boolean operation procedures for fabrication

4.3.4 Measurements and Evaluations

4.3.4.1 Solid Auricular Constructs

- Measurements

Five macrodimensions of the solid auricular constructs were recorded, and the descriptive statistics (mean and standard deviation) were calculated for each specific type.

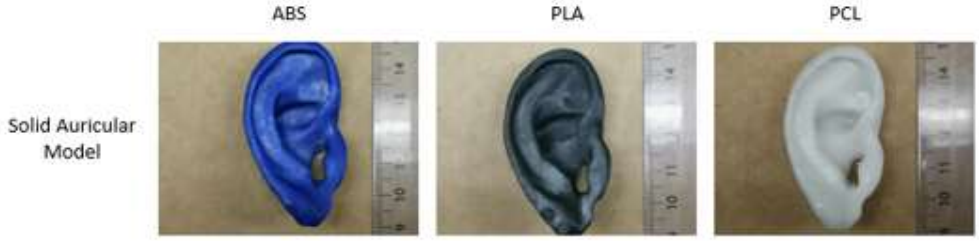

Figure 43. Presentation of solid auricular constructs

Dimension(mm)/Material	ABS			PLA			PCL		
	Mean	SD	N	Mean	SD	N	Mean	SD	N
PEL	51.73	0.104	5	51.75	0.109	5	51.72	0.145	5
MEL	25.47	0.113	5	25.47	0.107	5	25.43	0.083	5
PEB	28.41	0.115	5	28.37	0.127	5	28.38	0.110	5
MEB	31.42	0.100	5	31.42	0.107	5	31.36	0.137	5
Height	12.51	0.094	5	12.5	0.080	5	12.56	0.130	5

Table 9. Descriptive statistics for measurements of dimensions for solid auricular constructs

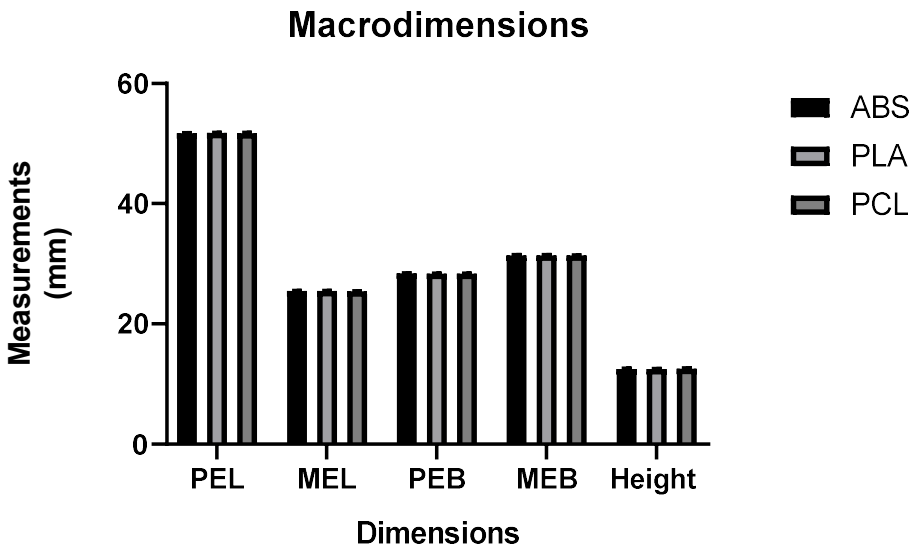

Figure 44. Descriptive statistics for measurements of dimensions for solid auricular constructs

4.3.4.2 Evaluations

Both descriptive statistics and inferential statistics are presented below. ANOVA was conducted to assess the solid auricular constructs in terms of five dimensions among three types of material. One-sample t-tests were also performed to compare the measurements of the PCL constructs with the reference measurements. No significant differences were found in any test ($P>0.05$). As the figures below indicate, shared ranges were found among the three columns; thus, there were no significant differences among these three groups regarding the respective dimensions.

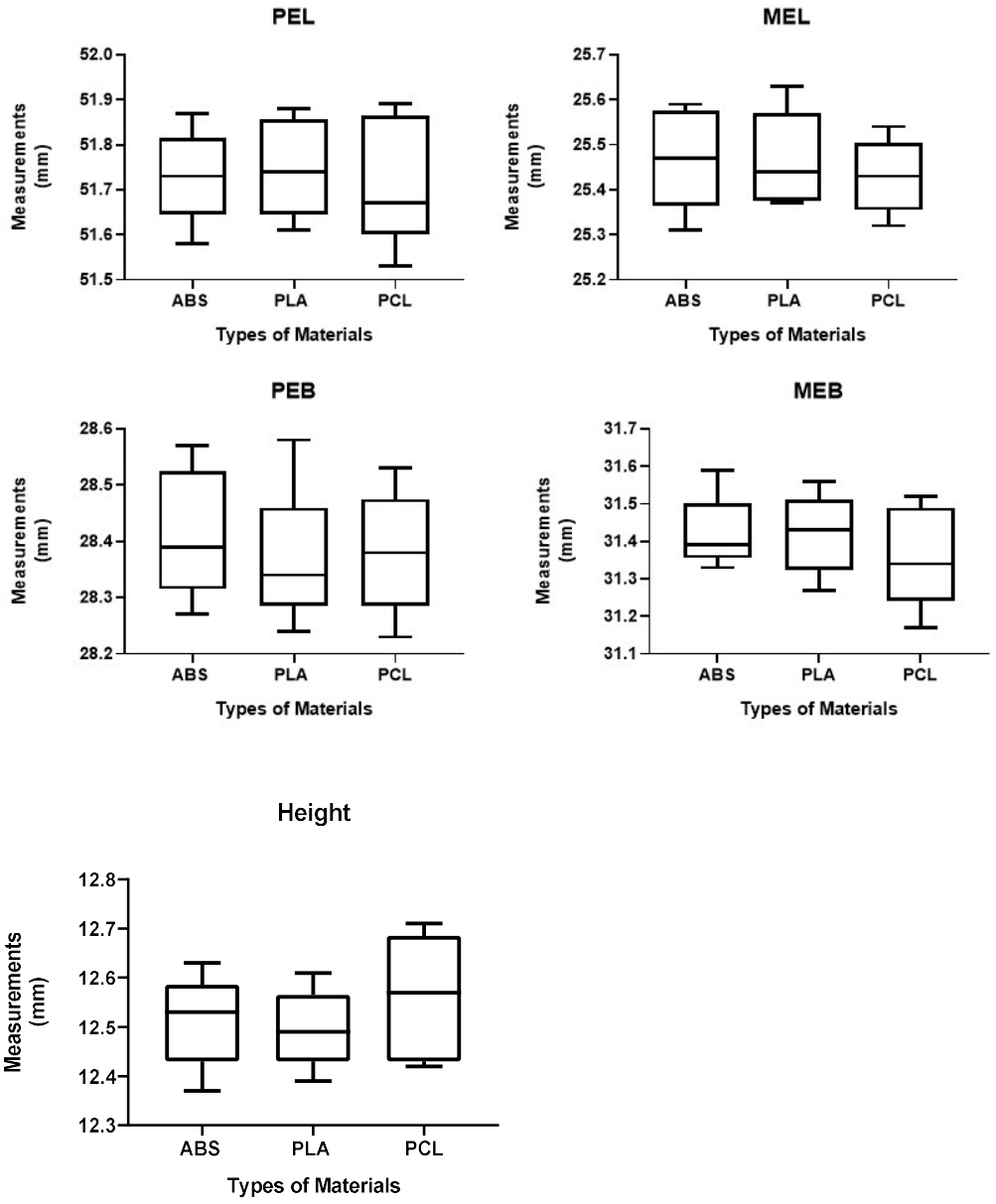

Figure 45. Comparison of dimensions of porous auricular constructs among types of materials

Statistical Test	ANOVA	One sample t test		
Dimensions		ABS	PLA	PCL
PEL	0.9339	0.8405	0.8781	0.7735

MEL	0.7944	0.7112	0.7557	0.6176
PEB	0.8049	0.799	0.5811	0.7046
MEB	0.6473	0.6764	0.6962	0.5483
Height	0.6069	0.6919	0.3951	0.6306

Table 10. Statistical test of dimensions of solid auricular constructs among types of materials.

Note: The significant threshold P value was set as P<0.05, P value for all statistical test were not significant.

4.3.4.3 Porous Auricular Constructs

- Measurements

Five macrodimensions and two microdimensions of the porous auricular constructs were recorded, and the descriptive statistics (mean and standard deviation) were calculated for each specific type.

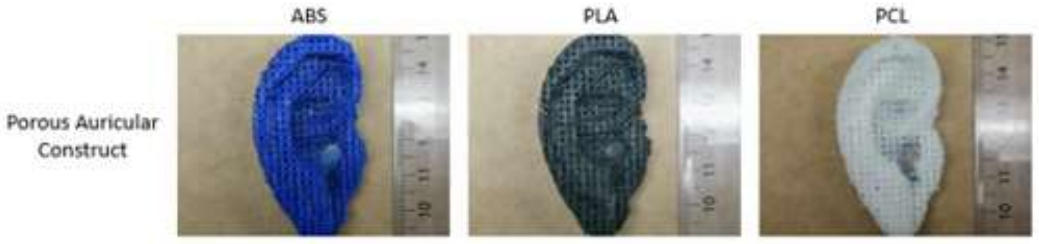

Figure 46. Presentation of solid auricular constructs

Dimension(mm)/Material	ABS			PLA			PCL		
	Mean	SD	N	Mean	SD	N	Mean	SD	N
PEL	51.74	0.117	5	51.75	0.104	5	51.73	0.146	5
MEL	25.46	0.098	5	25.48	0.113	5	25.43	0.089	5
PEB	28.39	0.127	5	28.37	0.105	5	28.39	0.121	5
MEB	31.41	0.105	5	31.39	0.121	5	31.36	0.120	5

Height	12.51	0.117	5	12.49	0.093	5	12.5	0.081	5
WRU	0.666	0.009	5	0.664	0.007	5	0.664	0.011	5
Pore Size	0.663	0.007	5	0.668	0.008	5	0.662	0.008	5

Table 11. Descriptive statistics for measurements of dimensions for porous auricular constructs

Note: The significant threshold P value was set as $P<0.05$, P value for all statistical test were not significant.

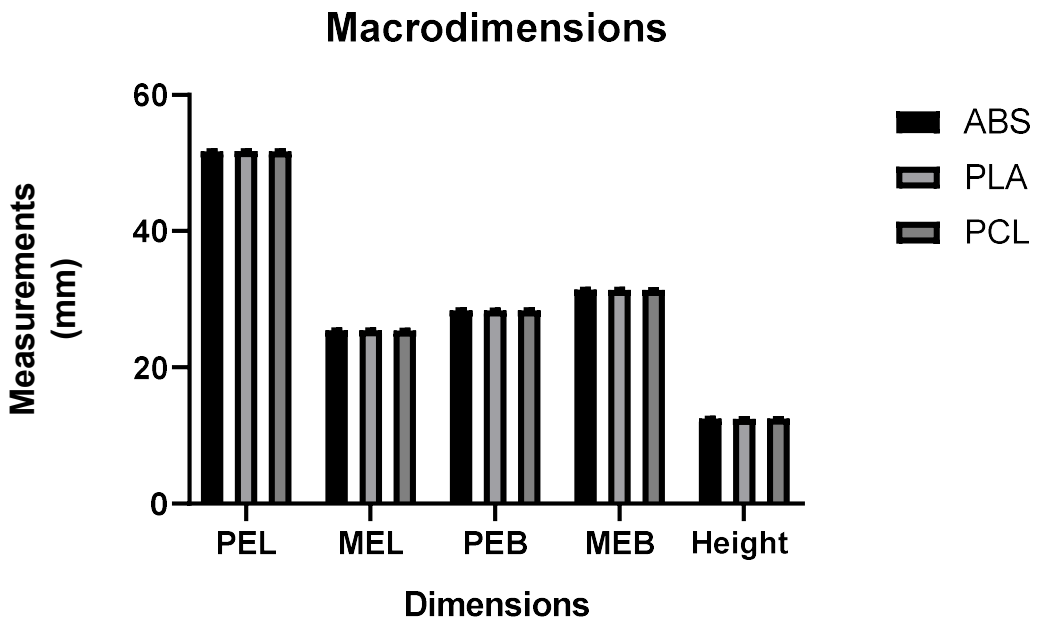

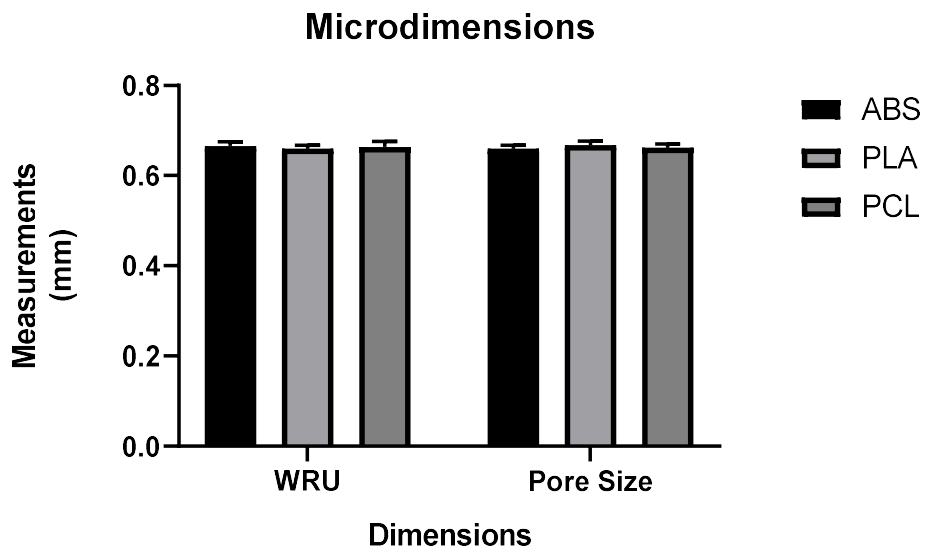

Figure 47. Descriptive statistics for measurements of dimensions for porous auricular constructs

- Evaluations

Both descriptive statistics and inferential statistics are presented below. ANOVA was conducted to assess the solid auricular constructs in terms of five macrodimensions and two microdimensions among three types of material. One-sample t-tests were also performed to compare the measurements of the PCL constructs with the reference measurements. No significant differences were found in any test ($P>0.05$). As the figures below indicate, shared ranges were found among the three columns; thus, there were no significant differences among these three groups regarding the respective dimensions.

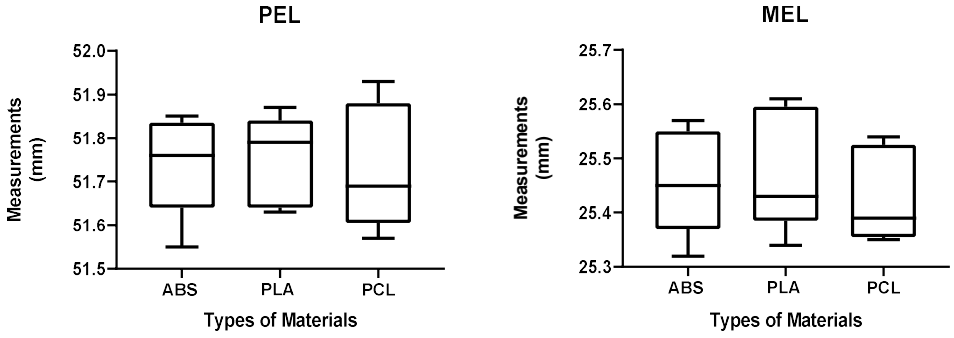

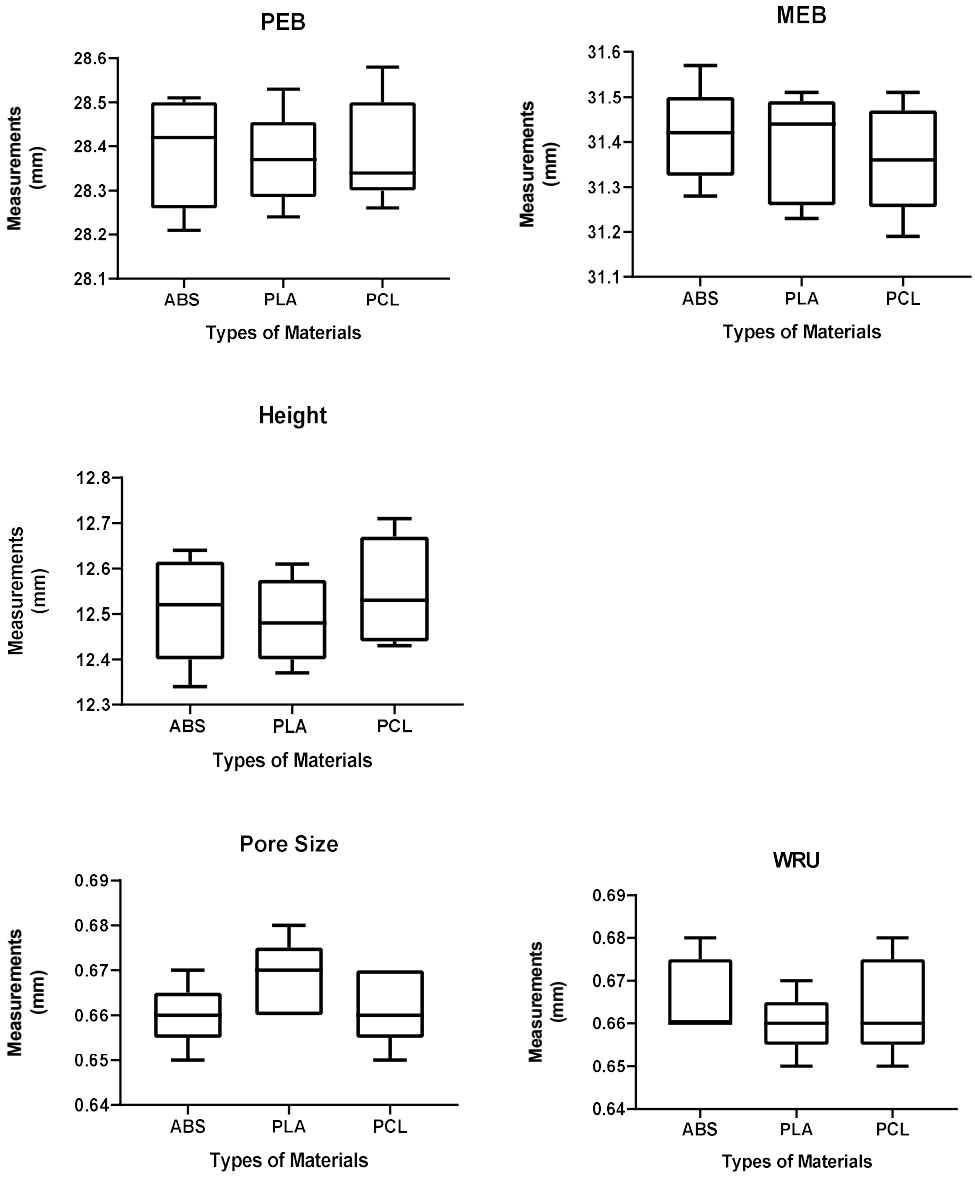

Figure 48. Comparison of dimensions of porous auricular constructs among types of materials

Statistical Test	ANOVA	One sample t test		
Dimensions		ABS	PLA	PCL
PEL	0.9739	0.9714	0.8416	0.9084
MEL	0.7549	0.8638	0.6104	0.6403

PEB	0.9621	0.8944	0.8419	0.8899
MEB	0.7816	0.511	0.8899	0.7547
Height	0.6613	0.7218	0.9283	0.3232
WRU	0.5971	0.8149	0.0913	0.5879
Pore Size	0.2915	0.0913	0.8025	0.2524

Table 12. Statistical test of dimensions of porous auricular constructs among types of materials

Note: The significant threshold P value was set as $P<0.05$, P value for all statistical test were not significant.

5 Discussion

5.1 Trend

Cartilage repair remains a potential challenge for most clinicians. Additionally, as a type of surgery with relatively high aesthetic concerns, ear reconstruction in microtia always calls for more individualized methods to gain optimal results according to personal needs.(23) Furthermore, the unpredictable outcomes are derived from a variety of differences, such as the condition of the recipient site, the specific geometry of the auricle, and the properties of the implant material/donor cartilage. Thus, a more objective, standardized, customized approach is required to close the gap between patients' specific needs and the capabilities of cartilage repair, which is mainly based on surgeons' accumulated subjective experience.(83) With the convergence of CAD and CAM, the technical development of 3D provides more opportunities to overcome issues in cartilage cell culture and could be a game-changer as a potentially revolutionary approach for auricular reconstruction and cartilage repair.(84, 85) One possible application is the production of a porous 3D scaffold to facilitate cell adhesion and growth of new cartilage tissue; another is the fabrication of either an individualized auricular mirroring framework to reflect the complex 3D structure of the unaffected ear as a reference for surgical simulation or an implant model to mimic the anatomy of the auricle while maintaining the porous structure. In our study, we developed a standardized, consistent CAD-CAM workflow by applying the Ultimaker 2+ with PCL filaments to fabricate 3D scaffolds for in vitro cell culture, a 3D auricular mirroring framework for surgical planning and a porous auricular construct as a potential candidate for in situ cell culture and implantation.

5.2 Significance

5.2.1 Hardware: Ultimaker 2+

5.2.1.1 Cost-effectiveness

While purchasing a 3D printer does require a significant investment for most clinics, this problem could be partially alleviated by introducing the relatively low-cost FDM machine Ultimaker 2+. The cost-effectiveness over time could become even more significant as the need to order commercial scaffolds or medical models is reduced. Furthermore, the open-filament system and variety of printing settings can be modified to adapt the manufacturing process to meet specific needs and serve a variety of purposes on a case-by-case basis to avoid the potential opportunity cost of purchasing other advanced 3D printers or ordering services from third-party companies.(86) Last but not least, this consistent workflow for fabricating scaffolds and models could be replaced with high transparency and potentially be applied at other institutes in a more accessible way.(87)

5.2.1.2 Extrusion upgrade kit

As an incremental upgrade to the Ultimaker 2, the Ultimaker 2+ is a more accurate and reliable desktop 3D printer for the purposes of a wide range of potential customers, such as academic institutions, small businesses, and health care services.

First, a flatter attached cooling fan was set on the extruder assembly; instead of being positioned at an angle to the extruder as was its predecessor, greater consistency could be achieved by this new cooling system.(88)

Second, the material feeder was improved to provide filaments more reliably and efficiently, instead of being stripped as the filaments moved inside the old feeder because the teeth of the feeder could not grip the filaments with enough friction. The pressure control system in this gear feeder solved this problem by easing this whole procedure and could be adjusted for different materials.(89)

Finally, the last feature of Ultimaker 2+ is the Upgrade Kit, which has several different replaceable nozzle specifications: 0.25, 0.4, 0.6, and 0.8 mm. This variety allows alternation between higher accuracy for increased detail or higher speed for increased efficiency.

5.2.2 Software

Customization could be achieved regarding both the scaffold design and individual needs of the patient by applying CAD and MRI/CT extraction software, respectively.(90, 91) In the laboratory, either the pattern or size of pores in scaffolds is capable to be customized for various cell types and microenvironments to test and determine the optimal algorithm for cell culture, and these precisely controlled porous structures could meet a variety of research needs in individual cases. In the clinic, unilateral defects could be identified and reconstructed by mirroring the anatomical counterpart on the reference side to create either a solid model for surgical simulation or an individualized implantable bioscaffold with an external auricular contour and an inner porous structure for in situ tissue engineering.

5.2.3 Materials

Appropriate selection of printing materials is vital for the long-term success of both implants and bioscaffolds. PCL, as the candidate material, has several inherent advantages compared with autologous cartilage, porous polyethylene implants, such as MEDPOR, and other types of compatible plastic filaments.(92, 93)

1. PCL is biocompatible and rarely induces a strong foreign body reaction.

2. PCL is biodegradable, which is ideal for serving as a temporary source of mechanical integrity for cell growth.

3. The potential of PCL to function as a biomaterial for both in vivo implants and in vitro scaffolds has been proven in previous works in the literature in cartilage engineering.(94)

4. PCL has been approved by the US Food and Drug Administration; thus, ethical concerns related to the clinical application of this material, especially in craniofacial surgery, are resolved.(95, 96)

PCL is a biodegradable and biocompatible polymer that is an ideal candidate for fabricating bioscaffolds.(97) Specifically, the slow degradation could also provide prolonged mechanical integrity while gradually disappearing in a physiological environment. Efforts were taken to make PCL printable with the Ultimaker 2+ by modifying the settings in Cura and comparing the resulting constructs with standard inherently compatible counterparts made from PLA and ABS to confirm its compatibility with this FDM machine in certain situations.

5.2.4 Limit Test

The purpose of the limit test was to explore the limit of accuracy of the Ultimaker 2+ in processing a specific type of filament. Both PLA and ABS showed matched results in the slicing software (Cura) for scaffold preparation and the Ultimaker 2+, as both of these materials are inherently compatible with this hardware. However, PCL is a type of polymer that is not in the default candidate list of compatible materials. The information in the software cannot be set as a reference and needs to be further tested to approach the actual limit.

Uniform scaling is a systematic method of shrinking the size of a test model by a specific unit in all three dimensions and is ideal for testing the 3D limit of accuracy. The limit was identified once the model could not be appropriately manufactured, collapsed or showed notable deviations at a specific size.

The identified limit could be applied as an original reference to develop an appropriate strategy for designing a model of interest printed with PCL. That is, we could either print the PCL model above this limit or use other approaches, such as indirect 3D printing, to avoid potential failure resulting from manufacturing out of the processable range. Following this logic, we applied customized postprocessing method to expand the scope of application for PCL material.

5.2.5 Evaluations

Regarding the macrostructures, both the length and width of the model scaffold were measured and evaluated to test the resolution on the X-Y plane, which is mainly determined by the minimum rotation of the stepper motor and mechanics of the Ultimaker 2+. The same procedure was conducted for the dimension of height as the representation of resolution on the Z axis, which is determined by the movements among different layers during the slice-by-slice printing process.

Regarding the microstructures, the width of the rectangular unit was measured and evaluated to test the dimensions of this substructures, while the same procedure was performed for the pore size to test the porous structure formed by perpendicular rectangular units. Pore size is a crucial variable in determining cellular behavior in later evaluations of cell culture and should be recorded and adjusted accordingly; thus, monitoring its accuracy is necessary.

Regarding the summary and descriptive statistics, as the SD of each dimension was presented and found to be in the acceptable range, the precision of 3D printing these models with PCL has been proven, which means that the Ultimaker 2+ is a reliable machine for printing these model scaffolds with PCL.

The purpose applying ANOVA to test all higher dimensions was to determine the potential compatibility of PCL for specific constructs. No significant differences were found among the three materials, ABS, PLA and PCL, indicating that PCL is as compatible as the reference materials ABS and PLA for this fabrication process.

The purpose of the one-sample tests was to test the accuracy of the printed model scaffolds compared with the reference measurements of the model design. As there were no significant differences in the values between the printed PCL models and the reference measurements, the PCL model scaffolds meet the accuracy standards to be regarded as satisfactory reflections of the designed model.

5.2.6 Postprocessing

The purpose of postprocessing was to extract a columnar bioscaffold from a cubic model scaffold manually. There are several potential obstacles to the direct fabrication of this columnar scaffold. First, the expected radius of the final bioscaffold (5 mm) is lower than the previously identified limit for PCL. Second, it is challenging to fabricate a PCL construct with a round edge as PCL filaments need a longer time to solidify after melting, which tends to leave strings on the rounded edge after each cycle of linear motion of the printer head. Third, the thin bottom layer of directly printed scaffolds cannot be set as porous and need to be removed to maintain the interconnectivity of the bioscaffold.

Indirect 3D fabrication avoids the above issues while maintaining the designed microstructures of the initial model scaffold. A biopsy punch was applied, and the general shape of the extracted scaffold was entirely determined by the round hole of this tool. A slicer was also applied to remove the nonporous bottom layer and expose the porous structure.

5.2.7 Image Mirroring

Finally, the mirror image of the normal auricular model for patients with unilateral microtia could serve as a 3D perception reference for simulation by mirroring its counterpart on the opposite side. The application of simulation models has been accepted as a safe, effective and time-saving method for training physicians and guiding surgery.(98, 99)

No commercially individualized auricular models for microtia patients available are far superior to traditional models, such as medical images or manual drawings of 2D slices, because the complex substructures and intricate convolutions of the auricle can only be presented by 3D output to achieve high shape fidelity and avoid systematic errors.

5.2.8 Boolean Operations

Boolean operations, as advanced 3D modeling methods, were applied in our design procedure to create features, such as holes, in the auricular model and yield scaffolds with complex microstructures.(100, 101) In this approach, the primary feature represented by a unit structure is constructed as the basic element, secondary feature are formed as pores by replicated flow of boolean operations.(102). Following this workflow, units with porous structure finally combine to construct customized ear construct. To create unit with expected geometry structure and properties remains as threshold issue. Instead of creating openings manually case by case, Boolean operations provide a more standardized and systematic way to design pores with a controllable, uniform distribution.

5.3 Limitations

5.3.1 Biological Properties of Bioscaffolds

In vitro and in situ cell cultures for testing biological properties of bioscaffolds are expected. In another project, our research group aims to compare the CAD-CAM 3D fabricated scaffolds made by Ultimaker 2+ with both blank control and current reference commercial scaffolds to assess their potential capacity to facilitate cell growth and proliferation.

5.3.2 Compatibility of PCL

The compatibility of the Ultimaker 2+ with PCL is not complete under some circumstances; for instance, the trial study of the default infill pattern settings in Cura cannot be conducted for PCL at the scale (5 mm) of a cell culture scaffold./ Infill pattern function in Ultimaker settings does not work very well for PCL, especially for the microlevel dimensions on small printouts (103) In contrast, the “inherently” fully compatible materials PLA and ABS can be regarded as standard materials for this test. Thus, we performed ANOVA to compare these three materials in terms of most evaluations to rule out potential incompatibility issues in certain situations.

5.3.3 Indirect 3D Printing

Due to the accuracy limitation of the Ultimaker 2+ FDM printer, for the fabrication of a cylindrical 3D cell culture scaffold, we followed the pathway of indirect 3D printing by converging both additive and subtractive manufacturing. It is challenging for the printer head to follow the path along round edges, especially when there are very small, delicate structures. Thus, indirect 3D printing provides an alternative method to complement direct AM methods. With the standardized postprocessing procedure described above, the final model achieves the same level of accuracy as the CAD simulation.

5.3.4 Bioprinting

In our study, a polymer was applied as a material for constructing scaffolds without the addition of bioactive substances or seed cells. Because cells cannot survive at the melting temperature of PCL. However, with the recent development of bioprinting, printing can be performed with bioink, a combination of bioactive factors, cells and biomaterials, to build up tissue directly in specific arrangements by following a similar layer-by-layer method as traditional 3D printing approaches.(104, 105) As an extension of traditional 3D printing, bioprinting can fabricate biological tissue, such as cartilage, and even entire organs from scratch for testing or direct implantation.(106, 107) The complex cell composition and surrounding microenvironment are the main challenges faced by this technology; although there is still a gap to fill before the full application of bioprinting, it has promise for the fabrication of specific anatomical structures of with living cells directly.(108)

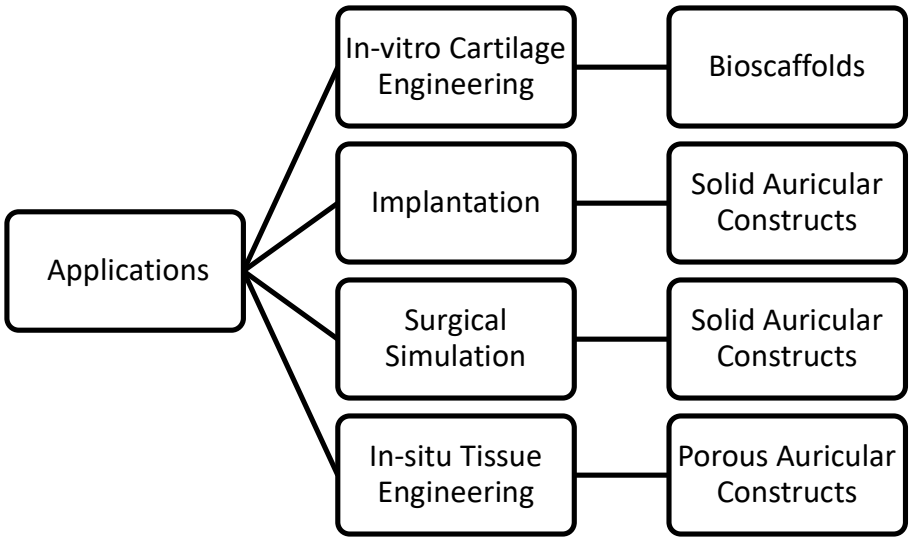

Figure 49. Potential applications of this work.

5.4 Potential Clinical Applications

5.4.1 Patient Communication

As more cooperative approaches between a plastic surgeon and their patients are actively recommended by the guidelines of the American Medical Association, it is essential to provide patients with relevant knowledge to enable them to understand and provide informed consent for interventions.(109) As information in the clinic is usually depicted verbally, further mutual communication might be improved at limited levels with the help of a 2D picture or display of patients' medical images.(110) However, it takes months to 2D readings and further conceptualize it in 3D due to the complexity of the 3D anatomy of target defects/organs. In addition, previous professional medical knowledge of histology and physiology are needed to make assessments through increasing medical imaging methods, such as CT and multisequence MRI.(111) As a result, patients find that 2D images and medical scans are challenging to interpret. Although individual patient could gain access to related information regarding their clinical status by searching on the Internet, inconsistent online interpretations tend to result in biased evaluations.

The solid auricular model fabricated through mirroring of the image extracted from the normal side on CT could serve as a bridge to close the gap of communication between doctors and patients. 1. The complex 3D anatomy of the auricle can be explained and evaluated more effectively. 2. The surgical procedure could be described more vividly through directly viewing and manipulating physical constructs. 3. The model could also be regarded as a reference target template to predict the outcome after the intervention. In summary, using the 3D-printed auricular model, patients and their families can receive a detailed explanation of the complexity of the microtia, the surgical procedures and the expected outcome, which could promote the understanding and cooperation of patients and family members.

5.4.2 Surgical Planning

Another application of the 3D-printed model as a reference for educating healthcare professionals or guiding intervention planning.

The complex anatomy of the auricle could be better assessed and understood using 3D physical constructs than 2D drawings and medical images, such as CT images. This auricular model, a simulation, can provide higher fidelity without any potential risks or invasive interventions. Significant improvement in medical education with the use of other 3D-printed simulated models has been systematically confirmed.(112)

Presurgical evaluation of the contour of 3D-printed replicates as a reflection of the anatomical structure, the auricle in this case, will enhance the understanding of its geometry.

Intraoperatively, using this patient-specific template to guide surgery can effectively reduce the operative time and improve the clinical outcome as the auricular model can be used as a guide for harvesting and carving cartilage to form the shape of the reconstructed ear.

It can also be applied postoperatively as a reference to evaluate the outcome and make modifications accordingly, which will greatly benefit the 3rd stage of ear reconstruction in microtia, when final correction of the substructure of the auricle is performed to achieve an optimal aesthetic outcome.

5.4.3 Implantation

3D-printed replicates of patient-customized anatomical structures at specific sites could be applied for implantation.

Ethical concerns regarding a variety of materials as implants have been cleared, especially with the approval of PCL by the Food and Drug Administration.(113)

The use of 3D fabricated implants as candidate substitutes for MEDPOR support in traditional microtia surgery has potential in terms of the customized contour that mimic the shape with greater fidelity and symmetry.(114)

Porous auricular constructs could also be potentially implanted as bioscaffolds for in situ cell culture. First and foremost, the shape and distribution of pores are adjustable to meet the optimal standards for cell culture.(47, 115) Furthermore, the customize shape reflecting the specific anatomy of the patient's auricle could induce cells to form engineered tissue in specific geometrical arrangements.

5.4.4 Cartilage Engineering

In recent decade, the advances of 3D printing technology have accelerated the development of the field of regenerative medicine. 3D printing renders the process of preparing engineering scaffolds for cartilage accurate and controllable, allowing the use of a rational design to prepare scaffolds for cell culture and tissue construction to become a reality. Through 3D printing, the precise preparation of scaffold structural features can be modified according to the cell biological behaviour, additionally, with improved mechanical properties scaffold is capable to promote the growth and spatial distribution of cells.(116)

Cartilage has a specific structure and composition according to its distribution, so the design for further preparation of cartilage tissue-engineered scaffolds via 3D printing will certainly further optimize the construction of cartilage tissue.

The microstructure of our bioscaffolds is expected to influence cell behaviour. The internal architecture was evaluated under a light microscope, and it was found that all scaffolds were composed of layers of crossed fibrous structures. In particular, pores were evenly distributed throughout all constructs. The results of model scaffolds showed that the shape and distribution of pores are precisely controllable. The porous structure formed by the fabricated rectangular units yielded scaffolds with a larger surface area, which would provide sufficient space for cell growth, and the pore channels were connected. Functional connectivity is expected to be beneficial to the exchange of nutrients and oxygen and the diffusion of cellular metabolites and is a critical factor for the formation of bioactive cartilage tissue.

6 Conclusion

The CAD-CAM workflow developed to fabricate scaffolds for cell culture and porous auricular models using the low-cost 3D printer Ultimaker 2+ with PCL has satisfied accuracy and precision. The specific compatibility of PCL with these procedures was confirmed by comparison with other standard compatible materials, PLA and ABS. The 3D bioscaffolds fabricated are potentially applicable for cartilage engineering. In addition, the use of CAD-CAM to fabricate personalized solid auricular models could permit plastic surgeons to build a customized framework for ear reconstruction using either costal cartilage or an alloplastic material to improve aesthetics and symmetry by individualized mapping and image mirroring, respectively. Finally, the porous auricular model could be applied as a patient-specific candidate scaffold with both biocompatibility and biodegradability for future auricular reconstruction via regenerative medicine pathways.

Summary

In recent years, the application of three-dimensional fabrication to fabricate customized porous scaffolds for cell culture has received much attention from the field of tissue engineering and plastic surgery. In this study, we applied a publicly accessible 3D printer-Ultimaker 2+ with biodegradable polymer-polycaprolactone (PCL) to fabricate both three-dimensional scaffolds and auricular porous constructs prepared for future in-vitro cell culture and in-situ tissue engineering respectively by using a customized CAD-CAM workflow.

For scaffolds, starting with original cubic scaffold, the resolution for printing scaffolds by PCL was gradually approached by applying method of uniform scaling, by evaluating both the procedures of limit test and constructs, results show lowest limit of Ulitmaker 2+ for fabricating scaffolds with PCL as 600 microns compared with inherent compatible material such as PLA and ABS at 300 microns. The accuracy and precision of the scaffold has also been tested by comparing with former standard counterparts and default measurements in CAD software (One sample t-test) ($P>0.05$). For auricular porous construct, we extracted 3D Data from MRI/CT scan and used its mirror image to create the shape of the porous scaffold including its microstructure. Following production, the accuracy and precision for constructing this final solid and porous auricle printouts showed promising results regarding a translation in a clinical setting.

In Conclusion, our study implemented a consistent CAD-CAM workflow for Ultimaker 2+ with PCL to fabricate both three-dimensional scaffolds and auricular porous constructs which are potentially applicable for future in-vitro cell culture and in-situ tissue engineering, respectively. The results of this study can help to improve surgical simulation and cartilage tissue engineering like for microtia or other cartilage defects.

Zusammenfassung

In den letzten Jahren hat die Anwendung der dreidimensionalen Fertigung zur Herstellung von patientenspezifischen porösen Gerüsten für die Zellkultur viel Aufmerksamkeit aus dem Bereich der Gewebetechnik und plastischen Chirurgie erhalten. In dieser Studie haben wir einen kommerziell erhältlichen 3D-Drucker-Ultimaker 2+ mit biologisch abbaubarem Polymer-Polycaprolacton (PCL) eingesetzt, um sowohl dreidimensionale Gerüste als auch poröse ohrförmige Konstrukte herzustellen, die für zukünftige In-vitro-Zellkulturen bzw. In-situ-Gewebetechnik mit einem maßgeschneiderten CAD-CAM-Workflow vorbereitet wurden.

An einfachen kubischen Gerüsten wurde die Druckauflösung des PCLs schrittweise durch steigende Skalierung ausgetestet. Die untere Grenze des Ulitmaker 2+ für die Herstellung von Gerüsten mit PCL konnte bei 600 Mikrometer bestimmte werden. Wohingehend die Grenze bei den inhärent kompatiblen Materialien wie PLA und ABS bei 300 Mikrometern lag. Die Genauigkeit der Gerüsterstellung wurde auch im Vergleich zu früheren Standard-Gegenstücken (ANVOA) ($P>0,05$) und Standardmessungen in CAD-Software (One Sample t-test) ($P>0.05$) getestet. Für das ohrförmige Konstrukt wurde die Form aus einem MRT/CT-Scan erfasst und ihr Spiegelbild für die Planung eines patientenspezifischen Gerüstes herangezogen. Die Präzision der porösen Aurikelgerüste ist vielversprechend hinsichtlich einer späteren klinischen Anwendung des Konzeptes.

Die Arbeit zeigt einen konsistenten CAD-CAM-Workflow für den Ultimaker 2+ zur PCL Herstellung sowohl dreidimensionaler Gerüste als auch Ohrförmiger Konstrukt. Dies könnte auch Grundlage für zukünftige Anwendungen in Kombination mit In-vitro-Zellkulturen bzw. In-situ-Gewebe-Engineering darstellen. Die Ergebnisse dieser Studie könnten zukünftig helfen, durch 3D Planung Knorpelgewebskonstrukte wie beispielsweise für die Behandlung der Mikrotie oder anderer Knorpeldefekte zu ermöglichen.

References

1. Brittberg M, Winalski CS. Evaluation of cartilage injuries and repair. JBJS. 2003;85:58-69.

2. Caplan AI, Elyaderani M, Mochizuki Y, Wakitani S, Goldberg VM. Principles of cartilage repair and regeneration. Clinical orthopaedics and related research. 1997(342):254-69.

3. Huey DJ, Hu JC, Athanasiou KA. Unlike bone, cartilage regeneration remains elusive. Science. 2012;338(6109):917-21.

4. Gaissmaier C, Koh JL, Weise K. Growth and differentiation factors for cartilage healing and repair. Injury. 2008;39(1):88-96.

5. Skoog T, Ohlsén L, Sohn SA. The chondrogenic potential of the perichondrium. Chirurgia plastica. 1975;3(2):91-103.

6. Robin Poole A, Matsui Y, Hinek A, Lee E. Cartilage macromolecules and the calcification of cartilage matrix. The Anatomical Record. 1989;224(2):167-79.

7. Riesle J, Hollander A, Langer R, Freed L, Vunjak‐Novakovic G. Collagen in tissue‐engineered cartilage: Types, structure, and crosslinks. Journal of cellular biochemistry. 1998;71(3):313-27.

8. Wright V, Dowson D. Lubrication and cartilage. Journal of anatomy. 1976;121(Pt 1):107.

9. Kuivaniemi H, Tromp G, Prockop DJ. Mutations in fibrillar collagens (types I, II, III, and XI), fibril‐associated collagen (type IX), and network‐forming collagen (type X) cause a spectrum of diseases of bone, cartilage, and blood vessels. Human mutation. 1997;9(4):300-15.

10. Alford JW, Cole BJ. Cartilage restoration, part 1: basic science, historical perspective, patient evaluation, and treatment options. The American journal of sports medicine.

2005;33(2):295-306.

11. Jackson DW, Scheer MJ, Simon TM. Cartilage substitutes: overview of basic science and treatment options. JAAOS-Journal of the American Academy of Orthopaedic Surgeons. 2001;9(1):37-52.

12. Steadman JR, Rodkey WG, Rodrigo JJ. Microfracture: surgical technique and rehabilitation to treat chondral defects. Clinical Orthopaedics and Related Research®. 2001;391:S362-S9.

13. Lewis PB, McCarty III LP, Kang RW, Cole BJ. Basic science and treatment options for articular cartilage injuries. Journal of Orthopaedic & Sports Physical Therapy. 2006;36(10):717-27.

14. Knutsen G, Engebretsen L, Ludvigsen TC, Drogset JO, Grøntvedt T, Solheim E, Strand T, Roberts S, Isaksen V, Johansen O. Autologous chondrocyte implantation compared with microfracture in the knee: a randomized trial. JBJS. 2004;86(3):455-64.

15. Peterson L, Vasiliadis HS, Brittberg M, Lindahl A. Autologous chondrocyte implantation: a long-term follow-up. The American journal of sports medicine. 2010;38(6):1117-24.

16. Marlovits S, Zeller P, Singer P, Resinger C, Vécsei V. Cartilage repair: generations of autologous chondrocyte transplantation. European journal of radiology. 2006;57(1):24-31.

17. Sittinger M, Perka C, Schultz O, Häupl T, Burmester G-R. Joint cartilage regeneration by tissue engineering. Zeitschrift für Rheumatologie. 1999;58(3):130-5.

18. Meyer U, Wiesmann HP. Bone and cartilage engineering: Springer Science & Business Media; 2006.

19. Luquetti DV, Heike CL, Hing AV, Cunningham ML, Cox TC. Microtia: epidemiology and genetics. American Journal of Medical Genetics Part A. 2012;158(1):124-39.

20. TANZER RC. Total reconstruction of the auricle: a 10-year report. Plastic and

reconstructive surgery. 1967;40(6):547-50.

21. Nagata S. A new method of total reconstruction of the auricle for microtia. Plastic and reconstructive surgery. 1993;92(2):187-201.

22. Brent B. Auricular repair with autogenous rib cartilage grafts: two decades of experience with 600 cases. Plastic and reconstructive surgery. 1992;90(3):355-74; discussion 75-6.

23. Ikada Y. Challenges in tissue engineering. Journal of the Royal Society Interface. 2006;3(10):589-601.

24. Rotter N, Haisch A, Bücheler M. Cartilage and bone tissue engineering for reconstructive head and neck surgery. European Archives of Oto-Rhino-Laryngology and Head & Neck. 2005;262(7):539-45.

25. Nussenbaum B, Teknos TN, Chepeha DB. Tissue engineering: the current status of this futuristic modality in head neck reconstruction. Current opinion in otolaryngology & head and neck surgery. 2004;12(4):311-5.

26. Vacanti C, Vacanti J. Bone and cartilage reconstruction with tissue engineering approaches. Otolaryngologic Clinics of North America. 1994;27(1):263-76.

27. Sittinger M, Bujia J, Minuth W, Hammer C, Burmester G. Engineering of cartilage tissue using bioresorbable polymer carriers in perfusion culture. Biomaterials. 1994;15(6):451-6.

28. Risbud MV, Sittinger M. Tissue engineering: advances in in vitro cartilage generation. TRENDS in Biotechnology. 2002;20(8):351-6.

29. Cancedda R, Cancedda FD, Castagnola P. Chondrocyte differentiation. International review of cytology: Elsevier; 1995. p. 265-358.

30. Barbero A, Grogan S, Schäfer D, Heberer M, Mainil-Varlet P, Martin I. Age related changes in human articular chondrocyte yield, proliferation and post-expansion chondrogenic

capacity. Osteoarthritis and cartilage. 2004;12(6):476-84.

31. Moskalewski S, Hyc A, Osiecka‐Iwan A. Immune response by host after allogeneic chondrocyte transplant to the cartilage. Microscopy research and technique. 2002;58(1):3-13.

32. Reddi AH. Morphogenesis and tissue engineering of bone and cartilage: inductive signals, stem cells, and biomimetic biomaterials. Tissue engineering. 2000;6(4):351-9.

33. Wang L, Tran I, Seshareddy K, Weiss ML, Detamore MS. A comparison of human bone marrow–derived mesenchymal stem cells and human umbilical cord–derived mesenchymal stromal cells for cartilage tissue engineering. Tissue Engineering Part A. 2009;15(8):2259-66.

34. Gao J, Dennis JE, Solchaga LA, Awadallah AS, Goldberg VM, Caplan AI. Tissue-engineered fabrication of an osteochondral composite graft using rat bone marrow-derived mesenchymal stem cells. Tissue engineering. 2001;7(4):363-71.

35. Ogawa R, Mizuno H, Hyakusoku H, Watanabe A, Migita M, Shimada T. Chondrogenic and osteogenic differentiation of adipose-derived stem cells isolated from GFP transgenic mice. Journal of Nippon Medical School. 2004;71(4):240-1.

36. Strem BM, Hicok KC, Zhu M, Wulur I, Alfonso Z, Schreiber RE, Fraser JK, Hedrick MH. Multipotential differentiation of adipose tissue-derived stem cells. The Keio journal of medicine. 2005;54(3):132-41.

37. Martin I, Wendt D, Heberer M. The role of bioreactors in tissue engineering. TRENDS in Biotechnology. 2004;22(2):80-6.

38. Chen H-C, Hu Y-C. Bioreactors for tissue engineering. Biotechnology letters. 2006;28(18):1415-23.

39. Zou H, Wieser R, Massagué J, Niswander L. Distinct roles of type I bone morphogenetic protein receptors in the formation and differentiation of cartilage. Genes & development. 1997;11(17):2191-203.

40. Reddi AH. Regulation of cartilage and bone differentiation by bone morphogenetic

proteins. Current opinion in cell biology. 1992;4(5):850-5.

41. Sporn MB, Roberts AB, Wakefield LM, Assoian RK. Transforming growth factor-beta: biological function and chemical structure. Science. 1986;233(4763):532-4.

42. Kim SE, Park JH, Cho YW, Chung H, Jeong SY, Lee EB, Kwon IC. Porous chitosan scaffold containing microspheres loaded with transforming growth factor-β1: Implications for cartilage tissue engineering. Journal of Controlled Release. 2003;91(3):365-74.

43. Cuevas P, Burgos J, Baird A. Basic fibroblast growth factor (FGF) promotes cartilage repair in vivo. Biochemical and biophysical research communications. 1988;156(2):611-8.

44. Trippel SB. Growth factor actions on articular cartilage. The Journal of rheumatology Supplement. 1995;43:129-32.

45. Schmidt M, Chen E, Lynch S. A review of the effects of insulin-like growth factor and platelet derived growth factor on in vivo cartilage healing and repair. Osteoarthritis and cartilage. 2006;14(5):403-12.

46. McQUILLAN DJ, Handley CJ, Campbell MA, Bolis S, Milway V, Herington A. Stimulation of proteoglycan biosynthesis by serum and insulin-like growth factor-I in cultured bovine articular cartilage. Biochemical Journal. 1986;240(2):423-30.

47. Hollister SJ. Porous scaffold design for tissue engineering. Nature materials. 2005;4(7):518.

48. Freed LE, Vunjak-Novakovic G, Biron RJ, Eagles DB, Lesnoy DC, Barlow SK, Langer R. Biodegradable polymer scaffolds for tissue engineering. Bio/technology. 1994;12(7):689.

49. Lee S-H, Shin H. Matrices and scaffolds for delivery of bioactive molecules in bone and cartilage tissue engineering. Advanced drug delivery reviews. 2007;59(4-5):339-59.

50. Song L, Baksh D, Tuan R. Mesenchymal stem cell-based cartilage tissue engineering: cells, scaffold and biology. Cytotherapy. 2004;6(6):596-601.

51. Huang AH, Farrell MJ, Mauck RL. Mechanics and mechanobiology of mesenchymal

stem cell-based engineered cartilage. Journal of biomechanics. 2010;43(1):128-36.

52. Woodfield T, Blitterswijk CV, Wijn JD, Sims T, Hollander A, Riesle J. Polymer scaffolds fabricated with pore-size gradients as a model for studying the zonal organization within tissue-engineered cartilage constructs. Tissue engineering. 2005;11(9-10):1297-311.

53. Kellomäki M, Törmälä P. Processing of resorbable poly-α-hydroxy acids for use as tissue-engineering scaffolds. Biopolymer methods in tissue engineering: Springer; 2004. p. 1-10.

54. O'brien FJ. Biomaterials & scaffolds for tissue engineering. Materials today. 2011;14(3):88-95.

55. Place ES, George JH, Williams CK, Stevens MM. Synthetic polymer scaffolds for tissue engineering. Chemical society reviews. 2009;38(4):1139-51.

56. Oh SH, Park IK, Kim JM, Lee JH. In vitro and in vivo characteristics of PCL scaffolds with pore size gradient fabricated by a centrifugation method. Biomaterials. 2007;28(9):1664-71.

57. Hollister SJ. Scaffold design and manufacturing: from concept to clinic. Advanced materials. 2009;21(32‐33):3330-42.

58. O'Brien FJ, Harley BA, Yannas IV, Gibson LJ. The effect of pore size on cell adhesion in collagen-GAG scaffolds. Biomaterials. 2005;26(4):433-41.

59. Derby B. Printing and prototyping of tissues and scaffolds. Science. 2012;338(6109):921-6.

60. O'Brien FJ, Harley BA, Yannas IV, Gibson L. Influence of freezing rate on pore structure in freeze-dried collagen-GAG scaffolds. Biomaterials. 2004;25(6):1077-86.

61. Yan Y, Xiong Z, Hu Y, Wang S, Zhang R, Zhang C. Layered manufacturing of tissue engineering scaffolds via multi-nozzle deposition. Materials Letters. 2003;57(18):2623-8.

62. Gauvin R, Chen Y-C, Lee JW, Soman P, Zorlutuna P, Nichol JW, Bae H, Chen S,

Khademhosseini A. Microfabrication of complex porous tissue engineering scaffolds using 3D projection stereolithography. Biomaterials. 2012;33(15):3824-34.

63. Khalil S, Nam J, Sun W. Multi-nozzle deposition for construction of 3D biopolymer tissue scaffolds. Rapid Prototyping Journal. 2005;11(1):9-17.

64. Jones AC, Milthorpe B, Averdunk H, Limaye A, Senden TJ, Sakellariou A, Sheppard AP, Sok RM, Knackstedt MA, Brandwood A. Analysis of 3D bone ingrowth into polymer scaffolds via micro-computed tomography imaging. Biomaterials. 2004;25(20):4947-54.

65. Carletti E, Motta A, Migliaresi C. Scaffolds for tissue engineering and 3D cell culture. 3D cell culture: Springer; 2011. p. 17-39.

66. Harley BA, Kim H-D, Zaman MH, Yannas IV, Lauffenburger DA, Gibson LJ. Microarchitecture of three-dimensional scaffolds influences cell migration behavior via junction interactions. Biophysical journal. 2008;95(8):4013-24.

67. Gebhardt A. Understanding additive manufacturing2011.

68. Kruth J-P, Leu M-C, Nakagawa T. Progress in additive manufacturing and rapid prototyping. Cirp Annals. 1998;47(2):525-40.

69. Weng Z, Zhou Y, Lin W, Senthil T, Wu L. Structure-property relationship of nano enhanced stereolithography resin for desktop SLA 3D printer. Composites Part A: Applied Science and Manufacturing. 2016;88:234-42.

70. Fina F, Goyanes A, Gaisford S, Basit AW. Selective laser sintering (SLS) 3D printing of medicines. International journal of pharmaceutics. 2017;529(1-2):285-93.

71. Bak D. Rapid prototyping or rapid production? 3D printing processes move industry towards the latter. Assembly Automation. 2003;23(4):340-5.

72. Dudek P. FDM 3D printing technology in manufacturing composite elements. Archives of Metallurgy and Materials. 2013;58(4):1415-8.

73. Melnikova R, Ehrmann A, Finsterbusch K, editors. 3D printing of textile-based

structures by Fused Deposition Modelling (FDM) with different polymer materials. IOP conference series: materials science and engineering; 2014: IOP Publishing.

74. Ultimaker B. Ultimaker 2: makes easy even easier. 2015.

75. Kelly JF. 3D Modeling and Printing with Tinkercad: Create and Print Your Own 3D Models: Que Publishing; 2014.

76. Sengupta AK, Das B. Human: An AutoCad based three dimensional anthropometric human model for workstation design. International Journal of Industrial Ergonomics. 1997;19(5):345-52.

77. Knighton MS, Moyer TC, Sidney KE, McKinley WD. Graphical interface for manipulation of 3D models. Google Patents; 2006.

78. Horvath J. Mastering 3D printing: Apress; 2014.

79. Hernandez DD. Factors affecting dimensional precision of consumer 3D printing. International Journal of Aviation, Aeronautics, and Aerospace. 2015;2(4):2.

80. Letcher T, Waytashek M, editors. Material property testing of 3D-printed specimen in PLA on an entry-level 3D printer. ASME 2014 international mechanical engineering congress and exposition; 2014: American Society of Mechanical Engineers.

81. Ahmad A, Leman Z, Azmir M, Muhamad K, Harun W, Juliawati A, Alias A, editors. Optimization of warpage defect in injection moulding process using ABS material. 2009 Third Asia International Conference on Modelling & Simulation; 2009: IEEE.

82. Cooper A, Bhattarai N, Zhang M. Fabrication and cellular compatibility of aligned chitosan–PCL fibers for nerve tissue regeneration. Carbohydrate Polymers. 2011;85(1):149-56.

83. McNickle AG, Provencher MT, Cole BJ. Overview of existing cartilage repair technology. Sports medicine and arthroscopy review. 2008;16(4):196-201.

84. Mota C, Puppi D, Chiellini F, Chiellini E. Additive manufacturing techniques for the production of tissue engineering constructs. Journal of tissue engineering and regenerative

medicine. 2015;9(3):174-90.

85. Melchels FP, Domingos MA, Klein TJ, Malda J, Bartolo PJ, Hutmacher DW. Additive manufacturing of tissues and organs. Progress in Polymer Science. 2012;37(8):1079-104.

86. Herrmann K-H, Gärtner C, Güllmar D, Krämer M, Reichenbach JR. 3D printing of MRI compatible components: Why every MRI research group should have a low-budget 3D printer. Medical engineering & physics. 2014;36(10):1373-80.

87. Walls S, Corney J, Vasantha A, Vijayumar G, editors. Relative energy consumption of low-cost 3d printers. 12th International Conference on Manufacturing Research; 2014.

88. Steenhuis H-J, Ulusemre T, Fang X. Technology Strategy and Developments in Consumer 3D Printers.

89. Virta M. The capabilities of the fused deposition modeling machine Ultimaker and its adjusting for the biomedical research purposes2014.

90. Ripley B, Levin D, Kelil T, Hermsen JL, Kim S, Maki JH, Wilson GJ. 3D printing from MRI Data: Harnessing strengths and minimizing weaknesses. Journal of Magnetic Resonance Imaging. 2017;45(3):635-45.

91. Wake N, Chandarana H, Huang W, Taneja S, Rosenkrantz A. Application of anatomically accurate, patient-specific 3D printed models from MRI data in urological oncology. Clinical radiology. 2016;71(6):610-4.

92. Lee J-Y, An J, Chua CK. Fundamentals and applications of 3D printing for novel materials. Applied Materials Today. 2017;7:120-33.

93. Skardal A, Atala A. Biomaterials for integration with 3-D bioprinting. Annals of biomedical engineering. 2015;43(3):730-46.

94. Cipitria A, Skelton A, Dargaville T, Dalton P, Hutmacher D. Design, fabrication and characterization of PCL electrospun scaffolds—a review. Journal of Materials Chemistry. 2011;21(26):9419-53.

95. Malikmammadov E, Tanir TE, Kiziltay A, Hasirci V, Hasirci N. PCL and PCL-based materials in biomedical applications. Journal of Biomaterials science, Polymer edition. 2018;29(7-9):863-93.

96. Kehoe S, Zhang X, Boyd D. FDA approved guidance conduits and wraps for peripheral nerve injury: a review of materials and efficacy. Injury. 2012;43(5):553-72.

97. Sun H, Mei L, Song C, Cui X, Wang P. The in vivo degradation, absorption and excretion of PCL-based implant. Biomaterials. 2006;27(9):1735-40.

98. Wilson N, Wang K, Dutton RW, Taylor C, editors. A software framework for creating patient specific geometric models from medical imaging data for simulation based medical planning of vascular surgery. International Conference on Medical Image Computing and Computer-Assisted Intervention; 2001: Springer.

99. Melchels F, Wiggenhauser PS, Warne D, Barry M, Ong FR, Chong WS, Hutmacher DW, Schantz J-T. CAD/CAM-assisted breast reconstruction. Biofabrication. 2011;3(3):034114.

100. Schroeder C, Regli WC, Shokoufandeh A, Sun W. Computer-aided design of porous artifacts. Computer-aided design. 2005;37(3):339-53.

101. Yoo D. New paradigms in hierarchical porous scaffold design for tissue engineering. Materials Science and Engineering: C. 2013;33(3):1759-72.

102. Hellestam C, Olsson J, Elfstoem I. Method and apparatus for manufacturing porous three-dimensional articles. Google Patents; 2014.

103. Lee J, Kim KE, Bang S, Noh I, Lee C. A desktop multi-material 3D bio-printing system with open-source hardware and software. International journal of precision engineering and manufacturing. 2017;18(4):605-12.

104. Mandrycky C, Wang Z, Kim K, Kim D-H. 3D bioprinting for engineering complex tissues. Biotechnology advances. 2016;34(4):422-34.

105. Tasoglu S, Demirci U. Bioprinting for stem cell research. Trends in biotechnology.

2013;31(1):10-9.

106. Cui X, Breitenkamp K, Finn M, Lotz M, D'Lima DD. Direct human cartilage repair using three-dimensional bioprinting technology. Tissue Engineering Part A. 2012;18(11-12):1304-12.

107. Jakab K, Norotte C, Marga F, Murphy K, Vunjak-Novakovic G, Forgacs G. Tissue engineering by self-assembly and bio-printing of living cells. Biofabrication. 2010;2(2):022001.

108. Mironov V, Prestwich G, Forgacs G. Bioprinting living structures. Journal of Materials Chemistry. 2007;17(20):2054-60.

109. Korsch BM, Gozzi EK, Francis V. Gaps in doctor-patient communication: I. Doctor-patient interaction and patient satisfaction. Pediatrics. 1968;42(5):855-71.

110. de Heras Ciechomski P, Constantinescu M, Garcia J, Olariu R, Dindoyal I, Le Huu S, Reyes M. Development and implementation of a web-enabled 3D consultation tool for breast augmentation surgery based on 3D-image reconstruction of 2D pictures. Journal of medical Internet research. 2012;14(1):e21.

111. Chesson RA, McKenzie GA, Mathers SA. What do patients know about ultrasound, CT and MRI? Clinical Radiology. 2002;57(6):477-82.

112. Vaccarezza M, Papa V. 3D printing: a valuable resource in human anatomy education. Anatomical science international. 2015;90(1):64-5.

113. Kim JY, Cho D-W. Blended PCL/PLGA scaffold fabrication using multi-head deposition system. Microelectronic Engineering. 2009;86(4-6):1447-50.

114. Romo T, Reitzen SD. Aesthetic microtia reconstruction with Medpor. Facial Plastic Surgery. 2008;24(01):120-8.

115. Adachi T, Osako Y, Tanaka M, Hojo M, Hollister SJ. Framework for optimal design of porous scaffold microstructure by computational simulation of bone regeneration. Biomaterials.

2006;27(21):3964-72.

116. Kuhne M, John T, El-Sayed K, Marzahn U, Aue A, Kohl B, Stoelzel K, Ertel W, Blottner D, Haisch A. Characterization of auricular chondrocytes and auricular/articular chondrocyte co-cultures in terms of an application in articular cartilage repair. International journal of molecular medicine. 2010;25(5):701-8.

Appendix

List of all products and devices

Acrylonitrile-butadiene-styrene filaments	(Formfutura, Netherlands)
AutoCAD 2018	(Autodesk, San Rafael, CA, USA)
Biopsy punch, 5.0 mm	(Stiefel, UK)
Cura 3.6.0	(Ultimaker BV, Utrecht, Netherlands)
Electronic digital caliper	(Wiha, Schonach, Germany)
GraphPad Prism 8.0.1	(GraphPad, San Diego, CA, USA)
Microsoft 3D Builder, win10 1703	(Microsoft, Redmond, WA, USA)
Microsoft 3D Viewer, win10 1703	(Microsoft, Redmond, WA, USA)
Polycaprolactone filaments	(3D4MAKERS, Netherlands)
Polylactic acid filaments	(Formfutura, Netherlands)
Thinkercad v2.0	(Autodesk, San Rafael, CA, USA)
Ultimaker 2	(Ultimaker BV, Utrecht, Netherlands)
Ultimaker Extrusion Upgrade Kit	(Ultimaker BV, Utrecht, Netherlands)
Materialise Mimics 20.0	(Materialise NV, Leuven, Belgium)
Materialise 3-matic 9.0	(Materialise NV, Leuven, Belgium)
Axio Observer	(ZEISS, Oberkochen, Germany)
ZEN	(ZEISS, Oberkochen, Germany)

List of Figures

List of Tables

List of Abbreviations

3D	Three-Dimensional
ABS	Acrylonitrile-Butadiene-Styrene
ADSCs	Adipose-Derived Mesenchymal Stem Cells
AM- Additive Manufacturing	Additive Manufacturing
ANOVA	Analysis of Variance
BMP	Bone Morphogenetic Protein
BMSCs	Bone Marrow-derived Mesenchymal Stem Cells
CAD	Computer Aided Design
CAM	Computer Aided Manufacturing
CT	Computed Tomography
DICOM	Digital Imaging and Communications in Medicine
ECM	Extracellular Matrix
FDM	Fused Deposition modeling
FGF	Fibroblast Growth Factor
IGF	Insulin-like Growth Factor
MRI	Magnetic Resonance Imaging
PCL	Polycaprolactone
PGA	Polymethyl Acetate
PLA	Polylactic Acid
PLGA	Polylactic-co-glycolic Acid
SD	Secure Digital
SLA	Selective Laser Sintering
SLS	Selective Laser Sintering
STL	Standard Tessellation Language
TGF-β	Transforming Growth Factor beta
USB	

WRU	Universal Serial Bus
PEL	Width of Rectangular Unit
MEL	Physiological Ear Length
PEB	Morphological Ear Breadth
MEB	Physiological Ear Breadth
	Morphological Ear Breadth

Acknowledgements

It is with immense gratitude that I acknowledge the support and help of many people during my cooperative doctoral program at Ludwig Maximilian University of Munich (LMU):

I wish to thank, first and foremost, Chefarzt Prof. Dr.med. Riccardo Giunta and Professor Dr. med. Thilo Schenck, my doctor father. The door to your office was always open for me to discuss the progress of my independent research. With your patient guidance, I could start and concentrate on this project of interest during my doctoral study. Thanks for providing me with so excellent platform to complete this independent project and your always kind support for my study at both LMU and Harvard.

I would also like to express my profound gratitude to Dr med. Severin Wiggenhauser, who helped me a lot for providing me with hardware, software and other materials with request to optimize this project. Without your consistent encouragement and feedback, I could not conduct this project with confidence and passion.

I would also like to show my warm thanks to my lab manger Mrs. Alexandra Birt who provided me with a good working environment at lab and helped me to order measuring tools, polycaprolactone filaments and other essential materials for this project.

Special gratitude goes out to my lab colleagues Constanze Kuhlmann, Jana Blum, Benedikt Fuchs who provided me with great help with introduction to the laboratory and the LMU administration. Thanks for the time that I spent with you in the lab and I will keep this treasured this good memory forever.

Thanks for China Scholarship Council, Chinese Medical Board and Fellowships from Harvard University who supported my joint graduate study at both LMU and Harvard these years.

Thanks for professors and colleagues from my joint graduate program and postdoctoral research fellowship at both Harvard T.H Chan School of Public Health and Harvard Medical School who provided me with comments for data analysis and interpretation.

Thanks for my colleagues and supervisor from my home institute in China-Plastic Surgery Hospital, Peking Union Medical College, who always supported me and provided me with sample image to work on.

Last but not the least, I would like to express my gratitude to my parents, my girlfriend, it is your positive attitude that shape me to be a passionate and confident person. Your encouragement always drives me to move forward to conquer challenges.

Eidesstattliche Versicherung

Chenhao Ma

Ich erkläre hiermit an Eides statt,

dass ich die vorliegende Dissertation mit dem Thema

The CAD-CAM workflow for 3D Fabrication of 3D Bioscaffolds and Customized Auricular Constructs with Polycaprolactone using Ultimaker 2+

selbständig verfasst, mich außer der angegebenen keiner weiteren Hilfsmittel bedient und alle Erkenntnisse, die aus dem Schrifttum ganz oder annähernd übernommen sind, als solche kenntlich gemacht und nach ihrer Herkunft unter der Bezeichnung der Fundstelle einzeln nachgewiesen habe.

Ich erkläre zudem, dass die hier vorgelegte Dissertation nicht in gleicher oder ähnlicher Form bei einer anderen Stelle zur Erlangung eines akademischen Grades eingereicht wurde.

Beijing, 28.5.2021 — Chenhao Ma

Ort, Datum — Unterschrift Doktorand